arXiv:submit/7923078 [econ.GN] 7 Aug 2026

Shared Bidding Algorithms and Competition: Evidence from Electricity Markets

Nicolas Eschenbaum*

August 2026

Abstract

Competing firms increasingly delegate market decisions to algorithms supplied by the same third-party providers. We study whether a shared algorithm leads competitors to internalise one another's profits, using data from the Australian National Electricity Market, where batteries' bids are observed at 5-minute frequency and can be linked to an autobidding provider. Bids constructed by the same provider co-move, and do so more strongly after a disclosure reform made the scarcity state easier to observe: the same information that steers batteries towards efficient arbitrage also synchronises the bids of competitors who share a provider. To separate co-movement from joint profit maximisation, we perform a conduct test by estimating each battery's dynamic value of stored energy and reclearing the market under counterfactual bids. We find that batteries forgo profitable dispatch in the evening peak when it would lower the profit of same-provider batteries owned by rival firms. The estimated conduct parameter is close to one. But this effect arises only where a provider's share of near-margin battery capacity exceeds roughly 30%. The identified conduct costs consumers an annualised $\$5.5$ million given the battery fleet from 2025, and concentration analysis based on ownership would treat these batteries as independent competitors and miss the impact of shared autobidding software.

Keywords: algorithmic bidding; algorithmic collusion; algorithm providers; market conduct; battery storage; electricity markets.
JEL codes: D43; D44; L41; L86; L94.

1. Introduction

Firms increasingly rely on third-party algorithms to choose their prices or bids. In many markets, firms' actions are now intermediated by an upstream layer of algorithm providers – forecast vendors, data analytics providers, or bidding platforms that serve multiple downstream competitors.

*Swiss Economics, Zürich, Switzerland. nicolas.eschenbaum@swiss-economics.ch.

This has led to antitrust authorities raising concerns that the use of algorithms may lead to algorithmic collusion (e.g., U.S. Department of Justice and Federal Trade Commission, 2017; Autorité de la concurrence and Bundeskartellamt, 2019; Competition and Markets Authority, 2021) and a growing literature studies whether algorithms learn anti-competitive strategies (e.g., Calvano et al., 2020; Asker et al., 2024).

In this paper, we provide empirical evidence on the effects that shared algorithms and algorithm provider concentration have on downstream market conduct. We develop a hand-collected mapping of autobidding providers to utility-scale batteries in the Australian National Electricity Market (NEM). Autobidding software allows battery owners to specify high-level goals and constraints (such as their risk appetite) and the autobidding software then automatically calculates and submits the optimised bid stacks.[1] We combine this with 5-minute bidding, price, and dispatch data of four bidding zones in the NEM to construct a detailed panel of market behaviour and upstream provider concentration in 2025/2026.

Electricity markets – and utility-scale batteries in particular – have recently faced regulatory scrutiny stemming from concerns about algorithmic collusion associated with the rapid expansion of storage (Australian Energy Market Commission, 2024; Dutch Authority for the Financial Markets, 2024). Batteries interact across multiple concurrent markets at high frequency – features typically associated with elevated collusion risk. At the same time, the complexity of the physical and market constraints, together with the speed of bidding, mean that effective operation requires algorithms, which are typically provided by third-party firms.

We document a substantial degree of software provider concentration in the NEM, with two systems – Tesla Autobidder and Fluence Mosaic – operating two-thirds of known-provider battery capacity. The use of common software produces substantial synchronisation in the level of bids and in the timing of rebids among same-provider batteries. A July 2025 disclosure reform (ERI) made the aggregate regional state of charge in the last 5-minute interval, and the per-battery levels from the previous trading day, public. Combined with the observation of same-provider batteries operating across multiple bidding regions, this lets us measure how a stronger public scarcity signal changes same-provider co-movement. The use of the same architecture, parameters, and bidding logic may be expected to lead to more similar bidding responses as the public signal of the underlying scarcity state becomes stronger. We find that improved scarcity observability indeed increases same-provider synchronisation. Both the level of bids and the timing of rebids are strongly correlated among same-provider batteries and this correlation increases post-ERI. The same disclosure also improves the steering of batteries towards dynamic arbitrage: bids rise in upper bid bands during scarce intervals and fall during abundant intervals, and battery bids respond more strongly to their own state of charge.

We then perform a conduct test of bidding behaviour. We first estimate a dynamic Bellman function to determine the opportunity cost of the state of charge of a battery. We proceed to construct local deviations to individual battery bid stacks and reclear the market to determine the counterfactual market outcome.[2] We focus on deviations that move withheld capacity – i.e., capacity in bid bands above the clearing price – down to the marginal bid band at the given

[1] Very similar autobidding software is also commonly used in online ad auctions, see Aggarwal et al. (2024).

[2] The counterfactual reclearing co-optimises energy and Frequency Control Ancillary Services (FCAS) markets simultaneously, and we calculate the change in profit across markets.

interval. If batteries are engaging in strategic withholding, this deviation should be profitable. Each deviation defines a revealed-preference moment inequality that tests whether behaviour can be rationalised by owner-level profit maximisation or instead requires internalisation of profits of same-provider batteries owned by other firms. A conduct parameter value of $\lambda = 0$ corresponds to owner-level incentives, while $\lambda = 1$ corresponds to full internalisation of same-provider, different-owner battery profits. Because the test requires same-provider batteries operated by different owners with relevant near-margin MW in the clearing interval, we can only run the test for batteries served by the two large commercial providers in our sample: Tesla Autobidder and Fluence Mosaic.

We estimate the conduct parameter as a continuous function of the focal provider's near-margin share over evening-peak hours, when battery market power is highest. The test rejects owner-level incentives in energy-market deviations whenever the same-provider share lies between roughly 30% and 70%. Below about 30% the test retains power but finds no internalisation: the improvement in fit stays near zero and rises steeply at 30%, pointing to a genuine concentration threshold. Above about 70% the provider's MW is again dominated by a single owner and the multi-owner sample the test relies on becomes too thin.[3] FCAS deviations show no conduct signal in either provider.

We then provide a series of robustness exercises that rule out alternative interpretations of the finding. First, unobserved owner-level costs cannot account for the results, because the required costs would have to exceed the maximum movement we see in our Bellman opportunity-cost estimates across numerical sensitivity checks, and in two Tesla bands no finite per-MWh charge can rationalise the data. Second, the results do not reflect hindsight. We date each operative quantity bid to its submission timestamp and find that the conduct signal is concentrated in rebids submitted within fifteen minutes of dispatch, when five-minute predispatch forecasts are accurate, and vanishes for bids lodged more than an hour ahead. Third, the results are specific to the provider coalition. For each focal deviation we construct placebo coalitions of different-provider batteries near the margin in the same interval, matched to the same-provider coalition on battery count and installed capacity so that they carry the same mechanical price exposure. None of 500 matched placebo coalitions improves the fit of the conduct objective as much as the actual same-provider coalition ($p \leq 0.010$). Finally, a positive control shows that the estimator recovers full internalisation of profits across batteries of the same owner, where joint-profit maximisation should be recovered by construction.

The remaining explanation is thus that the conduct test identifies algorithmic profit internalisation. Two features of the setting establish that the identified conduct is economically meaningful. First, these batteries are non-negligible price setters. The reclearing analysis shows that a single battery's most profitable owner-only deviation moves the regional clearing price by $\$1.28$/MWh at the median and by more than $\$6$/MWh in the upper decile. These are substantial price effects of a single battery owner, given that the market also includes other dispatchable assets such as gas or hydro plants. Second, the internalisation arises at the software provider rater than ownership level. In the identifying intervals the focal provider's near-margin capacity is spread across 2.2 separately owned firms on average, and 83% of the internalised profit spillover accrues to batteries

[3] In finite samples $\widehat{\lambda}$ in a low-power band can sit at the $[0, 1]$ boundary because the objective is essentially flat. We treat $\widehat{\lambda} = 1$ as evidence of same-provider conduct only when the moment objective falls materially below $Q_n(0)$ and the subsampling confidence set excludes zero.

owned by a different firm than the one deviating – i.e., firms that ownership-based concentration analysis treats as independent competitors. To the best of our knowledge, we are the first to provide empirical evidence on the effect of algorithm-provider concentration on downstream market conduct

To assess the dollar size of the identified conduct, we use the reclearing engine to compute, for each focal battery-interval in the identifying range, the regional clearing-price difference the owner-only counterfactual deviation would have generated. The implied price difference is about $1.28/MWh at the median and $2.70/MWh on average, corresponding to an annualised consumer cost of approximately $5.5 million ($3.1m attributable to Tesla Autobidder and $2.4m to Fluence Mosaic). This is a local partial-equilibrium estimate that holds all other bid stacks fixed and does not solve for a new market equilibrium under alternative conduct.[4]

Related Literature. There is a large and rapidly growing literature on algorithmic collusion. Seminal works have shown how reinforcement-learning algorithms may converge to supra-competitive pricing and policies that show patterns of collusive behaviour (Calvano et al., 2020; Asker et al., 2024; Banchio and Mantegazza, 2023). Related work has documented the emergence of algorithmic collusion in simulation studies across various scenarios and settings.[5] Abada and Lambin (2023) in particular study the operation of storage assets in electricity markets and consider the Tesla Autobidder software – one of the two main players in our setting – as their motivating example. Recent papers further emphasize that the relevant issue is not only autonomous learning, but also the delegation of decision-making, information processing, and implementation to a common third-party algorithm.[6]

Our work is most closely related to Calder-Wang and Kim (2026), who similarly use hand-collected data on algorithmic pricing adoption in multifamily rental markets and combine reduced-form evidence with a structural conduct test to distinguish own-profit from same-provider joint-profit incentives. In contrast to their work, we do not observe algorithm adoption over time, because in our setting autobidding is already widespread. Instead, we observe bid stacks themselves and exploit the fact that we can evaluate counterfactual market outcomes using a very accurate clearing engine. Rather than estimating the effect of algorithm adoption, our conduct test estimates whether observed battery bids are rationalised by owner-level incentives, and whether violations are systematically reduced when same-provider profit effects are internalised. We then relate the estimated effects to the provider's share of near-margin battery capacity in the bidding interval. This allows us to ask whether internalisation of same-provider profits becomes systematically more informative as provider concentration rises, and whether there exists a threshold level of concentration at which this becomes the case.

The only other empirical study of the effect of algorithm adoption on market conduct that we are aware of is Assad et al. (2024), who show that adoption of pricing algorithms by competing

[4] The utility-scale battery fleet has since grown substantially in the NEM and continues to grow, so the same identifying signal applied to a larger fleet would imply a correspondingly larger cost.

[5] See, for example, Eschenbaum et al. (2022); Klein (2021); Waltman and Kaymak (2008); Kimbrough and Murphy (2009); Cooper et al. (2015); Hansen et al. (2021); Kastius and Schlosser (2022); Sánchez-Cartas and Katsamakas (2022); den Boer et al. (2022); Abada et al. (2024).

[6] See Harrington (2021, 2025); Harrington and Ortner (2025); Sugaya and Wolitzky (2025); Aleksenko and Miklós-Thal (2026).

gasoline stations leads to increased market prices. A related empirical literature studies repricing software in online retail markets, where the algorithm reprices an existing posted price in response to rivals rather than constructing the price from primitives, and shows that the use of repricers can increase market prices (Brown and MacKay, 2023; Musolff, 2025). We contribute evidence from a market in which the algorithmic decision itself – a submitted bid stack across ten price bands – is directly observed, and the first empirical evidence on *bidding* algorithms rather than pricing or repricing software.

Moreover, two effects from the recent theoretical literature on common-algorithm providers arise in our setting. We show this with a simplified, stylised model in which common autobidding providers map scarcity signals into battery bid stacks. As in Harrington and Ortner (2025), provider concentration amplifies the aggregate price response to common scarcity information. And similarly to Aleksenko and Miklós-Thal (2026), consumer harm from common-information pricing can be decomposed into a cross-seller correlation channel and an across-state dispersion channel. The intuition is as follows. Because batteries face a dynamic opportunity cost of discharge, a higher scarcity estimate raises the opportunity cost and thus the bids, leading to correlated bids of same-provider batteries. As a result, the market outcome becomes a function of provider concentration which amplifies the aggregate price impact. The more concentrated the software provider layer is, the stronger the market price moves with the scarcity signal. Consumers then face the highest prices during those time intervals in which their consumption is highest, leading to a reduction in consumer welfare. Our simple model shows how these effects can arise in a setting with bids and dynamic storage.[7]

Our paper speaks to an active competition-policy debate. Competition authorities have warned that pricing and bidding algorithms may facilitate coordination when competitors rely on a common software intermediary, share competitively sensitive data through that intermediary, or allow software defaults and implementation architecture to substitute for independent decision-making (U.S. Department of Justice and Federal Trade Commission, 2017; Monopolkommission, 2018; Autorité de la concurrence and Bundeskartellamt, 2019; Competition and Markets Authority, 2018, 2021; Dutch Authority for the Financial Markets, 2024; Hovenkamp and Schrepel, 2026).

This issue has become a concern in electricity markets. The Australian Energy Market Commission (2024) argues that algorithmic bidding is already pervasive in the NEM, that the NEM is increasingly vulnerable to algorithmic collusion, and that policy needs to balance the efficiency gains from AI against the risk that more information and more capable algorithms make coordination easier to sustain. We directly contribute to this debate by measuring the provider layer, and testing whether same-provider profit effects become informative precisely when a provider controls a large share of the near-margin battery capacity. In our setting, battery owners are the nominal decision-makers. However, the complexity of calculating the optimal bids under the complex market constraints imposed by the market regulator, as well as the physical constraints of the battery and high frequency of bidding makes it likely that battery owners rarely override the bids that the autobidding software calculates.

Our conduct test builds on structural conduct testing and moment-inequality methods. In

[7] Our model is intentionally kept simple, and we abstain from a complete model of the repeated auction setting with capacity constraints and dynamic storage.

differentiated-products markets, conduct is often tested by estimating demand and recovering marginal costs under alternative conduct models, and testing whether the resulting cost shocks satisfy exclusion restrictions (Berry and Haile, 2014; Backus et al., 2021). This is the route followed by Calder-Wang and Kim (2026). In our setting, short-run load is approximately perfectly inelastic, so there is no differentiated-products demand system whose price elasticities can be used to infer markups in the usual way. The central clearing mechanism instead offers a different possibility: exact reclearing of feasible bid-stack deviations. The resulting revealed-preference inequalities builds on the moment-inequality approaches based on optimality or no-profitable-deviation restrictions (Bajari et al., 2007; Pakes et al., 2015; Ho and Pakes, 2014).

The object our conduct test estimates – a weight on rival profits in a firm's effective objective – is also the central object of the common-ownership literature, which asks whether diversified shareholders lead firms to internalise their competitors' profits (Azar et al., 2018; Backus et al., 2021). In our setting this spillover can be measured directly, because reclearing returns the dollar profit effect of a deviation on every rival battery. More importantly, the conduct parameter (or weight) that we estimate is associated with a different term: not who owns the asset, but who runs the bidding algorithm.

A related industrial-organisation literature studies strategic bidding and storage market power. Supply-function competition is the canonical framework for strategic bidding in uniform-price electricity auctions (Klemperer and Meyer, 1989; Vives, 2011; Holmberg, 2008), and repeated uniform-price auctions can facilitate tacit collusion by weakening deviation incentives (Fabra, 2003). Empirical work has used detailed bidding data to study strategic behaviour and dynamic constraints in electricity markets (Reguant, 2014). A newer literature studies how storage changes market outcomes, investment incentives, and the integration of renewable generation (Butters et al., 2021; Andrés-Cerezo and Fabra, 2023). Our contribution is to study utility-scale batteries as strategic bid-stack participants whose actions are increasingly intermediated by common autobidding providers.

Lastly, our analysis of bidding behaviour is also related to the operational literature that models batteries as dynamic optimisers that choose charge, discharge, and ancillary-service participation subject to state-of-charge, efficiency, capacity, degradation, and market constraints. This is directly relevant in the NEM, where batteries co-optimise energy and FCAS participation at high frequency. Closest to our work is Karimi-Arpanahi et al. (2024), who estimate battery energy storage system (BESS) operating characteristics from public NEM data and solve a receding-horizon scheduling problem across energy and FCAS markets, including the FCAS trapezium, while Prakash et al. (2025) study the role of future price information for storage scheduling in the NEM. We build on their formulation of batteries as constrained dynamic optimisers for our analysis and the Bellman estimation, but study the submitted bid stacks themselves and the provider layer that helps construct them.

The paper proceeds as follows. Section 2 describes battery bid construction in the NEM and discusses a stylised model that guides the empirical analysis. Section 3 constructs the empirical panel, documents synchronisation and state-responsive bidding around the ERI reform, estimates the dynamic value of stored energy, and implements the counterfactual-reclearing conduct test. The final section concludes.

2. Battery Bidding and Autobidder Providers

This section defines how battery optimisation maps into observed bids and why provider identity enters that mapping. We proceed in two steps. First, we describe the dynamic battery problem and the bid stack submitted to the NEM, as well as the role of autobidders. Second, we introduce a stylised model that isolates the main mechanisms studied in the empirical analysis.

Throughout, we denote batteries by i, j, owners by o, providers by k, regions by r, intervals by t, and bid bands by b. Upper-case Latin letters denote stocks, prices, and counts (S stored energy, P price, V the continuation value, K number of providers); bold lower-case letters denote vectors of the corresponding scalars ($\mathbf{b}$ a bid stack). Greek letters denote parameters, unobservables, and profit objects (θ scarcity, λ the conduct parameter, π a single-battery per-period profit flow, Π an owner-portfolio payoff inclusive of continuation value); calligraphic capitals denote sets and information structures ($\mathcal{B}$ the feasible stack, $\mathcal{I}$ an information set); and hats denote estimators ($\widehat{\lambda}$, $\widehat{m}_{it}$).

2.1. Utility-Scale Batteries and Bid Construction

Batteries' ability to shift generated energy across the trading day, i.e., dynamic arbitrage, becomes very influential in electricity markets with substantial photovoltaic (PV) generation. As a result, storage is now one of the fastest-expanding power-sector technologies.[8] For example, in ERCOT (the energy market in Texas), installed battery capacity reached 14.1 GW by July 2025, almost triple its early-2023 level, and batteries discharged more than 7 GW during the evening ramp for the first time (Electric Reliability Council of Texas, 2025). The NEM is smaller but follows the same trajectory: AEMO reports a record 64 GW connection pipeline in the December 2025 quarter, with battery storage accounting for 46% of projects and hybrid solar-battery projects for another 19.7% (Australian Energy Market Operator, 2026). As storage becomes a larger share of flexible capacity, the way batteries construct bid stacks can increasingly affect both arbitrage efficiency and price formation in the evening hours when PV production subsides (Butters et al., 2021; Andrés-Cerezo and Fabra, 2023).

Formally, a utility-scale battery is a constrained dynamic asset. Time is discrete: in each 5-minute NEM dispatch interval the battery chooses charge, discharge, and FCAS enablement subject to energy, power, and market-validation constraints.[9] Let S_{it} denote stored energy of battery i at interval t.[10] The shadow value of S_{it} is the intertemporal opportunity cost of discharge: using stored energy in the current interval lowers the option value of using the same energy later in the peak.

[8] The IEA reports 108 GW of new battery storage capacity deployed in 2025, around 40% more than in 2024, with installed capacity eleven times higher than in 2021 (International Energy Agency, 2026). In the United States, developers plan 24 GW of utility-scale battery additions in 2026, with Texas alone accounting for 12.9 GW of planned additions (U.S. Energy Information Administration, 2026).

[9] FCAS stands for Frequency Control Ancillary Services. In the NEM, AEMO procures these services to keep system frequency close to 50 Hz when realised generation and load differ from expected levels. Raise services increase net injection or reduce load when frequency is too low; lower services reduce net injection or increase load when frequency is too high. These services include both continuous regulation and contingency response over short horizons. Batteries are well suited to FCAS because inverter controls can change charge or discharge quickly, but FCAS enablement reserves headroom or footroom and is therefore jointly constrained with energy dispatch.

[10] $S_{it} \in [0, \bar{S}_i]$, where $\bar{S}_i$ is the battery's energy capacity.

Figure 1: Battery operation and the market-power state

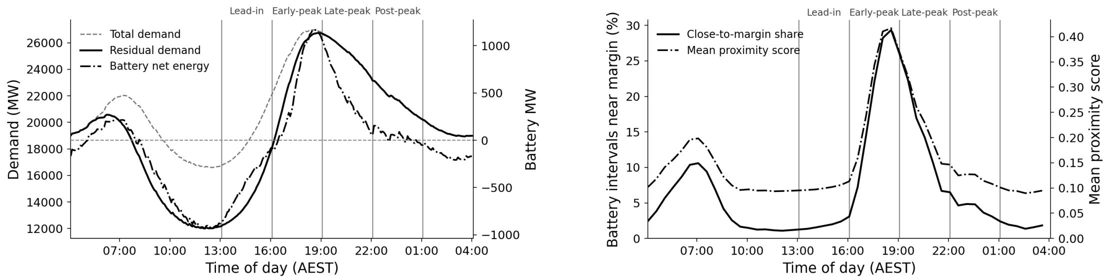

(a) Daily arbitrage (b) Near-margin battery capacity

Notes: Panel A plots average demand, residual demand, and net battery output over the day. Panel B measures when battery capacity is close to the regional clearing margin.

Figure 1 shows the two features of battery bidding that matter for the analysis. Panel A plots the daily arbitrage cycle. Solar generation compresses residual demand during the day, when batteries tend to charge, while the evening ramp creates the high-value discharge window. This makes battery bidding a finite-horizon inventory problem within the trading day. Panel B measures the corresponding market-power state. Batteries matter most for price formation when battery capacity is close to the regional clearing margin, which occurs primarily during the peak evening intervals.

Figure 1 focuses on the energy market because the energy clearing margin is the simplest way to show the dynamic arbitrage and price-setting logic. Our empirical analysis, however, evaluates operation and profits across both energy and FCAS markets. This distinction matters because FCAS enablement is jointly constrained with energy dispatch: capacity allocated to one market changes the headroom or footroom available in the other.

The NEM implements this decision through regional uniform-price auctions that clear every 5 minutes. Within each region, AEMO dispatches the least-cost feasible stack and sets the regional reference price (RRP) at the marginal accepted offer. A NEM energy bid is lodged for a trading day running from 4:00 a.m. on day t to 4:00 a.m. on day $t+1$ and contains 288 5-minute dispatch intervals. For each unit, participants set up to ten monotonically increasing price bands and, for each interval, the MW available in each band together with technical parameters such as maximum availability and ramp rates. For scheduled bidirectional batteries, bids are submitted separately for the load and generation sides, so a battery effectively has ten charge bands and ten discharge bands.

The timing of bids separates price choices from quantity choices. Price bands for trading day t must be lodged by 12:30 p.m. AEST on day $t-1$ and are then fixed for the trading day. Quantities and related technical parameters may be rebid after that deadline through the relevant dispatch interval, subject to the NEM rebidding rules: each rebid must provide a brief, specific, and verifiable reason and the time of the event giving rise to the rebid. For a given interval, the operative bid is the latest bid captured for dispatch for that interval.[11] The economically relevant

[11]For technical details, see AEMO's bidding specification, spot market operations timetable, and bidirectional-unit validation material.

Figure 2: Schematic generation-side bid stack with ten price bands

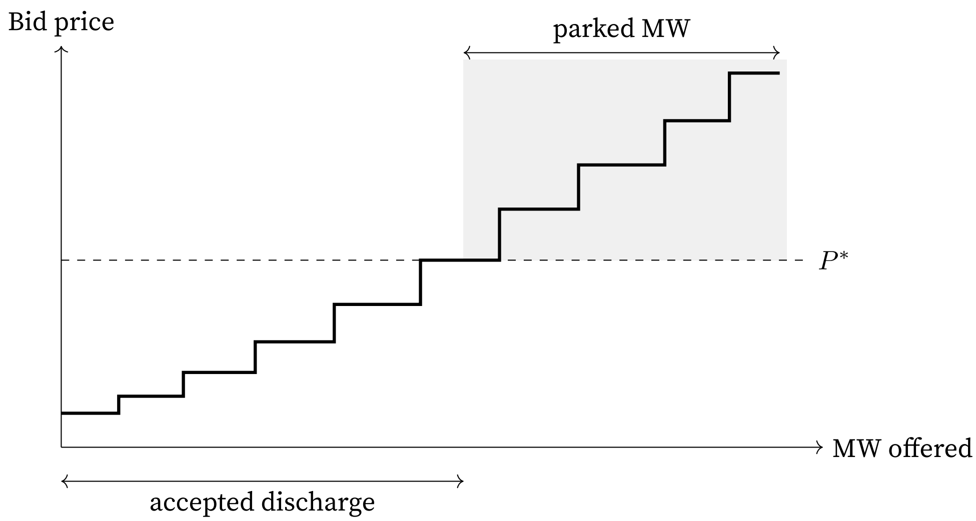

Notes: The clearing price P^* is set by the marginal accepted offer. Capacity above P^* is withheld from energy dispatch in that interval unless rebid or repriced.

object in our application is the generation-side stack, since it governs discharge offers into the regional energy auction. Figure 2 illustrates a battery's bid stack. For a given clearing price P^*, the accepted energy discharge of battery i is the cumulative accepted band quantity. Moving capacity from high bands towards the clearing band raises the probability of dispatch, but also uses scarce stored energy and can lower the market price.

The feasible stack is joint across markets. The difference between energy and FCAS bids is that the quantity offered in FCAS markets is enabled response capacity rather than energy dispatch. For batteries, FCAS enablement is feasible only conditional on the energy operating point, because raise and lower services require headroom and footroom. AEMO validates these relationships through service-specific trapezium constraints, which we describe formally in Appendix B.13. The submitted stack is therefore the output of a complex, high-frequency constrained dynamic optimisation problem.

Finally, an autobidder maps forecasts, telemetry, market data, owner settings, and risk preferences into this feasible stack. Public descriptions make clear that "autobidder" is a class of bid-construction and dispatch-control tools, not a single standardised product. AEMO describes auto-bidding systems as software that automatically carries out bids and rebids under pre-set parameters, typically using 5-minute pre-dispatch and dispatch data, so that auto-rebidding often occurs less than one hour ahead of dispatch.[12] Commercial offerings used or marketed for Australian batteries include Tesla's *Autobidder*, Fluence's *Mosaic*, Wärtsilä's *GEMS*/*IntelliBidder*, HARD Software's *Infolite Auto Bidding*, Habitat Energy's *EVOLVE* optimisation service, and newer NEM-specific products such as OptiGrid.

The relevant decision-maker remains the registered market participant, which may bid inter-

[12] See AEMO, *2025 General Power System Risk Review Report – Draft*, Section 5.9. Public document: `https://www.aemo.com.au/-/media/files/stakeholder_consultation/consultations/nem-consultations/2024/2025-general-power-system-risk-review/2025-draft-gpsrr-report.pdf`.

nally or contract optimisation services to a software or trading provider. Providers are therefore heterogeneous: some are stand-alone software vendors, some are integrated with the plant-control stack, some combine software with a trading desk, and some are in-house systems run by large asset owners. What they share is the same basic role in bid construction. The provider takes telemetry and market data as inputs, combines them with owner-supplied settings such as SoC limits, degradation or warranty constraints, FCAS participation choices, contract positions, and risk tolerances, and then forecasts prices and co-optimises charge, discharge, and offer construction for an asset or customer portfolio.

However, the complexity of calculating the optimal bid stacks over a trading day and across the sequence of 5-minute auctions – together with the technical difficulty of submitting them to the market operator – makes it difficult for an owner to override what the software has determined and submitted. An owner's agency over individual bids is therefore limited, and the bids the software constructs are unlikely to be changed.

This delegation creates the provider-layer object we study. In the empirical mapping, 42 usable batteries can be linked to 11 identified providers across 21 provider-region combinations; the two largest commercial providers are Tesla Autobidder and Fluence Mosaic.[13] A common provider can create correlated bid construction whenever clients share forecasts, update schedules, or implementation architecture, and can also be the level at which same-provider profit effects are internalised.

2.2. A Stylised Model

This section outlines a stylised model to explain how common providers affect batteries' bids. The aim is not to reproduce the NEM auction setting, but to isolate the key mechanisms of the setting. We start from the primitive objects of the empirical analysis and discuss three implications. *First*, autobidding makes bids load on provider-driven information, because the provider's algorithm turns the available information (private or public) into the bid stacks. *Second*, this common provider information channel generates bid co-movement, and it has a larger price effect when the provider's share is higher. Thus, even if we observe co-movement of same-provider batteries or stronger price effects in intervals where capacity is more concentrated among providers, we cannot conclude this implies coordinated conduct. *Third*, however, if the provider is implementing owner-level optimisation, then observed bid stacks must satisfy owner-level no-profitable-deviation inequalities; if they do not, same-provider profit internalisation is an alternative conduct hypothesis. This will be the basis for our conduct test.

Formally, consider a single bidding region r – one of the NEM's regional markets – and a 5-minute dispatch interval t. Batteries in the region are indexed by $i \in I_r$. Battery i is owned by o_i and uses autobidding provider k_i. Let $N_k := \{i : k_i = k\}$ denote the set of batteries using provider k. Battery i enters the interval with stored energy S_{it} and submits a feasible multimarket bid stack $\mathbf{b}_{it} \in \mathcal{B}_i(S_{it}, X_{rt})$, where X_{rt} collects public market states and technical constraints. The set $\mathcal{B}_i(\cdot)$ includes the energy bid bands, FCAS bid bands, power limits, state-of-charge restrictions, and the FCAS trapezium constraints described in Appendix B.13. Given the vector of submitted

[13]Appendix B.4 describes the provider mapping and the confidence classification.

stacks $\mathbf{b}_t = (\mathbf{b}_{it})_{i \in I_r}$, the market clearing engine maps bids and states into prices, dispatch, FCAS enablement, and current-period profits.

Let $\{\theta_{r\tau}\}_{\tau \geq t}$ denote the regional scarcity process. The current realisation θ_{rt} summarises contemporaneous tightness of the regional stack, while the future path $(\theta_{r,t+1}, \theta_{r,t+2}, \ldots)$ determines the continuation value of stored energy. Provider k observes an information set $\mathcal{I}_{krt}$, including public information and provider-specific forecasts. We write $m_{krt} := \mathbb{E}[\theta_{rt} \mid \mathcal{I}_{krt}]$ as shorthand for the provider's current-scarcity assessment. The same information set also induces beliefs over future scarcity, which enter continuation values below.

We now discuss how this conditioning on the provider-determined information set leads to co-movement due to a "responsive pricing" (or "responsive bidding") effect (Calder-Wang and Kim, 2026). That is, same-provider batteries will show co-movement even if the provider's algorithm maximises battery-owner profits.

Owner-level responsive autobidding. Let Π_{ot} denote owner o's current plus continuation payoff, including current energy and FCAS profits and the continuation value of stored energy after dispatch. Let $\mathcal{I}_{ot}$ denote the information available to the owner's portfolio, including the provider information sets for the owner's batteries, and let $\mathbb{E}_{ot}$ denote expectation under the owner's beliefs over scarcity and rival bid strategies.[14] Then owner-level responsive bidding solves

$$\mathbf{b}_{ot}^R \in \arg \max_{\mathbf{b}_o \in \mathcal{B}_o(S_t, X_{rt})} \mathbb{E}_{ot}[\Pi_{ot}(\mathbf{b}_o, \mathbf{b}_{-o,t}; S_t, X_{rt}, \{\theta_{r\tau}\}_{\tau \geq t}) \mid \mathcal{I}_{ot}] \,. \tag{1}$$

Here $\mathcal{B}_o$ is the product of the feasible bid-stack sets for the owner's batteries, and $\mathbf{b}_{-o,t}$ is shorthand for the rival stacks induced by the owner's beliefs about rival bidding rules. Note that equation (1) is not an equilibrium characterisation, but simply states that common software may change information, forecasts, and implementation, but it should not change which profits are maximised.

The responsive channel then follows from the dynamic opportunity cost of discharge. A higher provider scarcity assessment raises the expected continuation value of stored energy. Since raising the offer price reduces the probability or extent of current dispatch, the owner-level bid rule increases in the provider's scarcity assessment:

$$\frac{\partial b_i^R}{\partial m_{k_i,rt}} > 0. \tag{2}$$

The result is formally derived in Lemma 1 in Appendix A. Assuming monotone storage value and scarcity posterior (Assumptions 1–2), the provider's posterior shadow cost of discharge is weakly increasing in the scarcity assessment m_{krt}, and the local first-order condition then yields $\partial b_i^R / \partial m_{krt} > 0$.

However, this gives rise to co-movement among same-provider batteries. Linearizing the responsive bid around the observed state gives

$$b_{it}^R \approx \bar{b}_{it} + \psi_i(S_{it}, X_{rt}) + \phi_{it} m_{k_i,rt}, \qquad \phi_{it} := \frac{\partial b_i^R}{\partial m_{k_i,rt}} > 0. \tag{3}$$

[14] Equivalently, one could write an owner strategy $\sigma_o : \mathcal{I}_{ot} \to \mathcal{B}_o(S_t, X_{rt})$ and an expectation $\mathbb{E}_{\mu_{ot}, \sigma_{-o}}[\cdot]$ under owner o's beliefs μ_{ot} and rival strategies σ_{-o}. We keep this notation implicit because the empirical test only uses the resulting no-profitable-deviation restrictions.

For two batteries i and j using the same provider k, conditional on public controls, both bids load on the same provider-level object m_{krt}. Batteries using different providers load on different provider-level objects. Same-provider co-movement is therefore stronger whenever provider forecasts, preprocessing, or implementation rules create variation shared within provider but not across providers. This mechanism generates synchronised and state-contingent bids without any same-provider profit internalisation.

Concentration effects of third-party providers. This same co-movement effect also leads to the market outcome becoming a function of the degree of concentration among third-party providers. We develop a simple static equilibrium benchmark, in the spirit of Harrington and Ortner (2025), to formally prove this point. Appendix A solves an affine provider-posterior equilibrium whose aggregate response to a common scarcity signal is governed by a strategic concentration index $\Lambda(x)$ that depends on the vector of provider shares $x = (x_1, \ldots, x_K)$, the correlation across provider scarcity assessments, an own-action slope, and a strategic-complementarity coefficient (equation (27) in the appendix). Importantly, the aggregate response is increasing in $\Lambda(x)$ and $\Lambda(x)$ is Schur-convex in provider shares, so concentrating MW on fewer providers makes the common scarcity component more pronounced. Formally, Proposition 2 in the appendix shows for the affine static equilibrium that under any majorization-increasing (concentration-increasing) change in the provider-share vector x, (i) the unconditional mean action α_t is invariant, (ii) the common-response coefficient $\mathcal{S}_t$ is weakly increasing, and (iii) both the common component of aggregate variance $\rho_t \mathcal{V}_t \mathcal{S}_t^2$ and total variance $\operatorname{Var}(A_t)$ weakly increase, strictly along a dominant-provider family.

Figure 3 illustrates this logic using one scarcity path under three provider structures and the simple affine equilibrium structure developed in Appendix A. It depicts the response to a mean-zero scarcity path with a monopoly provider and three or ten symmetric providers, respectively. Because same-provider batteries condition on the same posterior, their bids co-move; as more capacity is attached to the same posterior, the aggregate response becomes steeper. This leads to stronger conditional response to common scarcity information and thus (relatively) higher bids during scarce periods and (relatively) lower bids during periods with abundance.

This also implies that concentration can have consumer-welfare implications even in the absence of coordinated conduct. Although the mean clearing price is unchanged when concentration rises, the second moments of prices are affected. Proposition 3 in Appendix A.3 proves this formally by decomposing the expected consumer loss into two channels. The first is a state-amplification channel. This channel arises as long as consumer demand co-moves with scarcity so that higher scarcity states also imply higher consumer demand. Because concentration makes the market price track the common scarcity state more closely, consumers pay a higher price precisely in the scarcer states when they consume more. The second is a price-variance channel. Concentration raises the variance of the clearing price, and in particular its common cross-provider component. This lowers welfare under a risk-averse consumer welfare standard. Both channels are weakly increasing under concentration-increasing changes in provider shares. Moreover, the variance channel can be expressed as the direct counterpart of the cross-seller price-correlation channel in Aleksenko and Miklós-Thal (2026): concentration shifts variance from diversifying cross-provider dispersion into a single common component.

Figure 3: Response to a common scarcity path under three provider structures

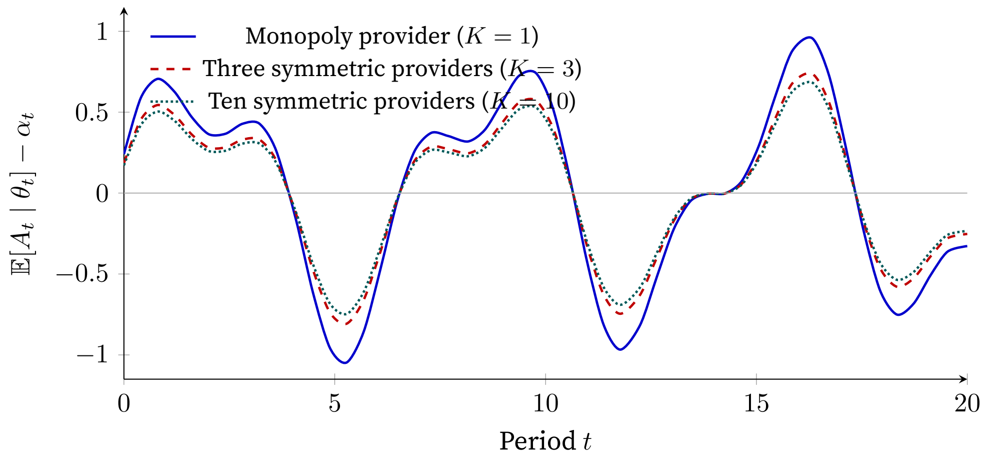

Notes: Simulated in the static affine equilibrium of Appendix A, for a monopoly provider and three or ten symmetric providers facing an identical scarcity path. The unconditional mean action α_t is fixed across cases.

Coordinated, same-provider conduct. The preceding steps show that responsive autobidding can lead to bids conditioning on common scarcity, same-provider batteries co-moving, the price effect of common responses increasing when provider capacity is concentrated, and a reduction in consumer welfare as provider concentration rises. But these patterns arise even when providers maximise owners' profits rather than joint profits across the fleet of batteries that use their software.

The conduct distinction we now consider is an objective-function restriction, not an additional implication of the stylised model. For a feasible unilateral deviation d from battery i's observed stack, that is, a reallocation of offered MW across the battery's price bands, let $\Delta\Pi_{o_i,t}(d)$ be the owner's deviation gain, a scalar dollar amount, and let $\Delta\Pi_{k_i,-o_i,t}(d)$ be the corresponding profit effect on same-provider batteries owned by other firms. Owner-level responsive optimisation requires the first inequality below; same-provider conduct with conduct parameter $\lambda \in [0, 1]$ replaces it with the second:[15]

$$\mathbb{E}_{it}[\Delta\Pi_{o_i,t}(d) \mid Z_{it}] \leq 0, \qquad \mathbb{E}_{it}[\Delta\Pi_{o_i,t}(d) + \lambda\Delta\Pi_{k_i,-o_i,t}(d) \mid Z_{it}] \leq 0. \tag{4}$$

The case $\lambda = 0$ is owner-level responsive optimisation. Positive λ means that the observed stack behaves as if the decision-maker internalises part of the profit effect on same-provider, different-owner batteries. The empirical conduct test therefore asks whether owner-level inequalities fail, and whether those failures are systematically reduced when same-provider profit effects are added.

Consider the focal owner o and a same-provider battery owned by a different firm, and a

[15]This is the analogue of the conduct-matrix step in Calder-Wang and Kim (2026): conduct assumptions determine which units' profit effects enter the no-deviation condition. Here each recleared deviation produces the two relevant entries, own-profit and same-provider, different-owner profit effects, and λ selects the linear combination. In our setting those entries are generated by exact reclearing of bid-stack deviations rather than by a product-demand model.

marginal change that moves ϵ MW of the focal's withheld capacity into the clearing band. Let

$$g_o := \left.\frac{\partial \Delta\Pi_{o_i,t}}{\partial \epsilon}\right|_{\epsilon=0}, \qquad g_k := \left.\frac{\partial \Delta\Pi_{k_i,-o_i,t}}{\partial \epsilon}\right|_{\epsilon=0}$$

denote the marginal effect of the change on the owner's own profit and on the same-provider peer. The change raises the focal owner's dispatch at a price above its opportunity cost, so $g_o > 0$. The same change lowers the regional price, so the peer loses inframarginal revenue, $g_k = -\zeta q_k < 0$, with $\zeta := -\partial P/\partial\epsilon > 0$ the price impact and q_k the peer's dispatch.

Under owner-level conduct the observed stack is not optimal, because $g_o > 0$ leaves a profitable deviation untaken and violates the first inequality in (4). Under same-provider conduct it is optimal once the weighted peer loss offsets the own gain,

$$g_o + \lambda g_k \le 0, \qquad \text{that is,} \qquad \lambda \ge \lambda^\star := \frac{g_o}{\zeta q_k}.$$

Observed restraint in dispatch therefore reveals $\lambda \ge \lambda^\star$, and the conduct test then recovers the smallest such λ across the sampled deviations. The threshold $\lambda^\star$ decreases in the same-provider peer's dispatch q_k, which rises with provider concentration, so the same restraint is rationalised by a smaller λ where same-provider capacity is more concentrated.

The empirical analysis in Section 3 proceeds in three steps. First, we use the ERI reform to study synchronisation and state-responsive bidding. Second, we estimate a rolling Bellman value function for stored energy that estimates the dynamic opportunity cost of bid-stack changes. Third, we construct a panel of bid stack deviations and use counterfactual reclearing of the resulting profit changes to test the owner-level and same-provider no-deviation inequalities.

3. Empirical Application

3.1. Data and Measurement

We build the empirical analysis from a battery-by-5-minute panel. The unit of observation is a battery i in dispatch interval t, and the panel covers April 1, 2025 through February 28, 2026.[16] It combines AEMO market data with two objects that are not recorded directly in the market files: the hand-built mapping from batteries to autobidder providers and a reconstructed asset-level state-of-charge series. Section 2 describes the institutional details of battery bidding in the NEM.

From AEMO, we observe the market primitives needed to reconstruct submitted and realised behaviour: bid prices and quantities, SCADA dispatch and charging, regional clearing prices, battery registration and capacity information, and post-ERI battery energy-storage fields. We then attach provider identity at the battery level using the mapping described in Appendix B.4. Analyses that require provider identity use the subset of batteries with a reliable provider assignment;

[16] We exclude six trading days from all analyses: 2025-06-11, 2025-06-12, 2025-06-18, 2025-06-26, 2025-07-02, and 2026-01-26. These are the days in the panel window with at least 300 interval-region observations whose regional reference price exceeds $1,000/MWh. The $1,000/MWh threshold sits well above the routine market regime (the 99th percentile of regional reference prices in the sample is approximately $311/MWh) and isolates sustained administered-price scarcity events whose squared-violation contribution would otherwise dominate the moment-inequality test. The exclusion removes about 1.7 percent of the panel.

Table 1: Analysis panel: information sources and sample

Information	Source	Construction
Battery units and capacities	AEMO/NEMOSIS registration data	Battery mapping and technical characteristics.
Bid quantities	AEMO MMS via NEMOSIS	Latest five-minute energy bid quantities.
Bid prices	AEMO MMS via NEMOSIS	Daily price bands matched to bid quantities.
Clearing prices	AEMO MMS via NEMOSIS	Regional five-minute clearing prices.
Dispatch	AEMO MMS via NEMOSIS	Charging, discharging, and net dispatch.
State of Charge	AEMO MMS via NEMOSIS + calibrated model	Public SoC plus reconstructed SoC.
Autobidding providers	Hand-built mapping from public sources	Provider identity and mapping confidence.
Panel summary		
Battery-by-five-minute observations		4,121,035
Batteries		52
Trading days		328
Time frame		April 1, 2025-February 28, 2026

analyses that only require bids, dispatch, prices, and state of charge use the full panel. Table 1 summarises the information in the panel and the source of each object.

The identification of software providers is based on public sources. For example, in some investor-relations documents of the software vendors, the filings list contracted deployments. In other cases, the owners have made public statements naming the provider. We further make use of combinations of known hardware-software-bundles. Of the 52 usable batteries in the panel, 42 can be linked to an autobidder provider.[17] These known-provider batteries account for 6.64 GW of discharge capacity and are served by 11 providers across 21 provider-region combinations. The two largest commercial providers are Tesla Autobidder, with 14 batteries and 2.32 GW, and Fluence Mosaic, with 10 batteries and 2.19 GW. Together they account for about two thirds of the known-provider capacity.

Provider concentration also varies substantially across regions. Among known-provider batteries, NSW1 has 11 batteries across 5 providers and a provider HHI of $4{,}620$ points, with Fluence the largest provider (63 percent). QLD1 has 10 batteries across 4 providers and an HHI of $4{,}180$, with Tesla the largest (59 percent). VIC1 is similarly concentrated, with 12 batteries across 5 providers and an HHI of $4{,}140$, again with Tesla the largest (57 percent). SA1 is more fragmented: 9 batteries across 7 providers and an HHI of $2{,}010$, with AGL in-house the largest (29 percent). This regional variation matters because the provider concentration relevant for bidding and prices is local to the dispatch region and the clearing interval, not only a national fleet share.

Beginning on July 1, 2025, AEMO expanded public reserve information by releasing additional battery and generator energy-state information, including the previous trading day's battery energy availability, regional daily energy limits, and regional battery state of charge. This disclosure reform is the Enhanced Reserve Information reform (ERI). For our purposes, ERI is an information-set

[17] In the appendix, we distinguish between confirmed and probable provider assignments based on the source. Note also that we cannot observe changes in the provider used over time.

change for batteries. Before ERI, market participants could observe prices, dispatch, and bids, but rival battery energy positions had to be inferred from market data. After ERI, aggregate battery energy-state information became part of the public market data. We use this change as a shock to the precision of the public signal about battery, and therefore market, scarcity.

Interpreting battery behaviour requires an estimate of each battery's current state of charge. State of charge is central for the analysis because it is the dynamic state that links current bidding to future opportunity cost. A battery with little stored energy has a high cost of additional discharge; a battery with ample stored energy can discharge at lower opportunity cost or preserve energy for later high-price intervals. However, asset-level SoC is not observed before ERI. We therefore reconstruct it from the physical stock-flow law that governs a battery, using the observed SCADA charge and discharge quantities as flows into and out of storage. Recovering battery operating characteristics such as round-trip efficiency from public NEM SCADA data has been done before in Karimi-Arpanahi et al. (2024). Let S_{it} denote stored energy, r_{it} charging MW, q_{it} discharging MW, and $\Delta = 1/12$ hours. For each battery we propagate[18]

$$S_{i,t+1} = \mathrm{clip}\left(\rho_i S_{it} + \eta_i^{\mathrm{ch}} r_{it}\Delta - \frac{q_{it}\Delta}{\eta_i^{\mathrm{dis}}} - \kappa_i\Delta,\ 0,\ \bar{S}_i\right), \tag{5}$$

where $\bar{S}_i$ is energy capacity, η_i^{ch} and η_i^{dis} are charge and discharge efficiencies, ρ_i is a self-discharge factor, κ_i captures auxiliary load, and the clipping operator enforces the physical storage bounds.

The calibrated model fits the public post-ERI storage data closely. In the unanchored validation exercise, which mimics a pre-ERI backcast, the median battery has a Pearson correlation of 0.956 with the public SoC series, an R^2 of 0.910, and an RMSE of 7.2 percent of energy capacity. In a separate multi-month holdout propagation, the median correlation is 0.979 and the median RMSE is 6.9 percent of capacity. Appendix B.5 describes the calibration and validation procedure, and Table B13 reports the full distribution of fit statistics.

All empirical SoC variables are built from this single reconstructed series.[19] Own SoC is the battery's reconstructed stored-energy share. Common battery scarcity is measured as one minus the regional battery SoC share, using public SoC where it is available and reconstructed SoC otherwise. We standardise this common-state measure within region-by-trading-period groups using the pre-ERI window. The common-state regressions below therefore compare how bids load on the same regional scarcity state before and after the disclosure reform, while the own-SoC regressions use the battery's private dynamic state.

3.2. Synchronisation and State-Responsive Bidding

We use ERI to study how a common information shock changes bid construction across batteries using the same autobidding provider. The stylised model in Section 2.2 implies that common software routines can make same-provider batteries move together, especially when those batteries

[18]The recursion allows battery-specific charge and discharge efficiencies, self-discharge, and auxiliary load, and clips the state to the physical interval $[0, \bar{S}_i]$. We calibrate these parameters separately by battery using the post-ERI public energy-storage fields, excluding the first week of public observations to reduce sensitivity to initial conditions.

[19]Before July 1, 2025, the series is the model propagation in (5), initialised at half of the asset's energy capacity because no public anchor exists. After ERI, the same model is re-anchored each day to the most recent public battery energy-storage field and then propagated forward with observed charge and discharge. This prevents mechanical drift while preserving the publication lag in public energy-state information.

operate in the same local market and face the same scarcity state. This subsection presents two pieces of evidence. The first is pairwise bid synchronisation. The second is that after ERI same-provider bids condition more strongly on the public common scarcity state, consistent with the disclosure improving the precision of the signal that a provider's algorithm maps into bids. A companion check that bids also load more on each battery's own dynamic state is reported in Appendix B.2.

For each battery pair (i, j), trading day s, and market family

$$f \in \{\text{energy discharge}, \text{ energy charge}, \text{ raise FCAS}, \text{ lower FCAS}\},$$

we compute, for each bid-stack outcome $Y \in \{\text{bid-band index}, \text{ rebid indicator}\}$ (as defined in Table 2), the raw within-day correlation

$$\rho_{ijs}^{Y,f} = \mathrm{corr}_{t \in s}(Y_{it}, Y_{jt}),$$

using the 5-minute intervals in which both batteries have the outcome observed. We then classify pairs into four groups: same provider and same region (SPSR), same provider and different region (SPDR), different provider and same region (DPSR), and different provider and different region (DPDR). Let $\bar{\rho}_{gs}^{Y,f}$ denote the average pair-day correlation for pair type g on day s. Separately for each market family and outcome, we estimate group-by-day difference-in-differences regressions of the form

$$\bar{\rho}_{gs}^{Y,f} = \alpha_g + \gamma_s + \sum_{c \in \{\text{SPSR,SPDR,DPSR}\}} \theta_c \, \mathbb{1}\{g = c\} \mathrm{Post}_s + \varepsilon_{gs}, \tag{6}$$

where $\mathbb{1}\{\cdot\}$ is the indicator function, α_g are pair-type fixed effects, and γ_s are trading-date fixed effects. DPDR is the omitted group. Our coefficient of interest is $\theta_{\text{SPSR}} - \theta_{\text{SPDR}}$. Same-provider batteries in different regions (SPDR) should co-move only through provider-wide channels such as a shared algorithm, common forecasts, or synchronised update routines, because they face different local scarcity states which should cause them to set different bid levels and show different rebid timing. Same-provider batteries in the same region (SPSR) on the other hand share the same local state. The difference $\theta_{\text{SPSR}} - \theta_{\text{SPDR}}$ therefore nets out the provider-wide component and isolates the extra synchronisation that arises when same-provider batteries respond to the same local scarcity.

Table 2 shows the main pattern for energy-discharge offers. Panel A uses the bid-band index, a quantity-weighted measure of where the battery places its offered MW in the ten bid bands. Same-provider batteries in the same region become more synchronised relative to same-provider batteries in different regions: the SPSR–SPDR gap rises by 0.045 after ERI. Panel B shows a related but distinct pattern for rebid timing. Rebid timing is already correlated for same-provider batteries in different regions, and rises from 0.196 to 0.252 for SPDR pairs after ERI. It rises more for SPSR pairs, from 0.216 to 0.354, producing a relative increase of 0.081. Thus, bid-update timing has a provider-wide component, while the bid-stack level itself becomes most synchronised when same-provider batteries operate in the same local market.

Table 3 reports the same SPSR-minus-SPDR estimate across market families and bid-stack outcomes. For energy discharge, the effect is largest in upper bid prices, with an estimate of 0.147;

Table 2: Energy-discharge synchronisation before and after ERI

Panel A: Energy-discharge bid-band index				
	Mean daily raw correlation			
Pair type	Pre-ERI	Post-ERI	Difference	Regression
Same provider, same region (SPSR)	0.369	0.371	$+0.002$	$+0.039^{***}$
				(0.014)
Same provider, different region (SPDR)	0.221	0.178	-0.043	-0.006
				(0.009)
Different provider, same region (DPSR)	0.271	0.226	-0.045	-0.008
				(0.007)
Different provider, different region (DPDR)	0.217	0.180	-0.037	omitted
$\theta_{\mathrm{SPSR}} - \theta_{\mathrm{SPDR}}$ (SPSR − SPDR)			$+0.045$	$+0.045^{***}$
				(0.015)
Panel B: Energy rebid timing				
	Mean daily raw correlation			
Pair type	Pre-ERI	Post-ERI	Difference	Regression
Same provider, same region (SPSR)	0.216	0.354	$+0.138$	$+0.153^{***}$
				(0.017)
Same provider, different region (SPDR)	0.196	0.252	$+0.057$	$+0.072^{***}$
				(0.018)
Different provider, same region (DPSR)	0.044	0.035	-0.010	$+0.006$
				(0.004)
Different provider, different region (DPDR)	0.050	0.035	-0.015	omitted
$\theta_{\mathrm{SPSR}} - \theta_{\mathrm{SPDR}}$ (SPSR − SPDR)			$+0.081$	$+0.081^{***}$
				(0.017)
Pair-type FE				Yes
Trading-date FE				Yes
N (group × day)				1,336
Trading dates				334

Notes: Entries are raw Pearson correlations, not Fisher-transformed correlations. For each battery pair and trading date, we compute the within-day correlation of the listed outcome across 5-minute intervals. Pre/post columns are simple averages of daily pair-type means. The Regression column reports $\hat{\theta}_g$ from (6); standard errors, in parentheses, are clustered by trading date. The bottom row in each panel reports the Wald test for $\theta_{\mathrm{SPSR}} - \theta_{\mathrm{SPDR}}$. $^{***}p < 0.01$, $^{**}p < 0.05$, $^{*}p < 0.10$.

Table 3: Synchronization effects across market families

Market family	Bid-band index	Upper-band price	Lower-band price	Rebid timing
Energy discharge	$+0.045^{***}$ (0.015)	$+0.147^{***}$ (0.030)	+0.051 (0.045)	$+0.081^{***}$ (0.017)
Energy charge	$+0.085^{***}$ (0.016)	+0.087 (0.070)	$+0.091^{***}$ (0.025)	$+0.081^{***}$ (0.017)
Raise FCAS	$+0.151^{***}$ (0.019)	$+0.081^{***}$ (0.021)	$+0.107^{***}$ (0.022)	$+0.087^{***}$ (0.027)
Lower FCAS	$+0.224^{***}$ (0.017)	$+0.295^{***}$ (0.021)	$+0.092^{***}$ (0.020)	$+0.072^{***}$ (0.027)

Notes: Entries report the SPSR–SPDR DiD coefficient from group-by-day regressions of raw within-day pairwise correlations. For each pair, trading date, market family, and outcome, we compute the Pearson correlation across 5-minute intervals in which both batteries have the outcome observed. Regressions include pair-type and trading-date fixed effects; standard errors, in parentheses, are clustered by trading date. Table 2 reports the detailed pre/post correlations for the two main energy-discharge outcomes; Appendix Table B1 reports the corresponding detail for the other market families. The maximum number of trading dates is 334. $^{***}p < 0.01$, $^{**}p < 0.05$, $^{*}p < 0.10$.

lower-band prices do not show a comparable effect. In energy charge, synchronisation rises in the bid-band index and lower-band prices. In FCAS markets, the effects are larger across the bid stack: the bid-band-index effect is 0.151 for raise FCAS and 0.224 for lower FCAS. Rebid-timing synchronisation is positive in every market family, with estimates between 0.072 and 0.087. This relative effect combines two patterns. In energy, same-provider different-region timing rises after ERI, consistent with provider-wide bid-update routines. In FCAS, the SPDR timing correlation is already high before ERI and changes little after the reform. Appendix Table B1 reports the corresponding pre/post correlations outside energy discharge.

The same reform also increases how strongly bids condition on the common scarcity state. We measure regional battery scarcity as one minus the regional state-of-charge share, split it into a tight and a loose component, and estimate how strongly quantity-weighted discharge bids load on the tight relative to the loose state before and after ERI, separately by evening window; Appendix B.2 gives the specification. Table 4 reports the result. In the upper discharge bands, which govern withholding, the post-ERI tight-minus-loose loading rises by $1{,}136$ AUD/MWh in the early-peak window and by a comparable amount in the lead-in window, while the lower bands, which secure baseline dispatch, show no such shift. The effect is concentrated in the lead-in and early-peak windows with the later windows showing no stable common-state response. Same-provider bids thus track the common scarcity signal more closely once that signal becomes more precise, rising in the upper bands during scarce intervals and easing during abundant ones, exactly the responsive-bidding channel of Section 2.2. A similar specification shows that bids also load more strongly on each battery's own reconstructed state of charge after ERI (Appendix B.2).

Table 4: Common-state responsiveness by evening window

Window	Upper bands	Lower bands	All bands
Lead-in	1,515* (819)	-33 (75)	792 (826)
Early peak	1,136*** (368)	-11 (22)	516 (479)
Late peak	-1,587 (1,077)	121* (62)	-3 (698)
Post-peak	324 (1,199)	106 (78)	1,230 (1,193)

Notes: Entries are post-ERI average changes in the tight-minus-loose loading of bid prices on the public regional scarcity signal. Each row is estimated in a separate regression restricted to the indicated trading-period window. Outcomes are quantity-weighted energy-discharge price bands. All specifications include battery fixed effects, region-by-date fixed effects, region-by-period fixed effects, and own-SoC event-study controls. Standard errors, in parentheses, are two-way clustered by battery and trading date. $^{***}p < 0.01$, $^{**}p < 0.05$, $^{*}p < 0.10$.

We next relate this common-provider bid behaviour to provider concentration. The synchronisation results show that autobidding providers induce co-movement in bid construction, especially when same-provider batteries face the same local market conditions. The model suggests that this channel should be more important when provider capacity is concentrated in the relevant market.

We begin with a regional concentration measure. For each region, we compute the installed provider HHI using battery capacity shares among known autobidder providers. We then form a region-day panel with two outcomes. Local synchronisation is the same-region SPSR correlation minus the same-region DPSR correlation. Market-action variance measures how much the region's bids move over the day: for each 5-minute interval we compute the offer-weighted average upper-band bid price across the region's batteries, and take the variance of this regional average across the intervals of the trading day.

Table 5: Provider concentration, bid synchronisation, and market-action variance

	(1)	(2)	(3)	(4)
	Synchronisation		Market-action variance	
	Local SPSR − DPSR	SPSR correlation	on local sync	on provider HHI
Provider HHI (10 p.p.)	+0.161***	+0.169***		+1.084***
	(0.021)	(0.018)		(0.378)
Local sync			+0.183	
			(0.882)	
Unit	Region day	Region day	Region day	Region day
Region FE	No	No	No	No
Date FE	Yes	Yes	Yes	Yes
N	738	738	738	738

Notes: The outcome is the upper-band energy-discharge price. Provider HHI is the installed capacity-share HHI across known autobidder providers, scaled so one unit equals a ten percentage point HHI increase. Local sync is SPSR minus DPSR mean pairwise correlation within region. Market-action variance is the within-day variance of the offer-weighted regional average bid price, reported in millions of squared AUD/MWh. Installed HHI is fixed within region, so specifications include date fixed effects but not region fixed effects. Columns (1)–(2) are weighted by SPSR pair-days; columns (3)–(4) by market intervals. Standard errors are clustered by trading date. $^{***}p < 0.01$, $^{**}p < 0.05$, $^{*}p < 0.10$.

Table 5 reports the reduced-form link for upper-band energy-discharge prices. A ten percentage point increase in installed provider HHI is associated with a 0.161 increase in the local synchronisation premium and a 0.169 increase in SPSR synchronisation. The same increase in HHI is also associated with a larger within-day variance of the regional average upper-band bid price. Appendix Table B2 repeats the same upper-band-price exercise across market families. The positive relationship between provider HHI and synchronisation is concentrated in energy discharge, while the relationship between provider HHI and bid-price variance is broader and is also present in FCAS. However, these estimates are descriptive: installed provider HHI is effectively cross-sectional, so the specifications include trading-date fixed effects but not region fixed effects. The result can therefore not be considered a causal estimate of the effect of provider concentration, but the signs and magnitudes are in line with the mechanism in Section 2.2. Regions with more concentrated providers show both more same-provider synchronisation and more within-day variance of the regional average bid price.

3.3. Dynamic Value of Stored Energy

The synchronisation evidence in Section 3.2 shows that common providers produce co-movement in bid construction, and Table 5 relates that co-movement to provider concentration. The conduct test in Section 3.4 asks whether the observed bids can be rationalised by owner-level dynamic incentives, or whether they internalise same-provider, different-owner profit effects. To run that test we first need an estimate of the dynamic opportunity cost of moving battery energy between intervals. For each battery i we estimate a single-battery value function $V_{i,\tau}(S, x)$ that maps own state of charge S and a market state x into the continuation value of stored energy. The value function solves the Bellman recursion

$$V_{i,\tau}(S,x) = \max_{S' \in \Gamma_i(S)} \Big\{ \pi_i(S,S',x,\tau) + \delta\, \mathbb{E}\big[V_{i,\tau+1}(S',x') \,\big|\, x\big] \Big\}, \tag{7}$$

where π_i collects current energy and FCAS profits net of throughput cost, δ is the discount factor, $\Gamma_i(S)$ enforces the SoC bounds and ramp limits, and the expectation is taken under a transition kernel for the market state x that we estimate non-parametrically from the trailing data window. The market state aggregates four conditioning variables: the time-of-day block, the residual-price bin (price relative to the regional mean profile, discretised into $N_p = 11$ empirical-quantile bins), the regional residual-demand state, and an aggregate-SoC signal that captures whether the regional storage fleet enters the interval close to empty, mid-range, or close to full. Conditioning on these variables lets the continuation value reflect both intraday arbitrage (price within the day) and dynamic scarcity (how much regional storage is available).

To keep the value function estimation tractable, we assume a finite horizon of a single trading day from $\tau = 1$ (06:00) to T (22:00). We fix the terminal value at 22:00 as the expected revenue from any remaining stored energy if it were discharged at 22:00 at the average overnight price of a 90-day trailing-window. Because overnight prices are stable and low relative to the daytime peak, and vary little over the 90-day period, this terminal value is small and is nearly the same across states, so the shadow values we use during the evening peak depend little on this estimated terminal value. The assumption of a finite horizon is important, as it allows us to avoid any infinite-horizon solve. π_i then co-optimises energy and FCAS using a hierarchical estimate of the FCAS headroom value (revenue per MWh of physical headroom, varying with block, residual demand, and residual price), so that deviations that reallocate capacity between the energy and FCAS sides of the stack are priced consistently.

We then calculate the implied shadow value of stored energy $\widehat{m}_{it}$,

$$\widehat{m}_{it} := \frac{\max\big\{\partial V_{i,\tau}/\partial S,\, 0\big\}}{\eta_i^{\text{dis}}} + c_i, \tag{8}$$

which yields the per-MWh dynamic opportunity cost of discharge at interval t, with η_i^{dis} the discharge efficiency and c_i the throughput cost. The non-negativity floor reflects the option value of waiting.

The Bellman is re-estimated each week on a 90-day trailing window so the price profile, transition kernel, and FCAS headroom values can absorb seasonal variation in market conditions. Within each window we construct the regional mean price profile, the residual-price bin edges, the non-parametric transition matrix (with a hierarchical fallback chain across conditioning groups when within-group support is thin), the FCAS headroom-value coefficients, and the overnight terminal value. The DP is then solved by backward induction on a 41-point SoC grid with 201 candidate next-period SoC controls per interval, separately by signal and residual-demand state. Asset parameters (energy capacity, discharge and charge power limits, charge and discharge efficiencies, self-discharge, and a parasitic-drain decomposition) are calibrated from the same SoC reconstruction model as in Section 3.1. Appendix B.3 reports the full state-space specification, the FCAS headroom-value construction, the rolling-pipeline coverage, the asset/SoC calibration parameters, the shadow-value profile across time blocks and SoC bins, and transition, FCAS, and deviation-valuation diagnostics.

We then use our estimated Bellman values to determine profits under counterfactual market outcomes. To turn a bid-stack edit into a counterfactual market outcome we use the open-source NEMDE replication `nempy` (Prakash, 2022), which reproduces AEMO's regional dispatch optimisation from the same MMS-DB and NEMDE-XML inputs that AEMO uses at clearing time. For each 5-minute interval, `nempy` solves the constrained least-cost dispatch problem

$$\min_{u,v,f,F} \sum_{i,b} p_{ib}^{E,\mathrm{gen}} u_{ib} - \sum_{i,b} p_{ib}^{E,\mathrm{load}} v_{ib} + \sum_{i,j,b} p_{ib}^{F,j} f_{ib}^{j} + \Phi(\text{slacks}) \tag{9}$$

subject to per-region energy balance with inter-regional flow and losses, inter-regional transmission limits, raise- and lower-FCAS service requirements at the regional and global levels, unit-level ramp rates and availability, the FCAS trapezium constraints that couple energy operating points to enabled FCAS quantities (Appendix B.13), fast-start unit constraints, and AEMO's set of generic network and security constraints. Decision variables are energy generation bid acceptances u_{ib} (units i, price bands b), energy load bid acceptances v_{ib}, FCAS service enablements f_{ib}^{j} across the ten regulation and contingency services, and aggregate interconnector flows F. The slack penalties $\Phi(\cdot)$ replicate AEMO's constraint-violation pricing so that infeasibilities are resolved at AEMO's preference ordering rather than producing infeasible solves. Regional reference prices recover as Lagrange multipliers on the regional energy-balance constraints.

The `nempy` library has been validated against historical AEMO dispatch outcomes in Prakash (2022), which shows high accuracy in replicating market clearing results. We report an end-to-end replication check against AEMO's published regional reference prices on our own panel in Appendix B.6. We find a median absolute discrepancy of $\$0.05$/MWh. More than 97% of intervals are reproduced within $\$20$ of AEMO's published RRP.[20]

As a final validation, we construct a randomly selected panel of broad counterfactual bid-stack deviations. Each deviation modifies the focal battery's submitted stack while holding all other batteries' stacks fixed, and the cleared interval is recomputed using (9) including the FCAS co-optimisation. We consider three types of deviations, illustrated in Figure 4: within-market downward and upward reallocations across the bid bands of a single market (energy or FCAS), and cross-market reallocations between energy and FCAS. Based on observed usage patterns we simplify by considering deviations between three sections of the ten bid bands. Top bands 8–10 are used to park energy, middle bands 4–7 are used near the clearing price, and low bands 1–3 are used to ensure dispatch in most intervals. The deviations always shift between two of these three sections. Shift sizes are fixed shares of the relevant offered MW and are capped by the available MW in the source band. We then randomly select 800 candidate rows per deviation type. Appendix Table B9 lists the full set of deviations with their shift sizes.

Each recleared deviation produces effects in three channels. Let $\Delta\Pi_{itd}^{E}$ and $\Delta\Pi_{itd}^{F}$ denote the

[20] Replication degrades when RRP approaches the price cap. This is expected, as this represents extreme scarcity intervals during which AEMO's full constraint set is difficult to reproduce. These intervals however are not concentrated in the evening-peak windows the conduct test focuses on.

Figure 4: Schematic bid-stack deviations

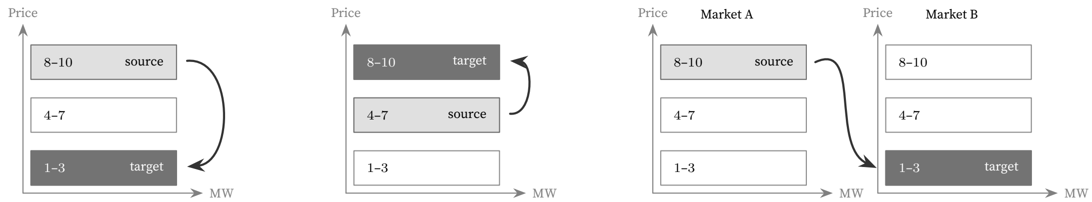

(a) Move down (b) Move up (c) Move across markets

Notes: Each panel uses three price-band groups: low bands 1–3, middle bands 4–7, and high bands 8–10. Light grey marks the source band from which quantity is removed; dark grey marks the target band into which the same quantity is added. Panel (a) illustrates within-market downward reallocations, Panel (b) illustrates within-market upward reallocations such as clearing-to-above withholding, and Panel (c) illustrates cross-market reallocations between energy and FCAS stacks.

changes in current energy and FCAS profit, and let

$$\Delta V_{itd} := \mathbb{E}\Big[V_{i,t+1}\big(S^{cf}_{i,t+1}, x'\big) \mid x_t\Big] - \mathbb{E}\big[V_{i,t+1}\big(S^{base}_{i,t+1}, x'\big) \mid x_t\big] \tag{10}$$

denote the change in continuation value induced by the deviation's effect on next-period state of charge, where $S^{cf}_{i,t+1}$ and $S^{base}_{i,t+1}$ are the recleared and observed next-period SoC and the expectation is taken under the same matrix that appears in (7). The focal owner's deviation gain on battery i at interval t is the sum of the three channels,

$$\Delta\Pi^{\text{own}}_{itd} := \Delta\Pi^{E}_{itd} + \Delta\Pi^{F}_{itd} + \Delta V_{itd}. \tag{11}$$

A battery-interval is incentive compatible if no sampled deviation yields a strictly positive own-profit gain. We report the share of battery-intervals with at least one deviation yielding a positive profit deviation gain above a given threshold ranging from \$1 to \$1,000 as a robustness check on Bellman measurement error.[21]

Table 6 reports the pre/post-ERI share of focal battery-intervals with at least one sampled deviation that increases profits relative to the observed bid stack by more than the listed threshold. We find that the shares of intervals with positive deviation gains post-ERI are below pre-ERI shares in every column of every deviation type. For example, for within energy deviations, we observe 21.7% of our sample with a \$1 difference in total profit (after accounting for the change in the continuation value) pre-ERI, which drops to 8.8% post-ERI. This is consistent with the reduced-form evidence that ERI led to better and more precise targeting of the underlying scarcity state and thus efficiency gains. We consistently observe that remaining profitable deviations are fewer but also, on average, economically smaller. The generally small differences that we find support the reliability of the Bellman estimation. If our Bellman values were imprecise, we should observe large deviation gains and many intervals with substantial differences between profit from observed bids and from the counterfactual deviation.

We now employ the state-of-charge calibration, Bellman value estimation, and validated re-clearing methodology to perform our conduct test.

[21] Appendix B.3 also reports the diagnostic under an alternative current-bin convention for ΔV_{itd}.

Table 6: Incentive-compatibility violations, pre/post-ERI, by deviation panel and dollar tolerance

			Share above			
Deviation family	Period	Intervals	\$1	\$10	\$100	\$1,000
Within energy	Pre-ERI	702	21.7%	17.4%	13.0%	10.8%
	Post-ERI	1,114	8.8%	3.7%	0.9%	0.3%
Within FCAS	Pre-ERI	388	19.1%	1.5%	0.3%	0.0%
	Post-ERI	853	6.0%	0.2%	0.0%	0.0%
Cross-market	Pre-ERI	1,035	23.8%	14.0%	6.0%	3.5%
	Post-ERI	1,506	10.2%	4.1%	1.3%	0.5%
Cross-FCAS	Pre-ERI	372	10.8%	0.5%	0.0%	0.0%
	Post-ERI	920	2.1%	0.0%	0.0%	0.0%

Notes: Pre/post-ERI share of battery-intervals in which at least one feasible sampled deviation yields a strictly positive own-profit gain exceeding the listed dollar tolerance. The own-profit gain combines the recleared change in current energy plus FCAS profit and the change in the Bellman continuation value, with continuation values evaluated under the kernel-expectation convention.

3.4. Conduct Test by Counterfactual Reclearing

We now turn to the conduct test itself. The starting point is the standard view of market power in uniform-price electricity auctions. In supply-function models, firms exercise market power by making their supply schedules less elastic or by offering less effective capacity near the clearing margin (Klemperer and Meyer, 1989; Vives, 2011; Holmberg, 2008). In repeated uniform-price auctions, collusive bidding similarly sustains high prices by weakening the incentive to expand supply, and deviations from a collusive arrangement are typically undercutting or output-expansion deviations that win more dispatch while rivals continue to bid less aggressively (Fabra, 2003). Storage adds an intertemporal layer: strategic storage owners internalise the price impact of when they buy and sell electricity, so market power can appear as smoothed or withheld discharge rather than purely as a static markup (Andrés-Cerezo and Fabra, 2023). This logic also arises with independent learning algorithms that can generate seemingly collusive battery decisions in a dynamic storage environment (Abada and Lambin, 2023). We therefore consider deviations that move part of the MW parked just above the regional clearing price down into the clearing band, thereby increasing the focal battery's dispatch and own profit while lowering the price and profits earned by other same-provider batteries in the region.

We formalise the test as follows. For a focal battery i in region r at interval t and a candidate deviation d, the reclearing engine returns, for every battery j in r, a change $\Delta\pi_{jtd}$ in current energy plus FCAS profit and a change ΔV_{jtd} in the continuation value of stored energy where each ΔV_{jtd} is obtained by applying j's Bellman value function from (7) to the next-period state of charge implied by j's recleared dispatch under d. For the focal $j = i$, $\Delta\pi_{itd} + \Delta V_{itd}$ coincides with the focal own-profit gain $\Delta\Pi^{\text{own}}_{itd} = \Delta\Pi^{E}_{itd} + \Delta\Pi^{F}_{itd} + \Delta V_{itd}$ defined in (11).

We then compute the focal owner's total deviation gain on its regional portfolio: i's own gain plus the gains on any other batteries the same firm operates in r,

$$\Delta\Pi_{o_i,t}(d) := \sum_{\substack{j:\, o_j = o_i \\ r_j = r_i}} \big[\Delta\pi_{jtd} + \Delta V_{jtd}\big]. \tag{12}$$

We also calculate the profit change for same-provider, different-owner batteries that share i's regional clearing, or

$$\Delta\Pi_{k_i,-o_i,t}(d) := \sum_{\substack{j:\, k_j=k_i,\, o_j\neq o_i \\ r_j=r_i}} \big[\Delta\pi_{jtd} + \Delta V_{jtd}\big]. \tag{13}$$

By construction, the deviations we consider can deliver positive $\Delta\Pi_{o_i,t}(d)$ – the focal owner gains by capturing additional dispatch at a price still above marginal cost – and negative $\Delta\Pi_{k_i,-o_i,t}(d)$ – same-provider peers see the recleared price fall and lose revenue on their inframarginal MW, and their stored energy depreciates in value at the lower realised price.

Under *owner-level* conduct ($\lambda = 0$), the observed bid is optimal at the focal owner's information set $\mathcal{I}_{ot}$ if no recleared deviation leaves a positive expected own-portfolio gain,

$$\mathbb{E}_{it}[\Delta\Pi_{o_i,t}(d) \mid Z_{it}] \leq 0 \quad \text{for every } d \text{ and every observable } Z_{it} \subseteq \mathcal{I}_{ot}. \tag{14}$$

Under *same-provider* conduct with weight $\lambda \in (0, 1]$, the bidder also values the recleared profit effect on same-provider peers,

$$\mathbb{E}_{it}[\Delta\Pi_{o_i,t}(d) + \lambda\, \Delta\Pi_{k_i,-o_i,t}(d) \mid Z_{it}] \leq 0 \quad \text{for every } d \text{ and every } Z_{it}. \tag{15}$$

Because $\Delta\Pi_{k_i,-o_i,t}(d)$ is typically negative on the deviations the test samples, a positive λ shrinks the left-hand side of (15): the bidder is rationalised in leaving a deviation on the table whenever the own-portfolio gain is more than offset by the recleared loss on same-provider peers, weighted by λ. Equivalently, a positive λ identifies bidding behaviour that looks like sub-optimal parking of high-band capacity unless the bidder is also pricing in the price-suppressing effect on same-provider peers.

To test these inequalities, we fix a candidate λ and calculate which observed deviations the corresponding hypothesis cannot rationalise. A deviation (i, t, d) contradicts hypothesis λ whenever its λ-weighted gain $\Delta\Pi_{o_i,t}(d) + \lambda\, \Delta\Pi_{k_i,-o_i,t}(d)$ is strictly positive – under that hypothesis the bidder would have left a positive expected payoff on the table by not deviating. Following Pakes et al. (2015), we accumulate the contradictions as follows

$$Q_n(\lambda) := \frac{1}{n} \sum_{(i,t,d)} w_{itd}\, \max\{\Delta\Pi_{o_i,t}(d) + \lambda\, \Delta\Pi_{k_i,-o_i,t}(d),\, 0\}^2, \tag{16}$$

where the sum is over the test panel described shortly and w_{itd} are stratification weights to ensure balance across coalitions and ERI periods. Deviations the hypothesis already rationalises contribute zero by construction, so $Q_n(\lambda)$ is also the squared dollar size of the contradictions left under hypothesis λ. The conduct estimator is the value of λ on $[0, 1]$ that minimises this contradiction count,

$$\widehat{\lambda} := \arg\min_{\lambda\in[0,1]} Q_n(\lambda), \tag{17}$$

and we report a 95% confidence set obtained by cluster subsampling at the (i, t) level (Romano and Shaikh, 2008), which respects the within-interval dependence between deviations drawn from the same focal battery. A value $\widehat{\lambda} = 0$ means that the owner-level hypothesis (14) already minimises the unrationalised contradictions and no positive λ improves on it. A value $\widehat{\lambda} > 0$ means that adding the same-provider spillover with weight $\widehat{\lambda}$ leaves fewer contradictions than $\lambda = 0$, and the magnitude of $\widehat{\lambda}$ measures how much of the spillover the observed bid behaves as if it internalises. In finite samples the minimiser can sit at a boundary even when the objective is nearly flat. We therefore treat $\widehat{\lambda} = 1$ as evidence of same-provider conduct only when the reduction in $Q_n(\widehat{\lambda})$ relative to $Q_n(0)$ is economically meaningful and the subsampling confidence set excludes zero.

We estimate the conduct parameter as a function of the focal provider's near-margin capacity share in the clearing interval. Let $s^{\text{prov}}_{k_i,r_i,t}$ denote provider k's share of near-margin battery MW in region r at interval t, defined as the MW within ± 1 price band of the clearing price operated by batteries served by k_i, divided by total near-margin battery MW in (r_i, t). This is a standard single-firm share but applied to the near-margin capacity of batteries only. Hence, this is not equivalent to the total market share which would need to account for competing capacity from gas, hydro, and other dispatchable plants. The per-interval near-margin share tracks the installed-capacity provider share reported in Section 3.1 on average: across the regions and providers in our sample, the median per-interval near-margin share lies within a few percentage points of the installed share, with per-interval dispersion that reflects which batteries are dispatchable at the margin in that interval (Appendix B.12). The near-margin window is the same concentration object measured at a finer (per-interval) resolution, not a separate measure. For each window centre s_0 on a grid in $[0.20, 0.85]$ we fit a local kernel-weighted version of (17),

$$\widehat{\lambda}(s_0) := \arg\min_{\lambda\in[0,1]} \sum_{(i,t,d)} K_h\left(s^{\text{prov}}_{k_i,r_i,t} - s_0\right)\, w_{itd}\, \max\{\Delta\Pi_{o_i,t}(d) + \lambda\,\Delta\Pi_{k_i,-o_i,t}(d),\, 0\}^2\,, \tag{18}$$

where K_h is a triangular kernel with bandwidth $h = 0.10$. Confidence sets are constructed by cluster subsampling at the (i, t) level as for the unweighted moment objective, with the same kernel weights applied inside each subsample draw. The estimator $\widehat{\lambda}(s_0)$ traces out a continuous profile of the conduct parameter across the identifying range of s^{prov} without committing to a discrete bin specification. Appendix B.8 reports the corresponding fit on 10-percentage-point s^{prov} bins as a complementary discrete view of the same estimand.

The test requires that the focal provider's near-margin set contain at least two distinct owners; otherwise the same-provider, different-owner partner set is empty and $\Delta\Pi_{k_i,-o_i,t}(d) \equiv 0$. We therefore restrict the sample to battery-intervals with $\text{HHI}^{\text{own}}_{k_i,r_i,t} < 1$, where $\text{HHI}^{\text{own}}_{k,r,t} = \sum_o (s^{\text{own}}_{o,k,r,t})^2$ is the Herfindahl index of owner shares inside the provider's near-margin set. We further restrict the deviation sample along three dimensions. First, we only keep focal batteries whose provider has at least one same-region battery operated by a different firm, so that the two-owner condition above can be met; in practice this confines the test to batteries served by the two largest commercial providers, 12 Tesla Autobidder batteries spanning NSW, QLD, SA, and VIC and 7 Fluence Mosaic batteries spanning NSW, QLD, and VIC. Second, we keep evening-peak intervals between 16:00 and 22:00 – the window in which Section 3.2 locates the ERI-driven upper-band responsiveness and in which regional prices are highest and most often set by batteries. Third, we drop intervals in which the focal battery offers no movable MW just above the clearing band, since we cannot construct a deviation for these intervals. For each interval we then construct nine deviations: three deviation sizes (10%, 25%, and 50% of the relevant offered MW) for each of three markets (energy, raise-FCAS, lower-FCAS). We retain only deviations that are feasible in the realised stack, meaning that the source band has movable MW and the bid-stack edit passes the reclearing-engine constraints. The final conduct-test panel consists of $49{,}481$ feasible deviations – $46{,}677$ in energy and $2{,}804$ in FCAS – over $15{,}882$ focal battery-intervals.

Figure 5: Conduct-test sample balance

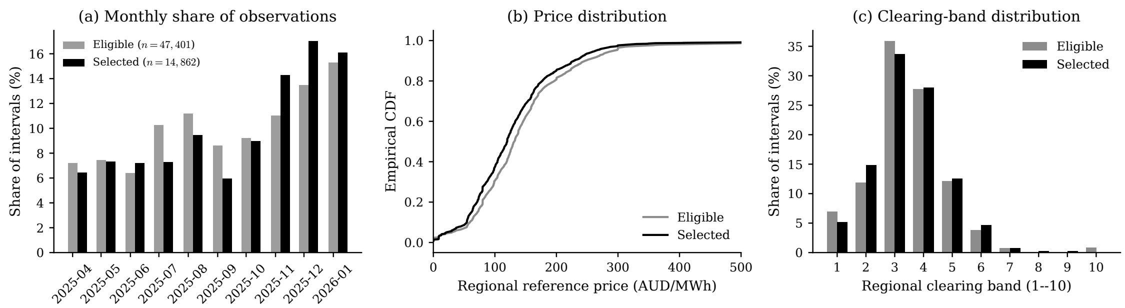

Notes: Comparison of the selected conduct-test panel with the eligible-but-not-selected evening-peak intervals. Panel (a): share of selected and eligible intervals by trading month. Panel (b): empirical CDF of the regional reference price, capped at $500/MWh for readability. Panel (c): share of intervals by regional clearing band.

Figure 5 compares the distribution of intervals over time, of regional reference prices, and of regional clearing-band placements between the deviation panel and the universe of eligible evening-peak intervals. The two distributions track each other closely on each dimension, so the panel is not selectively over-sampling outcome-relevant states within the test's identifying universe. Appendix B.7 reports the corresponding numerical balance table together with the full evening-peak set of all Tesla- and Fluence-managed battery-intervals for completeness.

Figure 6 shows the main results of the conduct test using the local kernel-weighted estimator (18) as a function of the focal-provider share on the deviation panel. The top row shows the point estimate $\widehat{\lambda}(s_0)$ at each window centre s_0 and the 95% cluster-subsampling confidence set. The bottom row plots the corresponding Q-reduction $1 - Q_n(\widehat{\lambda})/Q_n(0)$, measuring the share of the unrationalised deviation evidence at $\lambda = 0$ that the conduct hypothesis at $\widehat{\lambda}$ accounts for. Appendix Figure B1 shows the underlying $Q_n(\lambda)/Q_n(0)$ curves on the discrete share-band view, together with the FCAS panels, which we omit here. The same estimator applied to FCAS deviations finds no evidence of joint profit maximisation. However, this is because FCAS accounts for about 0.1% of these batteries' revenue in the evening peak, and enabled capacity clears at a median of well under one cent per MW per interval, so an equivalent deviation in the FCAS stack moves peer profits by almost nothing – the total same-provider spillover across all $2{,}804$ FCAS deviations is under $\$5$, compared to $\$559{,}000$ in energy discharge. Thus, the conduct signal is present where the spillover is large and absent where it is near-zero, which is the same dose-response pattern that produces the concentration threshold.

For both Tesla Autobidder and Fluence Mosaic, $\widehat{\lambda}$ is above 0.75 and mostly at the corner $\widehat{\lambda} = 1$ for provider shares between 20% and 70%. The estimates are informative where accounting for the profit change in same-provider, different-owner batteries meaningfully reduces Q_n, which holds for provider shares of roughly 30–70% for both providers. The 95% subsampling confidence sets exclude the owner-only null across this range. Outside this range the estimates are uninformative,

Figure 6: Conduct parameter $\widehat{\lambda}$ with 95% confidence set

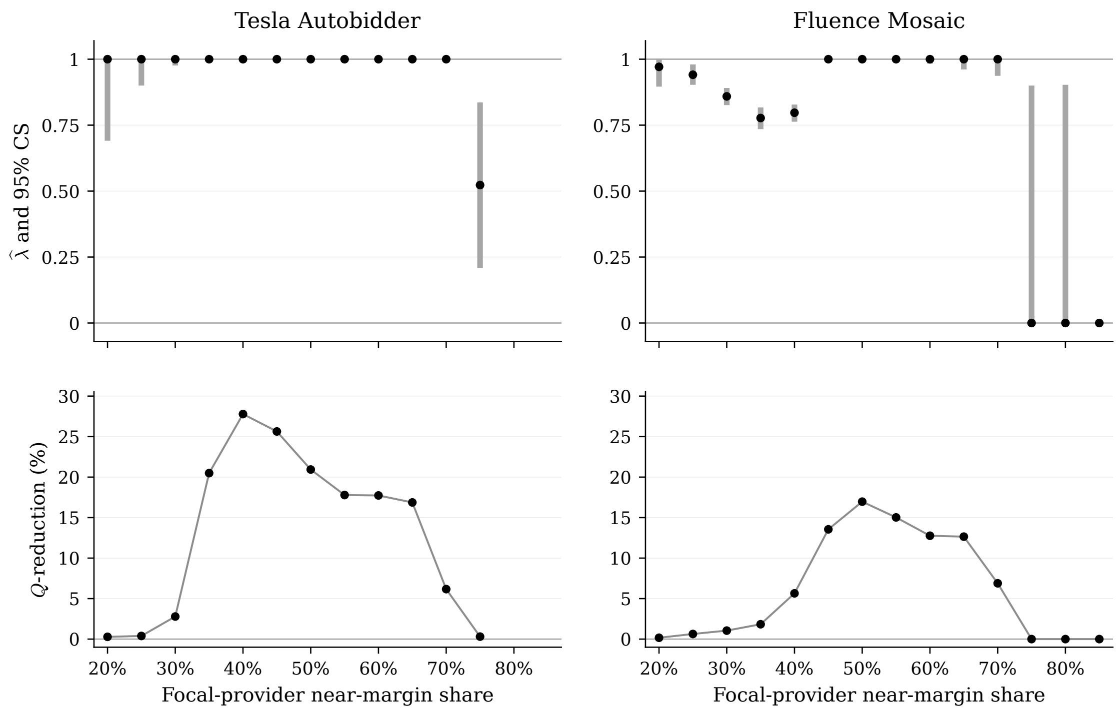

Notes: Local-window kernel-weighted fit of the two-tier conduct estimator on the deviation sample, separately for Tesla Autobidder (left) and Fluence Mosaic (right). Top row: point estimate $\widehat{\lambda}(s_0)$ at each window centre s_0 with a vertical 95% cluster-subsampling confidence set; dotted reference lines mark $\lambda = 0$ and $\lambda = 1$. Bottom row: Q-reduction $1 - Q_n(\widehat{\lambda})/Q_n(0)$ at the same window centres. Kernel is triangular with bandwidth $h = 0.10$. Windows with fewer than 50 multi-owner (i, t) clusters are omitted.

for different reasons at the two ends. Below 30% the identifying sample is large enough that an improvement in fit of the size found above 30% would be detected if same-provider internalisation were operating, yet the Q-reduction stays near zero and then rises discontinuously at 30%. This points to a genuine concentration threshold. Internalisation becomes detectable only once a provider controls a sufficiently large share of near-margin capacity. Above 70% the multi-owner identifying sample becomes too thin to estimate reliably.

The results therefore consistently show that joint-profit maximisation across same-provider batteries is a statistically significant improvement in fit over owner-level profit maximisation alone. Two features of the estimates are worth considering. First, the batteries in question are non-negligible price setters. Because the reclearing engine returns the counterfactual clearing price for every deviation, we can measure each battery's price impact directly rather than inferring it from an estimated residual demand curve. A single battery's most profitable owner-only deviation moves the regional price by $\$1.28$/MWh at the median, $\$2.70$/MWh on average and $\$6.24$/MWh in the upper decile, reaching roughly $\$59$/MWh at the maximum (Appendix B.10). Structural concentration screens exist to proxy for exactly this effect that we can directly calculate in our setting. In fact, the conduct test rejects the owner-only null at focal-provider near-margin shares between 30% and 70%. Because the per-interval near-margin share tracks the installed share on average, this identifying range corresponds to provider installed-capacity shares of approximately $20–60\%$, which is inside the range the classic wholesale-market-power literature treats as material unilateral conduct (Borenstein et al., 2002; Mansur, 2007) Second, the profit internalisation arises across ownership. In the identifying intervals the focal provider's near-margin capacity is held by 2.2 separately owned firms on average, and 83% of the same-provider spillover that the test finds internalised accrues to batteries owned by a different firm than the deviating one – precisely the pairs that ownership-based concentration analysis treats as independent competitors. The two partitions also differ in level: in QLD1 and VIC1, which together supply 73% of the identifying intervals, provider concentration among batteries is more than twice owner concentration. The identifying range of $30–70\%$ near-margin share corresponds to roughly $20–60\%$ of installed battery capacity, of the same order as the single-firm shares that trigger scrutiny under standard screens (Federal Energy Regulatory Commission, 2007), though we stress that our shares are computed within the battery segment and the comparison is a yardstick rather than a market-power finding

We now investigate possible alternative explanations for the results of the conduct test, and rule them out. All results of the robustness exercises are documented in Appendix B.11. First, the conduct test treats a positive recleared owner-portfolio gain as a contradiction of owner-level optimisation. A natural alternative explanation is that the estimated owner payoff omits private contract positions, tolling arrangements, degradation shadow costs, or other unobserved owner-level costs that make the owner-only deviations privately unattractive. We bound this omitted cost for each identifying band by solving for the smallest constant private cost c (in AUD per MWh of focal discharge) such that adding $c \cdot \text{exposure}_{itd}$ to the focal owner's deviation gain reduces the moment objective as much as the conduct hypothesis at $\widehat{\lambda}$.

The implied charges are well above the Bellman opportunity-cost benchmark of about $11/MWh, which is the largest movement in $\widehat{m}_{it}$ across our numerical sensitivity checks. For Tesla Autobidder, two of the four identifying bands ($40–50\%$ and $60–70\%$) even require an infinite cost – the irreducible part of the moment objective from positive own-gain rows with no corresponding dispatch exposure already exceeds $Q_n(\widehat{\lambda})$, so no finite per-MWh cost can rationalise the data – and the other two require $16 and $59/MWh, respectively. For Fluence, the three corner intervals at $\widehat{\lambda} = 1$ require $11, $15, and $28/MWh; the $30–40\%$ interior interval, the weakest in the identifying set, requires $8/MWh. This is the only interval that sits below the Bellman benchmark. In every other interval the implied cost is at least a factor above the benchmark or infinite.

Second, the deviation panel we construct and the reclearing calculation determine deviations and their value at the realised market outcome, instead of the expected market outcome prior to the 5-minute interval. An apparent owner-level violation could therefore in principle reflect hindsight – a deviation that looks profitable ex post but not under the information the bidder held when the operative bid was submitted. To rule out this possibility, we date each interval's operative quantity bid to its submission timestamp in the data and split the test by the lead time to dispatch. If the results are driven by hindsight, then they should be strongest for bids submitted well ahead of dispatch and weakest for bids submitted shortly before the dispatch interval. We find the opposite. The conduct test is strongest for rebids submitted within the final fifteen minutes prior to dispatch – when five-minute predispatch forecasts can be expected to be accurate and the no-profitable-deviation logic applies.

Third, a positive $\widehat{\lambda}$ could reflect a purely mechanical price externality rather than same-provider internalisation. Any deviation that lowers the clearing price reduces the inframarginal revenue of every battery near the margin, so same-provider profits may simply fall because same-provider batteries happen to be near the margin. Because the reclearing engine returns the profit change each deviation imposes on every regional battery, we can test this possibility directly. For each focal deviation we build placebo coalitions from the different-provider, different-owner batteries near the margin in the same region and interval, matched to the actual same-provider coalition on the number of batteries and on installed capacity, so that they carry the same mechanical price exposure by construction. Across 500 capacity-matched placebo coalitions – different-provider batteries carrying the same near-margin price exposure – not one improves the fit of the conduct objective as much as the actual same-provider coalition ($p = 0.002$ for both providers), and the same-provider improvement exceeds the 95th percentile of the placebo distribution. Moreover, if we do not match on capacity and construct a simpler count-matched placebo, we continue to obtain the same result ($p \leq 0.010$). This comparison also bounds owner-level objectives more complex than the per-MWh constant cost bound above. Some owners may hold generation portfolios and contract positions whose value rises with the regional price, an incentive denominated in price exposure rather than in discharge volume. Because any price-denominated objective scales with the recleared price change, a capacity-matched placebo coalition – which carries the same price exposure by construction – would rationalise the observed restraint as well as the same-provider coalition does. It does not. The conduct test results are therefore specific to the provider coalition, not a generic consequence of near-margin batteries losing revenue when the price falls.

Finally, we verify that the estimator recovers internalisation where theory requires it: we estimate the weight the focal owner places on its own other batteries, instead of imposing it. We indeed find a substantial improvement in fit and an estimated weight on same-owner batteries of approximately one, confirming that the method is able to detect joint-profit incentives when they should be present by construction.

Taken together, these robustness exercises leave same-provider profit internalisation as the most likely interpretation of the observed bidding behaviour and results of the conduct test. We now close by calculating the magnitude of the impact this conduct has. We estimate it to be around \$$5.5$m per year. We obtain this from the deviation panel: for each focal battery-interval in the identifying range, we take the owner-only best deviation d_{it}^{0} – the deviation that maximises the focal owner's recleared portfolio gain – and record the counterfactual regional price the reclearing engine returns. The gap between the observed and counterfactual price is the price increase that the owner's restraint sustains. We multiply it by regional demand for the 5-minute interval, sum across identified (r, t), and re-weight by inverse inclusion probability, giving \$$4.6$m over the sample window and \$$5.5$m annualised, of which Tesla Autobidder accounts for \$$3.1$m and Fluence Mosaic for \$$2.4$m.

This is likely a conservative bound on the cost of the identified conduct. The counterfactual is partial-equilibrium and unilateral: we compute the price increase from a single owner-only best deviation while holding all other bid stacks fixed, whereas fully coordinated same-provider bidding would move more capacity and raise prices further. It also counts only discrete deviations on the $\{10\%, 25\%, 50\%\}$ MW grid, and only within the identifying concentration bands. Finally, the magnitude is tied to the current fleet. Batteries account for 46% of AEMO's record 64 GW December-2025 connection pipeline (Australian Energy Market Operator, 2026), several times the 6.6 GW of known-provider capacity in our sample, so if provider shares persist as this capacity is commissioned, batteries will set the regional price in more intervals and the same per-interval conduct would scale the annual cost accordingly.

4. Conclusion

Whether and how algorithms may facilitate collusion is a central question in current competition policy debate, but direct empirical evidence is still scarce. Assad et al. (2024) show that the adoption of pricing algorithms raised margins among competing retail fuel stations, and Calder-Wang and Kim (2026) find that a common pricing algorithm in rental housing internalises competitors' profits.[22] We provide, to our knowledge, the first evidence of the effects of common third-party *bidding* algorithms, which construct an entire offer schedule from primitives rather than repricing a single posted price, and of concentration in the upstream layer of algorithm providers. We argue that the mechanism is not specific to batteries or electricity markets: where competitors delegate high-frequency decisions to a shared algorithmic provider, that provider maps common information into correlated conduct. We develop a simple stylised model to capture our setting of common third-party providers with dynamic storage and show that previously documented price and welfare effects from the literature arise in our setting as well (Harrington and Ortner, 2025; Aleksenko and Miklós-Thal, 2026).

To conduct our analysis, we hand-collect a mapping of autobidding providers to utility-scale batteries in the Australian National Electricity Market and combine it with public 5-minute bid, price, and dispatch data, as well as a reclearing engine that reproduces the regional clearing outcome from public market inputs and allows us to construct counterfactual market outcomes. We document substantial provider concentration, and then examine how this concentration affects downstream market conduct.

First, we find that bids constructed by the same provider move together more than bids constructed by different providers, and that the gap widens after the July 2025 ERI disclosure reform. The pattern is provider-specific: rebid timing has a provider-wide component, while bid-stack co-movement is strongest when same-provider batteries operate in the same region and face the same local scarcity state. The result is robust to alternative samples and specifications and is consistent with a common provider's algorithm converting shared scarcity information into correlated bids. We also find that the disclosure reform led to higher bids during periods of scarcity and lower bids during periods of abundance, showing the effect of the improved information about the market state.

Second, we relate this co-movement to regional provider concentration and find that both local co-movement and the within-day variance of the regional average bid price rise with the installed provider HHI. These reduced-form patterns are consistent with responsive bidding but cannot, on their own, separate that channel from coordinated conduct. We therefore turn to a structural test of the latter.

[22] A related empirical literature studies simpler repricing software that adjusts a posted price in response to rivals (Brown and MacKay, 2023; Musolff, 2025).

Third, to test for conduct, we estimate a Bellman opportunity-cost value for each battery, generate local feasible deviations from observed bid stacks, and reclear the market under each. The resulting profit changes define a revealed-preference moment inequality whose conduct parameter $\lambda \in [0, 1]$ measures the weight a battery's bidder places on same-provider, different-owner profits in its effective objective. For the dominant autobidding providers Tesla Autobidder and Fluence Mosaic, $\widehat{\lambda}$ is at or above 0.75 across focal-provider near-margin shares of roughly 30–70%, and the 95% subsampling confidence sets exclude the owner-only null throughout this range. Below 30% the test retains power but finds no internalisation, so the conduct emerges only above a concentration threshold; above 70% the multi-owner sample the test requires becomes too thin. Our conduct test shows that these batteries move prices: a single battery's best owner-only deviation shifts the regional clearing price by $\$1.28$/MWh at the median and by more than $\$6$/MWh in the upper decile. And the internalisation crosses ownership boundaries – 83% of the spillover it captures accrues to batteries owned by other firms, which ownership-based concentration analysis treats as independent competitors. FCAS deviations, by contrast, show no conduct signal.

A set of robustness exercises shows that this is not an artefact of measurement or of the test's construction. One, the unobserved owner-level cost required to rationalise the observed restraint under owner-only incentives exceeds our Bellman opportunity-cost benchmark in every identifying band. Two, the conduct signal is concentrated in rebids submitted within fifteen minutes of dispatch, when the realised outcome closely approximates the bidder's information set, so it does not reflect hindsight. Three, it is specific to the provider coalition: none of 500 placebo coalitions of different-provider batteries, matched on battery count and installed capacity and therefore carrying the same mechanical price exposure, improves the conduct fit as much as the actual same-provider coalition. Four, we confirm that the estimator correctly recovers full internalisation of profits across batteries of the same owner. We conclude by calculating that the identified withholding implies an annualised consumer-side cost of approximately $\$5.5$ million.

Our findings have implications beyond this market. The NEM is one of several wholesale electricity markets in which utility-scale batteries are expanding rapidly and a small number of third-party autobidder providers operate a growing share of installed capacity. As algorithmic bidding spreads, the relevant unit of concentration may become the provider whose software constructs the bid, not only the asset owner. Our results also speak to the disclosure debate in these markets: the July 2025 reform improved the scarcity information batteries can condition on, but the same richer signal let a concentrated provider's bids track the common state more tightly. Improved disclosure and stronger same-provider co-movement are two sides of one channel, and weighing them is a policy trade-off.

References

Ibrahim Abada and Xavier Lambin. Artificial intelligence: Can seemingly collusive outcomes be avoided? *Management Science*, 69(9):5042–5065, 2023. doi: 10.1287/mnsc.2022.4623.

Ibrahim Abada, Xavier Lambin, and Nikolay Tchakarov. Collusion by mistake: Does algorithmic sophistication drive supra-competitive profits? *European Journal of Operational Research*, 318(3): 927–953, 2024. doi: 10.1016/j.ejor.2024.06.006.

Gagan Aggarwal, Ashwinkumar Badanidiyuru, Santiago R. Balseiro, Kshipra Bhawalkar, Yuan Deng, Zhe Feng, Gagan Goel, Christopher Liaw, Haihao Lu, Mohammad Mahdian, Jieming Mao, Aranyak Mehta, Vahab Mirrokni, Renato Paes Leme, Andres Perlroth, Georgios Piliouras, Jon Schneider, Ariel Schvartzman, Balasubramanian Sivan, Kelly Spendlove, Yifeng Teng, Di Wang, Hanrui Zhang, Mingfei Zhao, Wennan Zhu, and Song Zuo. Auto-bidding and Auctions in Online Advertising: A Survey, 2024. URL `https://arxiv.org/abs/2408.07685`.

Stepan Aleksenko and Jeanine Miklós-Thal. Third-party pricing algorithms and information sharing. Working paper, 2026.

David Andrés-Cerezo and Natalia Fabra. Storing power: Market structure matters. *The RAND Journal of Economics*, 54(1):3–53, 2023. doi: 10.1111/1756-2171.12429.

John Asker, Chaim Fershtman, and Ariel Pakes. The impact of artificial intelligence design on pricing. *Journal of Economics & Management Strategy*, 33(2):276–304, 2024. doi: 10.1111/jems.12516.

Stephanie Assad, Robert Clark, Daniel Ershov, and Lei Xu. Algorithmic pricing and competition: Empirical evidence from the german retail gasoline market. *Journal of Political Economy*, 132(3): 723–771, 2024. doi: 10.1086/726906.

Australian Energy Market Commission. Ai and the future of energy regulation: Addressing the risk of algorithmic collusion. Staff working paper, Australian Energy Market Commission, July 2024.

Australian Energy Market Operator. FCAS Model in NEMDE. Technical report, Australian Energy Market Operator, 2021. URL `https://aemo.com.au/-/media/files/electricity/nem/security_and_reliability/dispatch/policy_and_process/fcas-model-in-nemde.pdf`.

Australian Energy Market Operator. Strong delivery, growing energy investment pipeline in december quarter, January 2026. URL `https://www.aemo.com.au/newsroom/media-release/strong-delivery-growing-energy-investment-pipeline-in-december-quarter`. Media release, January 28, 2026.

Autorité de la concurrence and Bundeskartellamt. Algorithms and competition. Technical report, Autorité de la concurrence and Bundeskartellamt, November 2019. URL `https://www.bundeskartellamt.de/SharedDocs/Publikation/EN/Berichte/Algorithms_and_Competition_Working-Paper.html`.

José Azar, Martin C. Schmalz, and Isabel Tecu. Anticompetitive effects of common ownership. *The Journal of Finance*, 73(4):1513–1565, 2018. doi: 10.1111/jofi.12698.

Matthew Backus, Christopher Conlon, and Michael Sinkinson. Common ownership and competition in the ready-to-eat cereal industry. NBER Working Paper 28350, National Bureau of Economic Research, 2021.

Patrick Bajari, C. Lanier Benkard, and Jonathan Levin. Estimating dynamic models of imperfect competition. *Econometrica*, 75(5):1331–1370, 2007. doi: 10.1111/j.1468-0262.2007.00796.x.

Martino Banchio and Giacomo Mantegazza. Artificial intelligence and spontaneous collusion, 2023. URL `https://arxiv.org/abs/2202.05946`.

Steven T. Berry and Philip A. Haile. Identification in differentiated products markets using market level data. *Econometrica*, 82(5):1749–1797, 2014. doi: 10.3982/ECTA9027.

Severin Borenstein, James B. Bushnell, and Frank A. Wolak. Measuring market inefficiencies in california's restructured wholesale electricity market. *American Economic Review*, 92(5):1376–1405, 2002. doi: 10.1257/000282802762024557.

Zach Y. Brown and Alexander MacKay. Competition in pricing algorithms. *American Economic Journal: Microeconomics*, 15(2):109–156, 2023. doi: 10.1257/mic.20210158.

R. Andrew Butters, Jackson Dorsey, and Gautam Gowrisankaran. Soaking up the sun: Battery investment, renewable energy, and market equilibrium. NBER Working Paper 29133, National Bureau of Economic Research, 2021.

Sophie Calder-Wang and Gi Heung Kim. Algorithmic pricing in multifamily rentals: Efficiency gains or price coordination? Working paper, version dated February 18, 2026, 2026.

Emilio Calvano, Giacomo Calzolari, Vincenzo Denicolò, and Sergio Pastorello. Artificial intelligence, algorithmic pricing, and collusion. *American Economic Review*, 110(10):3267–3297, 2020. doi: 10.1257/aer.20190623.

Competition and Markets Authority. Pricing algorithms: Economic working paper on the use of algorithms to facilitate collusion and personalised pricing. Technical report, Competition and Markets Authority, June 2018. URL `https://www.gov.uk/government/publications/pricing-algorithms-research-collusion-and-personalised-pricing`.

Competition and Markets Authority. Algorithms: How they can reduce competition and harm consumers. Technical report, Competition and Markets Authority, January 2021. URL `https://www.gov.uk/government/publications/algorithms-how-they-can-reduce-competition-and-harm-consumers`.

William L. Cooper, Tito Homem-de Mello, and Anton J. Kleywegt. Learning and pricing with models that do not explicitly incorporate competition. *Operations Research*, 63(1):86–103, 2015. doi: 10.1287/opre.2014.1341.

Arnoud V. den Boer, Janusz M. Meylahn, and Maarten Pieter Schinkel. Artificial collusion: Examining supracompetitive pricing by q-learning algorithms. Tinbergen Institute Discussion Paper TI 2022-067/VII, Tinbergen Institute, 2022. URL `https://ssrn.com/abstract=4213600`.

Dutch Authority for the Financial Markets. Algorithmic collusion in capital markets. Technical report, Dutch Authority for the Financial Markets, 2024. URL `https://www.afm.nl/en/sector/actueel/2023/november/trendzicht-2024`. Trend Monitor 2024.

Electric Reliability Council of Texas. ERCOT Monthly: July 2025, August 2025. URL `https://www.ercot.com/files/docs/2025/08/06/ERCOT-Monthly-July-2025.pdf`. Published August 6, 2025.

Nicolas Eschenbaum, Filip Mellgren, and Philipp Zahn. Robust algorithmic collusion, 2022. URL `https://arxiv.org/abs/2201.00345`.

Natalia Fabra. Tacit collusion in repeated auctions: Uniform versus discriminatory. *The Journal of Industrial Economics*, 51(3):271–293, 2003. doi: 10.1111/1467-6451.00201.

Federal Energy Regulatory Commission. Market-based rates for wholesale sales of electric energy, capacity and ancillary services by public utilities, order no. 697, June 2007. URL `https://www.ferc.gov/sites/default/files/2020-06/OrderNo.697.pdf`. 119 FERC ¶ 61,295; Docket No. RM04-7-000; issued June 21, 2007.

Karsten T. Hansen, Kanishka Misra, and Mallesh M. Pai. Frontiers: Algorithmic collusion: Supracompetitive prices via independent algorithms. *Marketing Science*, 40(1):1–12, 2021. doi: 10.1287/mksc.2020.1276.

Jr. Harrington, Joseph E. The effect of outsourcing pricing algorithms on market competition. Working paper, dated July 19, 2021, 2021.

Jr. Harrington, Joseph E. Hub-and-spoke collusion with a third-party pricing algorithm. Working paper, dated November 24, 2025, 2025.

Jr. Harrington, Joseph E. and Juan Ortner. The equilibrium design of a third-party pricing algorithm. Working paper, dated December 8, 2025, 2025.

Kate Ho and Ariel Pakes. Hospital choices, hospital prices, and financial incentives to physicians. *American Economic Review*, 104(12):3841–3884, 2014. doi: 10.1257/aer.104.12.3841.

Pär Holmberg. Unique supply function equilibrium with capacity constraints. *Energy Economics*, 30(1):148–172, 2008. doi: 10.1016/j.eneco.2006.10.005.

Herbert Hovenkamp and Thibault Schrepel. Cartel management services. Working paper, 2026.

International Energy Agency. Global Energy Review 2026. Technical report, International Energy Agency, Paris, 2026. URL `https://www.iea.org/reports/global-energy-review-2026/technology-battery-storage`. Technology: Battery storage.

Sahand Karimi-Arpanahi, Ali Pourmousavi Kani, and Nariman Mahdavi. Battery scheduling optimisation in energy and ancillary services markets: Quantifying unrealised revenue in the australian nem. In *Proceedings of the 15th ACM International Conference on Future and Sustainable Energy Systems*, e-Energy '24, pages 226–236, 2024. doi: 10.1145/3632775.3661960.

Alexander Kastius and Rainer Schlosser. Dynamic pricing under competition using reinforcement learning. *Journal of Revenue and Pricing Management*, 21(1):50–63, 2022. doi: 10.1057/s41272-021-00285-3.

Steven O. Kimbrough and Frederic H. Murphy. Learning to collude tacitly on production levels by oligopolistic agents. *Computational Economics*, 33(1):47–78, 2009. doi: 10.1007/s10614-008-9150-6.

Timo Klein. Autonomous algorithmic collusion: Q-learning under sequential pricing. *RAND Journal of Economics*, 52(3):538–558, 2021. doi: 10.1111/1756-2171.12383.

Paul D. Klemperer and Margaret A. Meyer. Supply function equilibria in oligopoly under uncertainty. *Econometrica*, 57(6):1243–1277, 1989. doi: 10.2307/1913707.

Erin T. Mansur. Upstream competition and vertical integration in electricity markets. *Journal of Law and Economics*, 50(1):125–156, 2007. doi: 10.1086/508309.

Monopolkommission. Algorithms and collusion. Excerpt from chapter i of biennial report xxii, German Monopolies Commission, 2018. URL `https://www.monopolkommission.de/index.php/en/press-releases/224-algorithms-and-collusion`.

Leon Musolff. Algorithmic pricing, price wars and tacit collusion: Evidence from e-commerce. *Management Science*, 2025. URL `https://lmusolff.com/papers/Algorithmic_Pricing.pdf`. Forthcoming.

Ariel Pakes, Jack Porter, Kate Ho, and Joy Ishii. Moment inequalities and their application. *Econometrica*, 83(1):315–334, 2015. doi: 10.3982/ECTA6865.

Abhijith Prakash. nempy: A Python package for modelling the Australian National Electricity Market dispatch procedure. *Journal of Open Source Software*, 7(70):3596, 2022. doi: 10.21105/joss.03596.

Abhijith Prakash, Anna Bruce, and Iain MacGill. The scheduling role of future pricing information in electricity markets with rising deployments of energy storage: An australian national electricity market case study. *Energy Economics*, 142:108191, 2025. doi: 10.1016/j.eneco.2025.108191.

Mar Reguant. Complementary bidding mechanisms and startup costs in electricity markets. *Review of Economic Studies*, 81(4):1708–1742, 2014. doi: 10.1093/restud/rdu022.

Joseph P. Romano and Azeem M. Shaikh. Inference for identifiable parameters in partially identified econometric models. *Journal of Statistical Planning and Inference*, 138(9):2786–2807, 2008. doi: 10.1016/j.jspi.2008.03.015.

Juan Manuel Sánchez-Cartas and Evangelos Katsamakas. Artificial intelligence, algorithmic competition and market structures. *IEEE Access*, 10:10575–10584, 2022. doi: 10.1109/ACCESS.2022.3144390.

Takuo Sugaya and Alexander Wolitzky. Collusion with optimal information disclosure. Working paper, dated January 17, 2025, 2025.

U.S. Department of Justice and Federal Trade Commission. Algorithms and collusion. Note by the United States DAF/COMP/WD(2017)41, Organisation for Economic Co-operation and Development, 2017. URL https://one.oecd.org/document/DAF/COMP/WD(2017)41/en/pdf.

U.S. Energy Information Administration. New U.S. electric generating capacity expected to reach a record high in 2026. Today in Energy, February 2026. URL https://www.eia.gov/todayinenergy/detail.php?id=67205. Published February 20, 2026.

Xavier Vives. Strategic supply function competition with private information. *Econometrica*, 79(6): 1919–1966, 2011. doi: 10.3982/ECTA8126.

Ludo Waltman and Uzay Kaymak. Q-learning agents in a cournot oligopoly model. *Journal of Economic Dynamics and Control*, 32(10):3275–3293, 2008. doi: 10.1016/j.jedc.2008.01.003.

A. Formal Model Details

This appendix provides the formal details behind the stylised model in Section 2.2. We define the strategy and belief objects suppressed in the main text, show the local responsive-bidding comparative static, and record a simple static affine equilibrium that illustrates the concentration channel.

A.1. Beliefs, Strategies, and Local Responsive Bidding

Let an owner-level bidding strategy be a map

$$\sigma_o : \mathcal{I}_{ot} \to \mathcal{B}_o(S_t, X_{rt}),$$

and let μ_{ot} denote owner o's belief over current and future scarcity, rival information, and rival bid strategies. The compact expectation $\mathbb{E}_{ot}[\cdot]$ in the main text is shorthand for expectation under (μ_{ot}, σ_{-o}). Thus the owner-level responsive benchmark is

$$\sigma_o(\mathcal{I}_{ot}) \in \arg \max_{\mathbf{b}_o \in \mathcal{B}_o(S_t, X_{rt})} \mathbb{E}_{\mu_{ot}, \sigma_{-o}} \left[\Pi_{ot}(\mathbf{b}_o, \sigma_{-o}(\mathcal{I}_{-o,t}); S_t, X_{rt}, \{\theta_{r\tau}\}_{\tau \geq t}) \mid \mathcal{I}_{ot} \right].$$

For the responsive-bidding comparative static below we require two regularity conditions: monotonicity of the continuation-value gap in the scarcity state, and monotonicity of the conditional distribution of next-period scarcity in the provider's current posterior.

Assumption 1 (Monotone storage value)**.** *For a fixed public state z and provider k, let*

$$\Delta V_k(z, \theta) := V_k^F(z, \theta) - V_k^E(z, \theta)$$

denote the continuation-value gain from retaining stored energy rather than depleting the battery. The map $\theta \mapsto \Delta V_k(z, \theta)$ is weakly increasing.

Assumption 2 (Monotone scarcity posterior)**.** *For each provider k and date t, the conditional distribution of $\theta_{r,t+1}$ given $m_{krt} = m$ is weakly increasing in m in the first-order stochastic dominance sense.*

The provider's posterior shadow cost of discharge is

$$\widehat{c}_k(z, m) := c_d + \delta\, \mathbb{E}[\Delta V_k(z, \theta_{r,t+1}) \,|\, z_t = z,\ m_{krt} = m]\,, \tag{19}$$

where c_d is the marginal throughput cost of discharge and δ is the discount factor.

Given these two assumptions, we can then state the following Lemma, which directly delivers the co-movement of same-provider batteries.

Lemma 1 (Posterior shadow cost monotonicity)**.** *Under Assumptions 1–2, the posterior shadow cost $\widehat{c}_k(z, m)$ is weakly increasing in m.*

Proof. For any $m' \geq m$, Assumption 2 implies that the conditional distribution of $\theta_{r,t+1}$ given $m_{krt} = m'$ first-order stochastically dominates the conditional distribution given $m_{krt} = m$. Since

$\theta \mapsto \Delta V_k(z, \theta)$ is weakly increasing by Assumption 1, the conditional expectation in (19) is weakly increasing in m. Adding c_d and multiplying by $\delta \geq 0$ preserve monotonicity. $\square$

To derive the local response to scarcity, take one near-margin generation block of battery i and hold the rest of the stack fixed. Let b_i denote the offer price for this block and let $q_i(b_i; \theta_{rt}, \mathbf{b}_{-i}, X_{rt})$ denote dispatched MW. Around the clearing margin, a higher offer price weakly lowers dispatch, so $q_{i,b} \leq 0$. The local owner payoff can be written as

$$U_i(b_i; m_{krt}) = \mathbb{E}[\pi_i(b_i; \theta_{rt}, \mathbf{b}_{-i}, X_{rt}) \mid \mathcal{I}_{krt}] + \delta\, \mathbb{E}[V_{i,t+1}(S_{it} - \Delta q_i(b_i; \theta_{rt}, \mathbf{b}_{-i}, X_{rt}), \theta_{r,t+1}) \mid \mathcal{I}_{krt}] \,. \tag{20}$$

At an interior optimum,

$$U_{i,b}(b_i^R; m_{krt}) = 0, \qquad U_{i,bb}(b_i^R; m_{krt}) < 0.$$

The implicit-function theorem gives

$$\frac{\partial b_i^R}{\partial m_{krt}} = -\frac{U_{i,bm}}{U_{i,bb}}.$$

Lemma 1 gives the storage part of the cross-partial: a higher provider scarcity posterior raises the expected shadow cost of discharge. Since $-\Delta q_{i,b} \geq 0$, a higher bid preserves energy by reducing current dispatch. When this dynamic force is not overturned by the current-profit term, $U_{i,bm} > 0$. Hence

$$\frac{\partial b_i^R}{\partial m_{krt}} > 0.$$

The same notation also gives the covariance logic in the main text. If

$$b_{it}^R \approx \bar{b}_{it} + \psi_i(S_{it}, X_{rt}) + \phi_{it} m_{k_i,rt}, \qquad \phi_{it} > 0,$$

then same-provider pairs load on the same provider-level object, whereas different-provider pairs load on distinct provider-level objects. Same-provider bid covariance exceeds cross-provider covariance whenever the provider-level object contains variation shared within provider but not across providers.

A.2. A Static Affine Benchmark

This subsection develops a static equilibrium benchmark. This closed-form benchmark uses Gaussian dynamics and signals. Under these assumptions the regularity conditions of Appendix A.1 hold automatically and the affine equilibrium has a closed form.

Let $(\theta_{r\tau})_{\tau \geq t}$ be a stationary mean-zero Gaussian process with $\mathrm{Var}(\theta_{r\tau}) = \tau_\theta^{-1}$ and $\mathrm{Cov}(\theta_{rt}, \theta_{r,t+1}) = \rho_\theta / \tau_\theta$ for some serial correlation $\rho_\theta \in [0, 1)$. In each interval, all providers observe the public signal

$$g_t = \theta_{rt} + \eta_{0t},$$

and provider k additionally observes the private signal

$$y_{kt} = \theta_{rt} + \eta_{kt},$$

where $\eta_{0t} \sim \mathcal{N}(0, \tau_g^{-1})$, $\eta_{kt} \sim \mathcal{N}(0, \tau_y^{-1})$, and all noise terms are mutually independent and independent of $(\theta_{r\tau})$. Provider k's contemporaneous posterior mean is

$$m_{kt} := \mathbb{E}[\theta_{rt} \mid g_t, y_{kt}]. \tag{21}$$

Lemma 2 (Gaussian posterior structure). *Let $T := \tau_\theta + \tau_g + \tau_y$. Then*

$$m_{kt} = \frac{\tau_g g_t + \tau_y y_{kt}}{T}, \qquad \mathcal{V}_t := \mathrm{Var}(m_{kt}) = \frac{\tau_g + \tau_y}{\tau_\theta T}, \tag{22}$$

and, for $j \neq k$,

$$\rho_t := \frac{\mathrm{Cov}(m_{kt}, m_{jt})}{\mathrm{Var}(m_{kt})} = 1 - \frac{\tau_\theta \tau_y}{(\tau_g + \tau_y)T} \in (0,1), \qquad \mathbb{E}[m_{jt} \mid m_{kt}] = \rho_t m_{kt}. \tag{23}$$

There exist mutually independent Gaussian random variables m_{gt}, $\widetilde{h}_t$ (both common across providers), and u_{kt} (provider-specific) such that

$$m_{kt} = m_{gt} + \widetilde{h}_t + u_{kt}.$$

The conditional distributions

$$\theta_{rt} \mid m_{krt} = m \ \sim \ \mathcal{N}(m,\, 1/T), \qquad \theta_{r,t+1} \mid m_{krt} = m \ \sim \ \mathcal{N}(\rho_\theta m,\, \sigma_+^2),$$

have variances that do not depend on m, so both are weakly first-order stochastically increasing in m (strictly so for $\theta_{r,t+1}$ when $\rho_\theta > 0$). In particular, Assumption 2 holds.

Proof. Gaussian updating gives the posterior mean in (22). Since the posterior variance is $1/T$, $\mathrm{Var}(m_{kt}) = \mathrm{Var}(\theta_{rt}) - 1/T = (\tau_g + \tau_y)/(\tau_\theta T)$.

Let

$$m_{gt} := \mathbb{E}[\theta_{rt} \mid g_t], \qquad r_t := \theta_{rt} - m_{gt}, \qquad \widetilde{h}_t := \frac{\tau_y}{T} r_t, \qquad u_{kt} := \frac{\tau_y}{T}\eta_{kt}.$$

Then $m_{kt} = m_{gt} + \widetilde{h}_t + u_{kt}$. The residual r_t is orthogonal to g_t, and hence independent of m_{gt} by Gaussianity; the provider-specific term u_{kt} depends only on η_{kt}, which is independent of all other primitives. This proves the independent decomposition. For $j \neq k$, $\mathrm{Cov}(m_{kt}, m_{jt}) = \mathrm{Var}(m_{gt} + \widetilde{h}_t)$, which gives (23). Joint normality and zero means imply $\mathbb{E}[m_{jt} \mid m_{kt}] = \rho_t m_{kt}$.

For the conditional distributions, write $\theta_{rt} = m_{kt} + r_{kt}$ where the posterior residual $r_{kt} \sim \mathcal{N}(0, 1/T)$ is independent of m_{kt}; this gives the first conditional distribution as a location family in m. For $\theta_{r,t+1}$, joint normality of $(\theta_{r,t+1}, m_{kt})$ gives

$$\mathrm{Cov}(\theta_{r,t+1}, m_{kt}) = \frac{\tau_g + \tau_y}{T}\mathrm{Cov}(\theta_{r,t+1}, \theta_{rt}) = \frac{(\tau_g + \tau_y)\rho_\theta}{\tau_\theta T} = \rho_\theta \mathcal{V}_t.$$

Linear projection then yields $\mathbb{E}[\theta_{r,t+1} \mid m_{kt} = m] = \rho_\theta m$ with conditional variance $\sigma_+^2 = \mathrm{Var}(\theta_{r,t+1}) - \rho_\theta^2 \mathcal{V}_t$ independent of m. Both conditional distributions are location families in m with m-invariant spread, hence weakly first-order stochastically increasing in m. $\square$

Now consider one region and one interval. Providers are indexed by $k = 1, \dots, K$, and provider k controls share $x_k \geq 0$, with $\sum_k x_k = 1$. All batteries using provider k receive the same posterior m_{kt} from Lemma 2 and choose the same scalar local action a_{kt}. Let

$$A_t := \sum_{k=1}^{K} x_k a_{kt}$$

denote the share-weighted aggregate action. We use the posterior variance $\mathcal{V}_t$ and the cross-provider posterior correlation ρ_t from Lemma 2 throughout.

The reduced payoff of a provider-k client from choosing action a is

$$\Pi_{kt}(a \mid m_{kt}) = (a - c_t)\Big(\psi_t + \xi_t m_{kt} - \beta_t a + d_t\, \mathbb{E}[A_t \mid m_{kt}]\Big), \tag{24}$$

where $\beta_t > 0$, $0 < d_t < \beta_t$, and $\xi_t > 0$. The coefficient ξ_t summarises the local scarcity loading of the reduced bid problem, including the dynamic opportunity-cost channel. The coefficient d_t captures strategic complementarity in local bid construction.

Definition 1 (Affine delegated equilibrium). *An affine delegated equilibrium is a vector $(\alpha_{kt}, \gamma_{kt})_{k=1}^K$ such that every client of provider k chooses*

$$a_{kt} = \alpha_{kt} + \gamma_{kt} m_{kt} \tag{25}$$

and this action is optimal under (24).

Proposition 1 (Affine provider-posterior benchmark). *There exists a unique affine delegated equilibrium. The intercepts coincide across providers, $\alpha_{kt} = \alpha_t$ for all k, with*

$$\alpha_t = \frac{\psi_t + \beta_t c_t}{2\beta_t - d_t}. \tag{26}$$

Let

$$\mathcal{S}_t := \sum_{k=1}^{K} x_k \gamma_{kt}, \qquad \Lambda_t(x) := \sum_{k=1}^{K} \frac{x_k}{2\beta_t - d_t(1-\rho_t)x_k}.$$

Then

$$\mathcal{S}_t = \frac{\xi_t \Lambda_t(x)}{1 - d_t \rho_t \Lambda_t(x)}, \qquad \gamma_{kt} = \frac{\xi_t}{1 - d_t \rho_t \Lambda_t(x)} \frac{1}{2\beta_t - d_t(1-\rho_t)x_k}. \tag{27}$$

Proof of Proposition 1. Fix t and suppress time subscripts. Under an affine conjecture

$$a_k = \alpha_k + \gamma_k m_k, \qquad A = \sum_{j=1}^{K} x_j(\alpha_j + \gamma_j m_j).$$

Let $\bar{\alpha} := \sum_j x_j \alpha_j$ and $S := \sum_j x_j \gamma_j$. From Lemma 2,

$$\mathbb{E}[m_j \mid m_k] = \rho m_k \qquad (j \neq k).$$

Therefore

$$\mathbb{E}[A \mid m_k] = \bar{\alpha} + \big[\rho S + (1-\rho) x_k \gamma_k\big] m_k. \tag{28}$$

For a provider-k client, the objective in (24) is strictly concave in a. The first-order condition is

$$2\beta a = \psi + \beta c + \xi m_k + d\,\mathbb{E}[A \mid m_k].$$

Substituting (28) and matching constant and slope terms gives

$$2\beta \alpha_k = \psi + \beta c + d\bar{\alpha}, \tag{29}$$

$$2\beta \gamma_k = \xi + d\big[\rho S + (1-\rho) x_k \gamma_k\big]. \tag{30}$$

The right-hand side of (29) is common across providers, so all intercepts coincide. With $\bar{\alpha} = \alpha$,

$$(2\beta - d)\alpha = \psi + \beta c,$$

which proves (26).

For the slopes, define

$$D_k := 2\beta - d(1-\rho) x_k, \qquad \Lambda(x) := \sum_{k=1}^{K} \frac{x_k}{D_k}.$$

Rearranging (30) gives

$$D_k \gamma_k = \xi + d\rho S, \qquad \gamma_k = \frac{\xi + d\rho S}{D_k}.$$

Multiplying by x_k and summing over k yields

$$S = (\xi + d\rho S)\Lambda(x),$$

so

$$S = \frac{\xi \Lambda(x)}{1 - d\rho \Lambda(x)}.$$

Substitution back into the expression for γ_k gives (27).

It remains only to verify that the denominator is positive. Since $0 < d < \beta$ and $x_k \leq 1$,

$$D_k \geq 2\beta - d(1-\rho) > 0, \qquad \Lambda(x) \leq \frac{1}{2\beta - d(1-\rho)}.$$

Hence

$$d\rho \Lambda(x) \leq \frac{d\rho}{2\beta - d(1-\rho)} < 1,$$

because $2\beta - d(1-\rho) - d\rho = 2\beta - d > 0$. The affine system is therefore well defined and unique. $\square$

Define

$$B_{2t} := \sum_{k=1}^{K} x_k \gamma_{kt}^2, \qquad Q_t := \sum_{k=1}^{K} x_k^2 \gamma_{kt}^2, \qquad \Delta_t^2 := \sum_{k=1}^{K} x_k (a_{kt} - A_t)^2.$$

In the affine delegated equilibrium, the aggregate action moments are

$$\operatorname{Cov}(A_t, \theta_t) = \mathcal{V}_t \mathcal{S}_t, \tag{31}$$

$$\operatorname{Var}(A_t) = \rho_t \mathcal{V}_t \mathcal{S}_t^2 + (1-\rho_t)\mathcal{V}_t Q_t, \tag{32}$$

$$\mathbb{E}[\Delta_t^2] = \mathcal{V}_t \big[B_{2t} - \rho_t \mathcal{S}_t^2 - (1-\rho_t) Q_t\big]. \tag{33}$$

These identities follow by substituting the affine rule into A_t and using the posterior decomposition in Lemma 2.

Proposition 2 (Concentration and responsiveness)**.** *Fix (τ_g, τ_y). Under any majorization-increasing perturbation of the provider-share vector x:*

(i) the unconditional mean action $\mathbb{E}[A_t] = \alpha_t$ is invariant;

(ii) the common-response object $\mathcal{S}_t$, and therefore $\operatorname{Cov}(A_t, \theta_t)$, is weakly increasing;

(iii) the common component $\rho_t \mathcal{V}_t \mathcal{S}_t^2$ and total variance $\operatorname{Var}(A_t)$ are weakly increasing.

Along the dominant-provider family

$$x(x_D) = \left(x_D, \frac{1-x_D}{K-1}, \dots, \frac{1-x_D}{K-1}\right), \qquad x_D \in [1/K, 1],$$

the increases in parts (ii) and (iii) are strict for interior $x_D > 1/K$.

Proof of Proposition 2. The intercept in (26) is independent of x, and $\mathbb{E}[m_{kt}] = 0$, so $\mathbb{E}[A_t] = \alpha_t$.

Fix (τ_g, τ_y), so ρ_t and $\mathcal{V}_t$ are fixed. Let

$$c_t^\rho := d_t(1-\rho_t), \qquad f(x) := \frac{x}{2\beta_t - c_t^\rho x}.$$

Since

$$f''(x) = \frac{4\beta_t c_t^\rho}{(2\beta_t - c_t^\rho x)^3} > 0,$$

$\Lambda_t(x) = \sum_k f(x_k)$ is Schur-convex by Karamata's inequality. The map

$$z \mapsto \frac{\xi_t z}{1 - d_t \rho_t z}$$

is increasing on the admissible domain, so $\mathcal{S}_t$ is weakly increasing under any majorization-increasing perturbation of x. Equation (31) then implies that $\operatorname{Cov}(A_t, \theta_t)$ is weakly increasing as well.

For the variance term, write

$$Q_t = \frac{\xi_t^2}{(1 - d_t \rho_t \Lambda_t(x))^2} \sum_{k=1}^{K} \frac{x_k^2}{(2\beta_t - c_t^\rho x_k)^2}.$$

Let $g(x) := x/(2\beta_t - c_t^\rho x)$. Since g, g', and g'' are positive on the admissible domain, $(g^2)'' = 2(g'^2 + g\,g'') > 0$, so g^2 is convex. The symmetric sum $\sum_k g(x_k)^2$ is therefore Schur-convex by Karamata's inequality, and weakly increases under any majorization-increasing perturbation of x. The multiplicative factor $(1 - d_t\rho_t\Lambda_t(x))^{-2}$ is positive and increasing in $\Lambda_t(x)$, which itself weakly increases under the same perturbation. A product of two non-negative quantities, each weakly increasing along a given perturbation, is itself weakly increasing along that perturbation, so Q_t is weakly increasing. Equation (32) then implies that total variance is weakly increasing; the common component $\rho_t\mathcal{V}_t\mathcal{S}_t^2$ rises because $\mathcal{S}_t$ rises.

Along the dominant-provider family, the convex primitives are strictly convex and x_D moves strictly away from the equal-share vector, so the increases in $\mathcal{S}_t$, the common component, and total variance are strict for interior $x_D > 1/K$. □

A.3. Consumer Welfare and Provider Concentration

The concentration result in Proposition 2 concerns the aggregate action. To translate it into a statement about consumers we add a price-formation map and a consumer-welfare standard. Throughout, (τ_g, τ_y) are held fixed, so the posterior variance $\mathcal{V}_t$ and cross-provider correlation ρ_t from Lemma 2 are fixed, and only the provider-share vector x varies.

Assumption 3 (Price formation and consumer standard)**.**

(W1) (Affine near-margin pass-through.) *The regional clearing price is affine and increasing in the aggregate near-margin action,*

$$P_t = \omega_0 + \omega_1 A_t, \qquad \omega_1 > 0.$$

(W2) (Exposure.) *Consumer load is weakly higher in scarcer states, $D_t = D_0 + \upsilon\,\theta_t$ with $\upsilon \geq 0$ and D_0 large enough that $D_t > 0$ on the relevant range; only the moments $\mathbb{E}[D_t] = D_0$ and $\mathrm{Cov}(D_t, \theta_t) = \upsilon/\tau_\theta$ enter below.*

(W3) (Consumer loss.) *Period consumer loss is expected payment plus a convex price-risk penalty,*

$$\mathcal{L}_t = P_t D_t + \tfrac{\kappa}{2}\big(P_t - \mathbb{E}P_t\big)^2, \qquad \kappa \geq 0.$$

Lemma 3 (Aggregate action moments)**.** *In the affine delegated equilibrium of Proposition 1, with $\mathbb{E}[\theta_t] = 0$ and $Q_t := \sum_k x_k^2\gamma_{kt}^2$,*

$$\mathbb{E}[A_t] = \alpha_t, \qquad \mathrm{Cov}(A_t, \theta_t) = \mathcal{V}_t\mathcal{S}_t, \qquad \mathrm{Var}(A_t) = \mathcal{V}_t\big(\rho_t\mathcal{S}_t^2 + (1-\rho_t)Q_t\big).$$

Proof. By Lemma 2 write $m_{kt} = w_t + u_{kt}$, where the common component $w_t := m_{gt} + \widetilde{h}_t$ satisfies $\mathrm{Var}(w_t) = \rho_t\mathcal{V}_t$ and $\mathrm{Cov}(w_t, \theta_t) = \mathcal{V}_t$, and the u_{kt} are mean-zero, mutually independent, independent of w_t and of θ_t, with $\mathrm{Var}(u_{kt}) = (1-\rho_t)\mathcal{V}_t$ and $\mathrm{Cov}(u_{kt}, \theta_t) = 0$. Since $a_{kt} = \alpha_t + \gamma_{kt}m_{kt}$ and $\sum_k x_k = 1$,

$$A_t = \alpha_t + \mathcal{S}_t\,w_t + \sum_k x_k\gamma_{kt}u_{kt}, \qquad \mathcal{S}_t = \sum_k x_k\gamma_{kt}.$$

Taking expectations gives $\mathbb{E}[A_t] = \alpha_t$. Since $\mathrm{Cov}(u_{kt}, \theta_t) = 0$, $\mathrm{Cov}(A_t, \theta_t) = \mathcal{S}_t \mathrm{Cov}(w_t, \theta_t) = \mathcal{V}_t \mathcal{S}_t$. By independence of w_t and $\{u_{kt}\}$, $\mathrm{Var}(A_t) = \mathcal{S}_t^2 \mathrm{Var}(w_t) + \sum_k x_k^2 \gamma_{kt}^2 \mathrm{Var}(u_{kt}) = \mathcal{V}_t \big(\rho_t \mathcal{S}_t^2 + (1-\rho_t) Q_t\big)$. These coincide with (31)–(32). □

Proposition 3 (Concentration raises expected consumer loss). *Under the affine delegated equilibrium and Assumption 3, expected consumer loss decomposes as*

$$\mathbb{E}[\mathcal{L}_t] = \; L_0 \; + \; \underbrace{\omega_1 \upsilon \, \mathcal{V}_t \mathcal{S}_t}_{\text{(I) state amplification}} \; + \; \underbrace{\tfrac{\kappa}{2} \, \omega_1^2 \, \mathcal{V}_t \big(\rho_t \mathcal{S}_t^2 + (1-\rho_t) Q_t\big)}_{\text{(II) price variance}}, \tag{34}$$

where $L_0 := \omega_0 D_0 + \omega_1 D_0 \alpha_t$ is independent of x. Terms (I) *and* (II) *equal* $\mathrm{Cov}(P_t, D_t)$ *and* $\frac{\kappa}{2}\mathrm{Var}(P_t)$*, respectively. The mean price $\mathbb{E}[P_t] = \omega_0 + \omega_1 \alpha_t$ is invariant to x, and along any majorization-increasing (concentration-increasing) change in x both* (I) *and* (II) *weakly increase, so $\mathbb{E}[\mathcal{L}_t]$ weakly increases; the increase is strict along the dominant-provider family $x(x_D)$ for interior $x_D \in (1/K, 1)$.*

Proof. First, by Proposition 1, $\alpha_t = (\psi_t + \beta_t c_t)/(2\beta_t - d_t)$ is independent of x, and $\mathbb{E}[m_{kt}] = 0$; hence $\mathbb{E}[A_t] = \alpha_t$ and $\mathbb{E}[P_t] = \omega_0 + \omega_1 \alpha_t$ are independent of x.

Second, using (W1)–(W2), $\mathbb{E}[\theta_t] = 0$, and Lemma 3,

$$\mathbb{E}[P_t D_t] = \mathbb{E}\big[(\omega_0 + \omega_1 A_t)(D_0 + \upsilon \theta_t)\big] = \omega_0 D_0 + \omega_1 D_0 \alpha_t + \omega_1 \upsilon \, \mathrm{Cov}(A_t, \theta_t) = L_0 + \omega_1 \upsilon \, \mathcal{V}_t \mathcal{S}_t,$$

and $\omega_1 \upsilon \, \mathcal{V}_t \mathcal{S}_t = \mathrm{Cov}(P_t, D_t)$.

Third, by (W3) and Lemma 3,

$$\tfrac{\kappa}{2} \mathbb{E}\big[(P_t - \mathbb{E}P_t)^2\big] = \tfrac{\kappa}{2} \mathrm{Var}(P_t) = \tfrac{\kappa}{2} \omega_1^2 \mathrm{Var}(A_t) = \tfrac{\kappa}{2} \omega_1^2 \mathcal{V}_t \big(\rho_t \mathcal{S}_t^2 + (1-\rho_t) Q_t\big).$$

Adding the two terms gives (34).

Finally, by Proposition 2(ii)–(iii), under a majorization-increasing change in x (with $\mathcal{V}_t, \rho_t$ fixed) both $\mathcal{S}_t$ and $\mathrm{Var}(A_t) = \mathcal{V}_t(\rho_t \mathcal{S}_t^2 + (1-\rho_t) Q_t)$ are weakly increasing, strictly so along $x(x_D)$ for interior x_D. Since $\omega_1 > 0$ and $\upsilon, \kappa, \mathcal{V}_t \geq 0$, terms (I) and (II) are weakly (strictly) increasing while L_0 is constant; hence $\mathbb{E}[\mathcal{L}_t]$ is weakly (strictly) increasing. □

Proposition 3 shows that all welfare consequences of concentration are driven by the two second moments in (34). If $\upsilon = \kappa = 0$ then $\mathbb{E}[\mathcal{L}_t] = L_0$ is invariant to x: because the mean action is invariant (Proposition 2(i)), provider concentration is welfare-neutral for a risk-neutral consumer facing inelastic demand and linear pricing. Channel (I) only needs demand to co-move with scarcity ($\upsilon > 0$): concentration makes the clearing price track scarcity more tightly ($\mathrm{Cov}(P_t, \theta_t) = \omega_1 \mathcal{V}_t \mathcal{S}_t$ rises), so consumers pay more precisely when they consume more. Channel (II) additionally requires a convex/risk-averse consumer standard ($\kappa > 0$): concentration raises aggregate price variance, and specifically its common component $\rho_t \mathcal{V}_t \mathcal{S}_t^2$.

Combining (32)–(33) yields the identity

$$\mathrm{Var}(A_t) = \mathcal{V}_t B_{2t} - \mathbb{E}[\Delta_t^2], \qquad \mathcal{V}_t B_{2t} = \sum_k x_k \mathrm{Var}(a_{kt}),$$

so Channel (II) equals $\frac{\kappa}{2}\omega_1^2\big(\sum_k x_k \mathrm{Var}(a_{kt}) - \mathbb{E}[\Delta_t^2]\big)$. That is, the aggregate price risk borne by consumers is the share-weighted average provider-level bid variance net of cross-provider dispersion $\mathbb{E}[\Delta_t^2]$. Concentration raises the aggregate by reallocating variance from the diversifying cross-provider dispersion into the common component. This is the counterpart, in the auction setting, of the cross-seller price-correlation channel in Aleksenko and Miklós-Thal (2026). Channel (I) is the corresponding counterpart of their across-state price-dispersion channel.

B. Empirical Appendix

B.1. Synchronisation Detail by Market Family

This appendix reports the synchronisation and concentration results for the market families summarised in Section 3.2. Table B1 gives the pre- and post-ERI pair-type correlations underlying the SPSR-minus-SPDR estimates of Table 3, for the three market families outside energy discharge: energy charge, raise FCAS, and lower FCAS. Reading the levels alongside the differences shows where a relative increase reflects a rise in same-region co-movement and where it reflects a flat or falling same-provider different-region baseline; in FCAS the different-region correlation is already high before the reform and changes little after it. Table B2 repeats the upper-band-price concentration exercise of Table 5 across the same market families. The association between installed provider HHI and synchronisation is concentrated in energy discharge, while the association with bid-price variance is present in FCAS as well.

Table B1: Detailed synchronisation correlations outside energy discharge

Market family	Outcome	SPSR pre	SPSR post	SPDR pre	SPDR post	Δ gap	DiD estimate
Energy charge	Bid-band index	0.332	0.378	0.174	0.135	0.085	+0.085*** (0.016)
	Upper-band price	0.352	0.415	0.091	0.057	0.097	+0.087 (0.070)
	Lower-band price	0.180	0.287	0.088	0.103	0.091	+0.091*** (0.025)
	Rebid timing	0.216	0.354	0.196	0.252	0.081	+0.081*** (0.017)
Raise FCAS	Bid-band index	0.153	0.270	0.116	0.081	0.151	+0.151*** (0.019)
	Upper-band price	0.156	0.230	0.074	0.066	0.081	+0.081*** (0.021)
	Lower-band price	0.299	0.298	0.231	0.123	0.107	+0.107*** (0.022)
	Rebid timing	0.325	0.411	0.318	0.317	0.087	+0.087*** (0.027)
Lower FCAS	Bid-band index	0.265	0.397	0.212	0.120	0.224	+0.224*** (0.017)
	Upper-band price	0.061	0.268	0.120	0.032	0.295	+0.295*** (0.021)
	Lower-band price	0.328	0.352	0.276	0.208	0.092	+0.092*** (0.020)
	Rebid timing	0.337	0.410	0.315	0.316	0.072	+0.072*** (0.027)

Notes: Entries are raw Pearson correlations, not Fisher-transformed correlations. Pre/post columns are simple averages of daily pair-type means. Δ gap is the post-minus-pre change in the SPSR–SPDR correlation gap. The DiD estimate is from group-by-day regressions with pair-type and trading-date fixed effects. Standard errors, in parentheses, are clustered by trading date. $^{***}p < 0.01$, $^{**}p < 0.05$, $^{*}p < 0.10$.

B.2. State-Responsive Bidding Checks

This appendix gives the specification behind the common-state result in Section 3.2 and reports the companion own-state check. Let z_{rt} denote public regional battery scarcity, measured as one minus the regional SoC share and standardised within region-by-trading period using the pre-ERI window. We split this signal into a tight-state component $T_{rt} = \max\{z_{rt}, 0\}$ and a loose-state

Table B2: Provider concentration, synchronisation, and variance across market families

	Synchronisation		Market-action variance		
Market family	Local sync	SPSR sync	Local sync	Provider HHI	N
Energy discharge	+0.161*** (0.021)	+0.169*** (0.018)	+0.183 (0.882)	+1.084*** (0.378)	738
Energy charge	-0.017 (0.057)	-0.021 (0.055)	-0.581 (0.784)	-0.947** (0.443)	258
Raise FCAS	-0.026* (0.016)	+0.005 (0.015)	+4.049*** (0.943)	+1.666*** (0.320)	951
Lower FCAS	-0.065*** (0.015)	-0.040*** (0.015)	+1.016 (0.993)	+2.203*** (0.384)	957

Notes: The outcome is the upper-band price in each bid-stack family. The first two columns report coefficients from regressions of local synchronisation and SPSR synchronisation on installed provider HHI. The next two columns report coefficients from regressions of within-day market-action variance on local sync and installed provider HHI. Provider HHI is scaled so one unit equals a ten percentage point HHI increase. Market-action variance is reported in millions of squared AUD/MWh. All specifications include trading-date fixed effects, omit region fixed effects because installed HHI is fixed within region, and cluster standard errors by trading date. Columns using synchronisation outcomes are weighted by SPSR pair-days; variance columns are weighted by market intervals. $^{***}p < 0.01$, $^{**}p < 0.05$, $^{*}p < 0.10$.

component $L_{rt} = \max\{-z_{rt}, 0\}$. For each evening window h, we estimate

$$Y_{irt} = \alpha_i + \gamma_{rd} + \mu_{rp} + \sum_{m \neq -1} \left(\delta^T_{mh} T_{rt} + \delta^L_{mh} L_{rt}\right) \mathbb{1}\{m(t) = m\} + G_h(\mathrm{SoC}_{it}, m(t)) + \varepsilon_{irt}, \quad (35)$$

where Y_{irt} is a quantity-weighted bid-price outcome, α_i are battery fixed effects, γ_{rd} are region-by-date fixed effects, μ_{rp} are region-by-period fixed effects, and $G_h(\mathrm{SoC}_{it}, m(t))$ collects own-SoC controls and their event-study interactions. The reported object is the post-ERI average of $\delta^T_{mh} - \delta^L_{mh}$: the change in the loading of bids on scarce states relative to abundant states.

The full common-state table by window and band group, including the results summarised in Section 3.2, is Table 4 in the main text.

The own-SoC specification replaces the public scarcity loading in (35) with phase-specific slopes on the battery's own reconstructed state of charge, again interacted with event months. This exercise validates that the same bid-stack outcomes respond to the dynamic state that determines the opportunity cost of stored energy.

Table B3: Post-ERI own-SoC bid conditioning across markets

Market family	Phase	All bands	Upper bands	Lower bands
Energy discharge	Lead-in	3,288*** (849)	4,960*** (829)	-953*** (126)
	Peak-early	3,947*** (1,022)	6,003*** (1,051)	-264*** (82)
	Peak-late	-2,284* (1,182)	-1,247 (1,481)	231 (196)
	Post-peak	-2,342** (1,075)	-718 (1,387)	417 (317)
Energy charge	Lead-in	992*** (272)	1,235** (496)	-125** (57)
	Peak-early	-193 (221)	-867 (860)	-164*** (54)
	Peak-late	-68 (366)	-615 (1,063)	353*** (96)
	Post-peak	-2 (339)	854 (904)	344*** (79)
Raise FCAS	Lead-in	6,657*** (746)	6,692*** (817)	-4*** (1)
	Peak-early	5,964*** (832)	7,011*** (906)	-3*** (1)
	Peak-late	-1,015 (1,220)	1,045 (1,293)	-3*** (1)
	Post-peak	-1,525 (1,237)	353 (1,269)	-3*** (1)
Lower FCAS	Lead-in	6,186*** (776)	5,571*** (674)	-3*** (1)
	Peak-early	5,236*** (869)	3,677*** (732)	-1 (1)
	Peak-late	-312 (1,092)	-164 (1,415)	-2** (1)
	Post-peak	-1,770* (1,046)	-1,020 (1,141)	-2*** (1)

Notes: Entries are post-ERI average changes in the slope of bid prices on own SoC, in AUD/MWh for a 0-to-1 SoC change. Specifications include battery fixed effects and region-by-period-by-date fixed effects. Standard errors are clustered by trading date, matching Regression 3.

Table B3 shows strong own-state responsiveness in the same windows in which the common-state result is economically relevant. For energy discharge, the post-ERI slope of upper bid prices on own SoC is $4{,}960$ AUD/MWh in the lead-in window and $6{,}003$ AUD/MWh in the early-peak window. Lower-band discharge prices move in the opposite direction over the same intervals.

B.3. Bellman Estimation and Deviation Valuation

This appendix describes the dynamic value-function estimates used to price the opportunity cost of state-of-charge changes in the recleared deviation analysis. The implementation builds on the battery and FCAS optimisation implementation of Karimi-Arpanahi et al. (2024), Prakash et al. (2025), Butters et al. (2021), and Australian Energy Market Operator (2021).

State space. Time within a trading day is indexed by $\tau \in \{1, \dots, T\}$ with $\Delta = 5/60$ hours. For each region r we estimate a mean price profile $\bar{p}_{r,h}$ on the trailing window, where $h \equiv h(\tau)$ is the hour-of-day bin. The realised regional price decomposes as

$$p_{rt} = \bar{p}_{r,h(t)} + \varepsilon_{rt}, \qquad \varepsilon_{rt} \in \{e_{r1}, \dots, e_{rN_p}\}, \tag{36}$$

with the residual ε_{rt} discretised into N_p price bins by empirical quantiles of the same window; we write k_t for the active bin index. The exogenous transition kernel for the discretised residual price is

$$k_{t+1} \sim \widehat{P}_{r,b(t),z_t,\sigma_t}(k_t, \cdot), \tag{37}$$

where $b(t) \in \{\text{morning}, \text{peak1}, \text{peak2}\}$ is the time-of-day block, z_t is a three-level regional residual-demand state, and σ_t is a four-level aggregate battery-SoC signal (low/mid/high SoC tertile, plus an unconditional fallback). Transitions are estimated non-parametrically from the trailing window separately for each (r, b, z, σ) group, with a fallback chain that successively pools σ and then z when group support is thin; the fallback status of each visited group is recorded in the transition diagnostics below.

The endogenous state is the own state of charge $S_{i,t} \in [0, \bar{S}_i]$. We write dispatch in signed form q_{it}, with $q_{it} > 0$ for discharge and $q_{it} < 0$ for charge, and decompose $q_{it} = q_{it}^+ - q_{it}^-$ where $q_{it}^+ := \max\{q_{it}, 0\}$ and $q_{it}^- := \max\{-q_{it}, 0\}$. Using the same calibrated asset parameters as the SoC reconstruction in Appendix B.5, the stock-flow recursion is

$$S_{i,t+1} = \rho_i \, S_{it} - \kappa_{it} \, \Delta - \frac{q_{it}^+ \, \Delta}{\eta_i^{\text{dis}}} + q_{it}^- \, \eta_i^{\text{ch}} \, \Delta, \qquad 0 \le S_{i,t+1} \le \bar{S}_i. \tag{38}$$

The parasitic drain κ_{it} is split into a constant aux-load component α_i and an FCAS-attributable component $\beta_i F_{it}$ that scales with expected enabled FCAS MW at the operating point, using the typical-utilisation decomposition documented in Karimi-Arpanahi et al. (2024).

Flow payoff and FCAS headroom values. Conditional on the operating point q_{it} and the next-period state $S_{i,t+1}$, the per-interval flow payoff under the energy-and-FCAS market scope is

$$\pi_i(S_{it}, S_{i,t+1}, k_t, \tau) = q_{it}\, p_{rt}\, \Delta - c_i\, |q_{it}|\, \Delta + \sum_m a^m_{ibzk}\, H^m_i(q_{it}, S_{i,t+1})\, \Delta, \tag{39}$$

where c_i is a throughput (wear) cost in AUD/MWh, $H^m_i(q, S')$ is the physical raise- or lower-headroom that the battery can deliver for FCAS service m at (q, S') subject to the trapezium and energy-duration constraints of Appendix B.13, and a^m_{ibzk} is the estimated FCAS revenue per MWh of physical headroom for service m in the (b, z, k) group. The a^m_{ibzk} coefficients are estimated on the trailing window from the NEMDE/FCAS clearing logic of Australian Energy Market Operator (2021) and Karimi-Arpanahi et al. (2024), using a hierarchical fallback chain that backs off from the full $\{$battery $\times$ block $\times\ z \times k\}$ group to coarser pools when within-group observations are thin. Optional shrinkage towards the parent group and upper-tail winsorisation are available but are disabled in the production configuration reported here.

Bellman recursion and shadow value. For each battery i, signal state σ, residual-demand state z, and trading day, the value function $V^{\sigma z}_{i\tau}$ is obtained by backward induction on

$$V^{\sigma z}_{i\tau}(S, k) = \max_{S' \in \Gamma_i(S)} \left\{ \pi_i(S, S', k, \tau) + \delta \sum_\ell \widehat{P}_{r,b(\tau),\sigma,z}(k, \ell)\, V^{\sigma z}_{i,\tau+1}(S', \ell) \right\}, \tag{40}$$

with $\delta = 1$ within the trading day (intraday discounting is negligible at 5-minute resolution) and a terminal value $V^{\sigma z}_{i,T+1}(\cdot, \cdot)$ taken from an overnight-value profile estimated on the trailing window. The feasibility correspondence $\Gamma_i(S)$ enforces the SoC bounds and the asset's discharge and charge power limits.

The shadow value of stored energy is the derivative of V with respect to own SoC,

$$\nu_{it} := \left. \frac{\partial V^{\sigma_t z_t}_{i\tau}(S, k_t)}{\partial S} \right|_{S = S_{it}}, \qquad \widehat{m}_{it} := \frac{\max\{\nu_{it}, 0\}}{\eta^{\text{dis}}_i} + c_i. \tag{41}$$

The non-negativity floor reflects the fact that storage value is never negative for a battery with the option to wait; the discharge-efficiency adjustment converts the SoC shadow value into a per-MWh marginal cost of discharge at the meter; and adding c_i folds in the throughput cost. The quantity $\widehat{m}_{it}$ is the per-MWh dynamic opportunity cost used in the deviation reclearing of Section 3.3 and in the conduct test of Section 3.4.

Rolling estimation. The Bellman is re-estimated each week on a 90-day trailing window. For anchor date a, the estimation window is $[a - 90,\ a - 1]$ and the target week of evaluated intervals is $[a,\ a + 6]$. Within an anchor, we sequentially construct the regional mean price profile, residual-price bin edges, transition kernel with group fallbacks, FCAS headroom-value coefficients, and an overnight terminal value; we then solve the backward induction (40) and evaluate the value function only at the target-week intervals required by the deviation panel. The production configuration uses $N_p = 11$ residual-price bins, $N_S = 41$ own-SoC grid points, and 201 candidate next-period SoC controls per interval; sensitivity tests at $N_S = 21$ and 501 controls shift $\widehat{m}_{it}$ by less than

11 AUD/MWh, well below its typical magnitude. The estimated value functions currently cover 2025-04-01 13:05 through 2026-02-02 21:55, from 44 successful weekly anchors and three failed anchors at 2026-02-03, 2026-02-10, and 2026-02-17. Table B4 reports the coverage by month and asset.

Table B4: Bellman rolling-pipeline coverage

Item	Value
Weekly anchors attempted	47
Weekly anchors successful	44
Weekly anchors failed	3
Date range of evaluated intervals	2025-04-01 13:05 – 2026-02-02 21:55
Regions covered	4
Batteries (DUIDs) covered	51
Battery-intervals evaluated	1,379,979
Battery-intervals pre-ERI / post-ERI	335,552 / 1,044,427
Share of intervals with non-missing $\widehat{m}_{it}$	100.0%
Share of intervals with $\lambda_{it} = 0$ (option-value floor)	13.8%

Notes: Coverage of the rolling weekly Bellman estimation. Failed anchors: 2026-02-03, 2026-02-10, 2026-02-17. $\lambda_{it} = 0$ indicates intervals at which the implied shadow value is non-positive and the option-value floor binds; $\widehat{m}_{it}$ is the corresponding throughput cost c_i.

Table B5 reports the asset-level calibration parameters used by the DP, alongside SoC RMSE and bias on the calibration window. These parameters are inherited from the SoC reconstruction in Appendix B.5; the table is included here so that the Bellman appendix is self-contained.

Table B5: Bellman asset and SoC calibration parameters by battery

DUID	Region	$\bar{S}_i$ (MWh)	$\bar{P}_i^{\text{dis}}$ (MW)	$\bar{P}_i^{\text{ch}}$ (MW)	η_i^c	η_i^d	κ_i (MW)	RMSE (% $\bar{S}_i$)	Bias (% $\bar{S}_i$)
BHB1	NSW1	50.0	49.7	45.2	0.999	0.999	0.257	0.1	-0.0
CAPBES1	NSW1	199.9	100.0	91.6	0.999	0.999	0.318	0.1	-0.0
DPNTB1	NSW1	46.5	25.0	25.0	0.923	0.923	0.000	0.1	-0.0
LDBESS1	NSW1	1086.2	75.1	74.7	0.952	0.952	5.000	0.0	-0.0
LIMBESS1	NSW1	534.6	50.0	50.8	0.999	0.999	1.904	0.1	-0.0
ORABESS1	NSW1	1660.0	43.2	48.0	0.889	0.889	0.313	0.0	0.0
QBYNB1	NSW1	15.2	10.0	9.3	0.994	0.994	0.047	0.1	0.0
QPSFB2	NSW1	40.0	3.0	19.0	0.900	0.900	0.000	0.0	-0.0
RESS1	NSW1	117.1	60.0	60.0	0.917	0.917	0.165	0.0	0.0
RIVNB2	NSW1	126.4	65.0	65.0	0.922	0.922	0.185	0.1	-0.0
SMTHBES1	NSW1	130.0	65.0	65.0	0.999	0.999	0.589	0.1	-0.0
WALGRV1	NSW1	78.0	49.2	46.2	0.961	0.961	0.095	0.1	-0.0
WTAHB1	NSW1	1154.0	638.0	299.7	0.927	0.927	1.732	0.1	-0.0
BBATTERY1	QLD1	95.6	50.0	50.0	0.985	0.985	0.257	0.0	-0.0
BRNDBES1	QLD1	410.0	205.0	205.0	0.980	0.980	0.888	0.1	-0.0
CHBESS1	QLD1	197.2	100.0	99.9	0.954	0.954	0.452	0.1	-0.0
GREENB1	QLD1	400.0	199.5	199.3	0.979	0.979	1.816	0.0	-0.0
KEPBG1	QLD1	4.0	2.0	0.0	0.949	0.949	0.000		
SNB01	QLD1	544.3	260.0	248.3	0.901	0.901	0.373	0.1	0.0

Continued on next page

DUID	Region	$\bar{S}_i$ (MWh)	$\bar{P}_i^{\mathrm{dis}}$ (MW)	$\bar{P}_i^{\mathrm{ch}}$ (MW)	η_i^c	η_i^d	κ_i (MW)	RMSE (% $\bar{S}_i$)	Bias (% $\bar{S}_i$)
SWANBBF1	QLD1	410.5	248.8	236.1	0.896	0.896	0.536	0.1	-0.0
TARBESS1	QLD1	600.0	300.0	299.2	0.999	0.999	2.970	0.1	-0.0
ULPBESS1	QLD1	298.0	155.0	153.2	0.999	0.999	3.976	0.1	-0.0
WANDB1	QLD1	150.0	90.1	74.9	0.977	0.977	0.976	0.1	-0.0
WDBESS1	QLD1	400.0	254.9	253.6	0.999	0.999	0.968	0.2	-0.1
WDBESS2	QLD1	510.0	255.0	255.0	0.999	0.999	2.289	0.1	-0.0
ADPBA1	SA1	6.0	6.1	6.0	0.999	0.999	0.002	0.5	-0.4
BLYTHB1	SA1	400.0	199.9	199.1	0.999	0.999	2.293	0.1	-0.0
BOWWBA1	SA1	2.0	2.0	2.0	0.999	0.999	0.000	0.7	-0.6
BUNGAMB1	SA1	300.0	30.0	25.4	0.999	0.999	4.354	0.0	-0.0
CBWWBA1	SA1	2.0	2.0	2.0	0.999	0.999	0.000	0.6	-0.5
CGBESS01	SA1	120.0	20.1	20.2	0.999	0.999	2.297	0.0	-0.0
DALNTH1	SA1	11.7	10.0	6.0	0.927	0.927	0.149	0.1	0.0
HPR1	SA1	169.5	80.0	80.6	0.980	0.980	0.865	0.0	-0.0
HVWWBA1	SA1	4.0	4.0	4.0	0.999	0.999	0.000	0.6	-0.5
LBB1	SA1	43.4	24.1	24.3	0.951	0.951	0.000	0.0	-0.0
LGAPBS1	SA1	10.0	9.0	13.0	0.898	0.898	0.086	0.0	0.0
MANNUMB1	SA1	200.0	99.8	99.8	0.958	0.958	0.343	0.1	-0.0
TB2B1	SA1	41.0	40.5	38.6	0.999	0.999	0.339	0.1	-0.0
TEMPB1	SA1	285.0	111.0	111.0	0.999	0.999	2.019	0.1	-0.0
TIB1	SA1	250.0	152.7	184.0	0.993	0.993	2.338	0.1	-0.0
BALB1	VIC1	28.4	30.0	30.0	0.959	0.959	0.071	0.1	-0.0
BULBES1	VIC1	31.9	19.9	20.0	0.952	0.952	0.022	0.1	-0.0
GANNB1	VIC1	37.2	25.3	25.3	0.928	0.928	0.000	0.1	-0.0
HBESS1	VIC1	150.0	149.3	141.0	0.999	0.999	1.175	0.1	-0.0
KESSB1	VIC1	370.0	185.0	185.0	0.758	0.758	0.000	0.4	-0.1
LVES1	VIC1	200.0	100.0	100.0	0.999	0.999	1.084	0.1	-0.0
MREHA1	VIC1	400.0	200.0	200.0	0.974	0.974	0.152	0.1	-0.0
MREHA2	VIC1	400.0	199.7	199.8	0.964	0.964	0.457	0.1	-0.0
MREHA3	VIC1	800.0	200.0	200.0	0.992	0.992	1.074	0.0	-0.0
PIBESS1	VIC1	11.5	5.0	5.0	0.952	0.952	0.009	0.1	-0.0
RANGEB1	VIC1	400.0	200.0	200.0	0.943	0.943	0.000	0.1	-0.0
VBB1	VIC1	450.0	221.0	233.3	0.933	0.933	0.000	0.2	0.1

Notes: Per-battery parameters used in the Bellman recursion. $\bar{S}_i$ is the energy capacity used in the DP, $\bar{P}_i^{\mathrm{dis}}$ and $\bar{P}_i^{\mathrm{ch}}$ the discharge and charge power limits, η_i^c and η_i^d the charge and discharge efficiencies, and κ_i the calibrated parasitic drain in MW (which the DP decomposes into a constant aux-load component and an FCAS-attributable component scaling with expected enabled FCAS MW). RMSE and bias are evaluated on the un-anchored post-ERI calibration window and expressed as a percentage of $\bar{S}_i$.

Table B6 reports the distribution of $\widehat{m}_{it}$ across battery-intervals, summarised by time block, own-SoC bin, and aggregate market-SoC bin. Consistent with the dynamic arbitrage logic in Section 2, the median rises in the evening-peak block and falls when both own and market SoC are high; the lowest values cluster in intervals with high own SoC and high market SoC, where storage value is small and the option-value floor frequently binds.

Transition diagnostics. Table B7 reports kernel quality pooled across anchors. Row-sum errors on the unconditional kernel are machine-zero; the table also reports the minimum group counts

Table B6: $\widehat{m}_{it}$ summary by block and SoC bin

Time block	Own SoC	Market SoC bin: Low	Mid	High
Peak 1 (09–15)	Low	95 [48, 148]	74 [33, 113]	58 [19, 86]
Peak 1 (09–15)	Mid	58 [19, 94]	35 [1, 79]	9 [1, 46]
Peak 1 (09–15)	High	5 [1, 37]	1 [1, 38]	1 [1, 18]
Peak 2 (15–22)	Low	151 [117, 212]	163 [115, 269]	97 [74, 140]
Peak 2 (15–22)	Mid	131 [101, 174]	132 [89, 193]	74 [37, 120]
Peak 2 (15–22)	High	95 [53, 135]	93 [37, 149]	38 [1, 88]

Notes: Median $\widehat{m}_{it}$ in AUD/MWh with 25th and 75th percentiles in brackets, computed across all battery-intervals in the rolling evaluation panel. Own SoC is the battery's lagged stored-energy share; market SoC is the regional fleet's stored-energy share at the same interval (sum of asset-level SoC over the region, divided by the regional capacity). Bins are low/mid/high tertiles. Time block follows the Bellman conditioning convention (morning = 06:00–09:00, peak 1 = 09:00–15:00, peak 2 = 15:00–22:00; the rolling evaluation panel only retains peak 1 and peak 2 intervals).

in the unconditional, signal-conditioned, residual-demand-conditioned, and fully-conditioned versions of the kernel, which together govern the fallback chain used in solving (40).

Table B7: Transition kernel diagnostics

Conditioning of $\widehat{P}_{r,b,\sigma,z}(k,\cdot)$	Intervals	Share	Share with row support $n_{r,b,\sigma,z,k} \geq$ 30	100	1,000
Signal + residual demand ($\sigma + z$)	485,138	35.2%	93.8%	54.6%	0.2%
Residual demand only (z, σ pooled)	894,841	64.8%	98.2%	92.6%	8.6%

Notes: Transition-kernel diagnostics evaluated at the (r, b, σ, z, k) states actually visited by the rolling evaluation panel (total 1,379,979 battery-intervals). The conditioning level used at solve time is $\sigma + z$ when the aggregate-SoC signal is named (low, mid, high) and z-only otherwise. "Row support" is the number of within-window 5-min observations the kernel row was estimated from. The maximum row-sum error across visited rows is 2.2e-16 (95th percentile 1.1e-16); the share of evaluated intervals with non-missing $\widehat{m}_{it}$ is 100.0%.

FCAS diagnostics. Table B8 reports the distribution of the estimated FCAS headroom-value coefficients a^m_{ibzk} across services, together with the share of groups whose coefficients are set by a pooled-fallback estimator rather than the fully conditioned group. These objects are first-order for the Bellman because they govern how much shadow value $\widehat{m}_{it}$ is attributable to energy arbitrage versus FCAS option value.

Deviation menu. Table B9 reports the full set of operators used in the broad deviation panel of Section 3.3. Each operator is a clearing-relative reallocation that takes the bid band-group structure described in the main text as given. Shift sizes are fixed shares of the relevant offered MW and are capped by available movable MW in the source band.

Continuation values for deviation reclearing. For a sampled stack deviation d at battery-interval (i, t), exact reclearing produces a counterfactual energy operating point and FCAS enablement, hence a counterfactual next-period state of charge $S^{cf}_{i,t+1}$. We define the deviation in continuation

Table B8: FCAS headroom-value diagnostics

		Headroom value (AUD/MWh of headroom)			Pooled
Service	Cells	Median	p75	p95	fallback
Raise (all)	180,675	0.20	1.02	4.35	11.2%
Raise reg	180,675	0.09	0.58	2.35	11.2%
Raise cont	180,675	0.01	0.21	2.34	11.2%
Lower (all)	180,675	0.11	0.63	4.47	11.2%
Lower reg	180,675	0.01	0.21	1.11	11.2%
Lower cont	180,675	0.03	0.23	3.82	11.2%

Notes: Distribution of estimated FCAS headroom-value coefficients a^m_{ibzk} across (d, b, z, k) cells, pooled across the 44 successful weekly anchors. The coefficient enters the flow payoff as $a^m_{ibzk}\, H^m_i\, \Delta$ and is measured in AUD per MWh of physical headroom (MW of headroom $\times$ interval length in hours). "Cells" is the count of (battery, block, residual-demand state, residual-price bin) cells with a finite estimate. "Pooled fallback" is the share of cells whose value is set by a coarser hierarchical-fallback estimator (region-by-block-by-bin, or region-by-block) rather than the fully conditioned cell, before any optional shrinkage or upper-tail winsorization. "Raise (all)" and "Lower (all)" aggregate over regulation and contingency services within each direction.

value as

$$\Delta V_{itd} := \mathbb{E}_{\ell|k_t}\left[V_{i,t+1}(S^{cf}_{i,t+1}, \ell)\right] - \mathbb{E}_{\ell|k_t}\left[V_{i,t+1}(S^{base}_{i,t+1}, \ell)\right], \tag{42}$$

with the expectation taken under the same kernel $\widehat{P}_{r,b(t),\sigma_t,z_t}(k_t, \cdot)$ used in solving (40). The deviation's effect on owner-level total payoff is the recleared change in current energy and FCAS profit plus ΔV_{itd}, and this is the object summarised by the incentive-compatibility diagnostic in Section 3.3.

As a robustness alternative, ΔV_{itd} can be evaluated at the contemporaneous residual-price bin $\ell = k_t$ rather than averaged under the kernel. This is the natural counterpart to the information set available at the deviation interval, but it departs from the kernel used to solve (40). Table B10 reports both conventions side by side together with the contribution of ΔV_{itd} to the total recleared deviation gain.

The two conventions are economically indistinguishable on the realised deviation panel: the median absolute discrepancy in ΔV_{itd} is zero AUD across all four panels and the 90th-percentile discrepancy does not exceed $\$6$. The share of deviations whose IC classification flips between conventions is below 1.5% at the 1 AUD tolerance and near zero at the 100 AUD tolerance. The IC pre/post pattern reported in Table 6 is therefore not driven by the choice of continuation convention.

Incentive-compatibility violations by provider concentration. Table B11 splits the pre/post-ERI IC diagnostic of Table 6 by the focal battery's provider-group parked share in the same interval (Tesla, Fluence, Major-IOU, and Other), bucketed into 20-percentage-point bins. The summary statistic in each group is the share of focal battery-intervals on which the maximum owner-level deviation gain M^O_{it} across the sampled broad deviation menu exceeds a dollar threshold $\tau \in \{1, 100, 1000\}$. The pre/post drop in IC violation shares holds inside every concentration bucket and at every threshold, so the post-ERI improvement in incentive compatibility is not driven by the changing concentration mix of the deviation panel over time.

Table B9: Deviation menu for the incentive-compatibility diagnostic

Family	Deviation	Selected obs.	Evaluable obs.
Within energy	Discharge energy 8–10 → 4–7 (10%)	800	800
Within energy	Discharge energy 8–10 → 1–3 (3.5%)	800	800
Within energy	Charge energy 4–7 → 1–3 (10%)	800	800
Within FCAS	Raise FCAS 8–10 → 1–3 (2%)	800	647
Within FCAS	Lower FCAS 8–10 → 1–3 (2.5%)	800	638
Cross-market	Raise FCAS 8–10 → discharge energy 4–7 (10%)	800	422
Cross-market	Raise FCAS 8–10 → discharge energy 1–3 (3.5%)	800	418
Cross-market	Lower FCAS 8–10 → discharge energy 1–3 (3.5%)	800	405
Cross-market	Discharge energy 8–10 → raise FCAS 1–3 (3.5%)	800	647
Cross-market	Discharge energy 8–10 → lower FCAS 1–3 (3.5%)	800	632
Cross-market	Raise FCAS 8–10 → charge energy 1–3 (10%)	800	324
Cross-market	Lower FCAS 8–10 → charge energy 1–3 (10%)	800	344
Cross-FCAS	Raise FCAS 8–10 → lower FCAS 1–3 (2%)	800	681
Cross-FCAS	Lower FCAS 8–10 → raise FCAS 1–3 (2.5%)	800	611
Total		11,200	8,169

Notes: One observation is a focal battery by five-minute interval by deviation type. Selected observations are the fixed-budget counterfactual-reclearing target bank. Evaluable observations require a successful exact bid-stack edit and reclear, and a valid Bellman match for the focal battery. Shift percentages are applied to the relevant offered MW and capped by available MW in the source band.

B.4. Software Provider Identification

The empirical analysis requires a mapping from individual battery dispatch units (DUIDs) to autobidder software providers. Because AEMO registration data do not record which software platform operates a given battery, we assemble this mapping from public sources. Table B12 reports the complete result.

Each assignment carries one of two confidence levels. *Confirmed* (●) assignments rely on direct public evidence naming the software platform for a specific battery: vendor investor-relations filings (e.g., Fluence 10-K and 10-Q filings listing contracted deployments), manufacturer product pages identifying the deployed platform (e.g., Wärtsilä GEMS, Energy Vault VaultOS), or asset-owner public statements naming the provider (e.g., Iberdrola confirming Tesla Autobidder for its Australian portfolio). *Probable* (○) assignments rely on strong indirect evidence, typically the combination of hardware identification (e.g., Tesla Megapack units) with the manufacturer's known software-bundling pattern (e.g., Tesla's standard Autobidder revenue-sharing arrangement), or a market participant's known intermediary role for a portfolio of tolled assets (e.g., EnergyAustralia's intermediary function for several BESS assets). Batteries with no public evidence linking them to any provider are marked as unknown and excluded from all provider-level specifications.

Of the 60 registered battery DUIDs across the four NEM regions, 48 can be linked to a software provider: 30 with confirmed evidence and 18 with probable evidence. After consolidating the Kennedy gen-load pair into a single physical asset, harmonising provider labels, and restricting to the set of usable grid-scale batteries, the mapping yields 42 known-provider batteries served by 11 distinct providers across 21 provider-region combinations.

Table B10: Deviation-valuation diagnostics

Deviation family	Deviations	$\lvert\Delta V\rvert/$ $\lvert G^O\rvert$ (med.)	$\lvert\Delta V_{\text{exp}} - \Delta V_{\text{bin}}\rvert$ Median (AUD)	p90 (AUD)	IC-sign flip share $\tau = 1$	$\tau = 100$
Within energy	2,400	70.7%	0.00	5.41	1.42%	0.08%
Within FCAS	1,285	0.0%	0.00	0.00	0.00%	0.08%
Cross-market	3,192	0.0%	0.00	1.40	1.32%	0.13%
Cross-FCAS	1,292	0.0%	0.00	0.00	0.00%	0.00%

Notes: Diagnostics for the continuation-value contribution to the recleared deviation gain G^O_{itd}. Sample is focal-asset rows from the four broad deviation panels with valid Bellman conditioning. Column three is the median ratio $|\Delta V_{itd}|/|G^O_{itd}|$, capped at one. Columns four and five compare ΔV_{itd} evaluated under the kernel-expectation convention used in the main results ('exp') against the contemporaneous-bin convention ('bin'). The last two columns report the share of deviations whose IC classification changes across conventions at tolerance τ AUD.

Table B11: Incentive-compatibility violations by focal-provider parked share, pre/post-ERI

Provider-group parked share	Period	Intervals	Mean share	Share with $M^O_{it} > \tau$ at $\tau =$ 1 AUD	100 AUD	1,000 AUD
0–20%	Pre-ERI	631	9.1%	14.9%	2.2%	1.6%
0–20%	Post-ERI	1,218	9.1%	8.0%	0.2%	0.0%
20–40%	Pre-ERI	628	30.4%	22.6%	5.1%	1.8%
20–40%	Post-ERI	1,373	28.7%	5.5%	0.7%	0.4%
40–60%	Pre-ERI	603	48.9%	18.9%	3.8%	2.8%
40–60%	Post-ERI	801	49.6%	9.1%	0.9%	0.1%
60–80%	Pre-ERI	153	69.3%	15.7%	3.9%	3.9%
60–80%	Post-ERI	375	69.5%	8.8%	1.1%	0.0%
80–100%	Pre-ERI	167	86.3%	30.5%	28.1%	27.5%
80–100%	Post-ERI	98	85.1%	4.1%	0.0%	0.0%

Notes: Provider-group parked share is the focal battery's provider-group share of regional parked discharge capacity in the sampled interval. Provider groups are Tesla, Fluence, Major-IOU, and Other. The table is restricted to rows for which this all-interval concentration measure is observed (8,169 of 8,169 evaluable deviation rows). One interval observation is a focal battery by five-minute interval. M^O_{it} is the maximum owner-level gain across the sampled broad deviation menu for that battery-interval.

Table B12: Battery-to-provider mapping

DUID	Station	Participant	Provider	C
NSW1				
BHB1	Broken Hill Battery	AGL	AGL in-house	•
LDBESS1	Liddell BESS	AGL	AGL in-house	•
DPNTB1	Darlington Point ESS	EA/Edify	EA intermediary	○
RIVNB2	Riverina ESS 2	EA/Edify	EA intermediary	○
NESBESS1	New England BESS	ACEN/NESF	Energy Vault VaultOS	•
NESBESS2	New England BESS	ACEN/NESF	Energy Vault VaultOS	•
CAPBES1	Capital Battery	GPG/Naturgy	Fluence Mosaic	•

Continued on next page

DUID	Station	Participant	Provider	C
MLB01	Mortlake BESS	Origin Energy	Fluence Mosaic	•
ORABESS1	Orana BESS	Akaysha/BlackRock	Fluence Mosaic	•
QBYNB1	Queanbeyan BESS	GPG/Naturgy	Fluence Mosaic	•
WTAHB1	Waratah Super Battery	Akaysha/BlackRock	Fluence Mosaic	•
RESS1	Riverina ESS 1	Shell Energy	Shell Energy interm.	○
SMTHBES1	Smithfield BESS	Iberdrola	Tesla Autobidder	○
WALGRV1	Wallgrove BESS	Iberdrola	Tesla Autobidder	•
ERB01	Eraring BESS	Origin Energy	Wärtsilä GEMS	•
LIMBESS1	Limondale Battery	RWE	—	—
QPSFB2	Quorn Park Solar Hybrid	Potentia/Enel	—	—
QLD1				
CHBESS1	Chinchilla BESS	CS Energy	CS Energy in-house	○
GREENB1	Greenbank BESS	CS Energy	CS Energy in-house	○
WANDB1	Wandoan BESS	Vena Energy/AGL	Doosan GridTech	•
BRNDBES1	Brendale BESS	Akaysha	Fluence Mosaic	•
ULPBESS1	Ulinda Park BESS	Akaysha	Fluence Mosaic	•
BBATTERY1	Bouldercombe Battery	Genex Power	Tesla Autobidder	•
SWANBBF1	Swanbank BESS	CleanCo	Tesla Autobidder	○
TARBESS1	Tarong BESS	Stanwell	Tesla Autobidder	○
WDBESS1	Western Downs BESS	Neoen	Tesla Autobidder	•
WDBESS2	Western Downs BESS	Neoen	Tesla Autobidder	•
KEPBG1	Kennedy Energy Park	Windlab/Eurus	—	—
KEPBL1	Kennedy Energy Park	Windlab/Eurus	—	—
SNB01	Supernode BESS	Quinbrook	—	—
SNB02	Supernode BESS	Quinbrook	—	—
SA1				
DALNTH1	Dalrymple North BESS	AGL	AGL in-house	•
TIB1	Torrens Island BESS	AGL	AGL in-house	•
TB2B1	Tailem Bend 2	Vena Energy	Doosan GridTech	•
LGAPBS1	Lincoln Gap WF Battery	Ratch/Nexif	Fluence Mosaic	○
MANNUMB1	Mannum BESS	Epic Energy	Habitat Energy	•
BLYTHB1	Blyth BESS	Neoen	Neoen/NHOA	○
HPR1	Hornsdale Power Reserve	Neoen	Tesla Autobidder	•
LBB1	Lake Bonney BESS	Iberdrola	Tesla Autobidder	•
BUNGAMB1	Bungama BESS	Amp Energy	Wärtsilä GEMS	•

Continued on next page

DUID	Station	Participant	Provider	C
ADPBA1	Adelaide Desal. Plant	SA Water	—	—
BOWWBA1	Bolivar Waste Water	SA Water	—	—
CBWWBA1	Christies Beach WWTP	SA Water	—	—
CGBESS01	Clements Gap BESS	Pacific Blue	—	—
HVWWBA1	Happy Valley WTP	SA Water	—	—
TEMPB1	Templers BESS	ZEN Energy/ZEBRE	—	—
VIC1				
BALB1	Ballarat BESS	EA/AusNet	EA intermediary	○
GANNB1	Gannawarra ESS	EA/Edify	EA intermediary	○
HBESS1	Hazelwood BESS	ENGIE/Eku Energy	Fluence Mosaic	•
LVES1	Latrobe Valley BESS	Tilt Renewables	Fluence Mosaic	•
RANGEB1	Rangebank BESS	Shell Energy/Eku	Fluence Mosaic	•
TRGBESS1	Terang BESS	FRV	Fluence Mosaic	•
MOORABS1	Moorabool Wind Farm	Goldwind	Goldwind in-house	○
KESSB1	Koorangie ESS	Shell Energy	Shell Energy interm.	○
BULBES1	Bulgana Green Power Hub	Neoen/HMC	Tesla Autobidder	○
MREHA1	Melbourne REH A1	Equis Energy	Tesla Autobidder	○
MREHA2	Melbourne REH A2	Equis Energy	Tesla Autobidder	○
MREHA3	Melbourne REH A3	SEC Energy	Tesla Autobidder	○
VBB1	Victorian Big Battery	Neoen/HMC	Tesla Autobidder	•
PIBESS1	Phillip Island BESS	Mondo/AusNet	Ubi Platform	•

Notes: Column "C" denotes confidence: ● = confirmed (direct public evidence naming the software platform), ○ = probable (strong indirect evidence, typically hardware identification combined with the manufacturer's known bundling pattern), – = unknown (excluded from provider-level specifications). "EA" abbreviates EnergyAustralia. "Participant" is the asset owner or offtaker; "Provider" is the identified software platform operator. DUIDs follow AEMO's Dispatch Unit Identifier convention. Multiple DUIDs sharing a station name (e.g., WDBESS1/WDBESS2) are separate dispatch units of the same physical battery.

B.5. State-of-Charge Reconstruction

We build a battery-level state-of-charge (SoC) series at 5-minute frequency. Before the ERI reform on July 1, 2025, battery state is not public, so SoC must be reconstructed from observable SCADA dispatch data. After ERI, AEMO publishes end-of-interval energy storage fields with a one-day lag, which we use both to calibrate the model and to anchor its post-reform output. This subsection describes the stock-flow model, the calibration procedure, and the validation results.

Model. For each battery i with nameplate energy capacity $E_i^{\max}$, we propagate a 5-minute stock-flow recursion driven by SCADA charge and discharge metering. Let P_{it}^{chg} and P_{it}^{dis} denote the observed charging and discharging power (MW) at interval t, and let $\Delta = 5/60$ h. The modelled state of charge evolves as

$$S_{i,t} = \mathrm{clip}\left(\rho_i \, S_{i,t-1} + \eta_i^{\mathrm{ch}} \, P_{it}^{\mathrm{chg}} \, \Delta - \frac{P_{it}^{\mathrm{dis}} \, \Delta}{\eta_i^{\mathrm{dis}}} - \kappa_i \, \Delta, \quad 0, \quad E_i^{\max}\right), \tag{43}$$

where $\eta_i^{\mathrm{ch}} \in [0.70, 0.99]$ is the charge efficiency, $\eta_i^{\mathrm{dis}} \in [0.70, 0.99]$ the discharge efficiency, $\rho_i \in [0.999, 1.0]$ a per-interval self-discharge factor, and $\kappa_i \in [0.0, 2.0]$ MW an auxiliary parasitic load. The clip operator enforces the physical bounds $S_{i,t} \in [0, E_i^{\max}]$.

Calibration. The four parameters $(\eta_i^{\mathrm{ch}}, \eta_i^{\mathrm{dis}}, \rho_i, \kappa_i)$ are calibrated separately for each battery by minimising the root mean squared error between $S_{i,t}$ and the public post-ERI energy-storage field published by AEMO (July 2025 through January 2026). The first seven days of each battery's public series are excluded to avoid initial-condition bias. Optimisation uses L-BFGS-B with the bounds stated above. Across the 42 known-provider batteries, the calibrated charge efficiency has a median of 0.955 (IQR $[0.913, 0.977]$), the discharge efficiency a median of 0.990 (most batteries at the upper bound), the self-discharge factor a median of 0.9997 (implying negligible inter-interval leakage), and the auxiliary load a median of 0.20 MW.

SoC series construction. The calibrated model produces three SoC objects for each battery-interval. *Pre-ERI* (before July 1, 2025): $S_{i,t}$ is the pure model propagation from (43), initialised at half capacity. Because no public anchor exists, pre-reform SoC is entirely model-driven. *Post-ERI*: the model is re-anchored daily at midnight to the previous trading day's publicly released end-of-interval energy storage, then propagated forward through the day using (43). This daily anchoring prevents drift and ensures that the modelled series reflects the information set available to market participants at the start of each trading day.

Empirical SoC variables. We define the common-state variable $\mathrm{CommonSoC}_{rt}$ as the leave-one-out regional SoC share: for battery i in region r at interval t,

$$\mathrm{CommonSoC}_{rt}^{(-i)} := \frac{\sum_{j \in r,\, j \neq i} S_{j,t-288}}{\sum_{j \in r,\, j \neq i} E_j^{\max}},$$

where the lag of 288 intervals corresponds to one trading day. The own-state control $\mathrm{SoC}_{it} := S_{i,t-288}/E_i^{\max}$ is the corresponding battery-level lagged share. Both variables are predetermined with respect to current-interval bids.

Validation. We assess model accuracy using two exercises on the post-ERI window where public SoC is observed. The first ("un-anchored") runs the calibrated model from the first ERI observation *without* daily re-anchoring, mimicking the pre-reform backcast where no public anchor exists. The second ("quasi-holdout") anchors the model at a single date (November 1, 2025) and propagates forward un-anchored through January 2026, testing multi-month accuracy with parameters trained on the full July–January window. Table B13 reports the results for the 42 known-provider batteries used in the empirical analysis.

Table B13: SoC model validation: known-provider batteries

	P10	P25	Median	P75	P90
Panel A: Un-anchored full window (Jul 2025 – Jan 2026)					
Pearson ρ	0.643	0.924	0.956	0.983	0.988
R^2	0.393	0.846	0.910	0.964	0.974
RMSE (% of $E^{\max}$)	3.1	5.3	7.2	10.3	15.0
MAE (% of $E^{\max}$)	2.0	3.4	4.6	7.2	11.4
Panel B: Quasi-holdout (anchored Nov 1, propagated to Jan 2026)					
Pearson ρ	0.601	0.930	0.979	0.989	0.993
RMSE (% of $E^{\max}$)	3.2	4.5	6.9	9.6	12.2

Notes: Distribution is across 42 known-provider batteries. Panel A runs the calibrated stock-flow model from the first post-ERI observation without daily re-anchoring; this exercise mimics the pre-reform backcast. Panel B anchors the model once at November 1, 2025 and propagates forward without re-anchoring, testing multi-month drift. Percentiles are unweighted across batteries. Of the 42 batteries, 33 have un-anchored Pearson $\rho \geq 0.90$ and 32 have $R^2 \geq 0.80$. The lower-tail batteries (P10) are predominantly recently commissioned assets with short calibration windows or near-dormant units with minimal cycling.

B.6. Reclearing-Engine Validation

The deviation analysis relies on `nempy` (Prakash, 2022) to reproduce AEMO's regional dispatch outcome from the same MMS-DB and NEMDE-XML inputs that AEMO uses at clearing time. As a direct check that this reproduction is accurate enough for our purposes, the deviation scan also computes a baseline clearing for every focal interval – the engine is run on the observed bid stack with no counterfactual edit. Comparing this baseline price to AEMO's published regional reference price (RRP) for the same interval is therefore an end-to-end test of the input pipeline plus the optimiser.

Table B14 reports the resulting price discrepancy on the $3{,}956$ unique (interval, region) pairs in the deviation panel. Pooled across all intervals the median absolute price discrepancy is \$$0.05$ per MWh, and 72.5% of intervals are reproduced within \$$1$ of the published RRP, 89.5% within \$$5$, and 97.2% within \$$20$. Replication is essentially exact across all four NEM regions and across both the pre- and post-ERI windows. Accuracy degrades, as expected, in price-cap and other extreme-price intervals where AEMO's full constraint set is hardest to reproduce from public inputs: among intervals with $\mathrm{RRP} > \$1{,}000$ the share within \$$20$ falls to 73%. These intervals are rare in the deviation panel, are not concentrated in the evening-peak windows the conduct test focuses on, and produce engine prices that differ from RRP by amounts that are still small relative to the price level itself.

B.7. Conduct-Test Sample Balance

Table B15 reports the numerical balance check accompanying Figure 5 in the main text. For each variable the table reports means and medians across three groups of Tesla- and Fluence-managed battery-intervals in evening-peak hours (16:00–22:00). The *Full* columns cover all such intervals in the panel window. The *Eligible* columns restrict to intervals satisfying the four structural preconditions under which the conduct test has power: (i) the focal provider's near-margin set contains more than one owner ($\mathrm{HHI}^{\mathrm{own}}_{\mathrm{within\ prov}} < 1$); (ii) the focal provider has positive near-margin share

Table B14: Reclearing-engine validation against AEMO's published RRP

			Share with $\lvert\Delta p\rvert \leq$		
Cut	Intervals	Median $\lvert\Delta p\rvert$	\$1	\$5	\$20
Panel A: pooled					
All intervals	3,956	0.05	72.5%	89.5%	97.2%
Panel B: by period					
Pre-ERI	1,335	0.02	83.1%	94.5%	97.8%
Post-ERI	2,621	0.11	67.1%	87.0%	96.9%
Panel C: by region					
NSW1	769	0.05	71.1%	86.3%	94.1%
QLD1	946	0.01	80.5%	91.3%	97.1%
SA1	1,295	0.24	66.3%	89.7%	98.1%
VIC1	946	0.03	74.2%	90.1%	98.4%
Panel D: by observed RRP magnitude (AUD/MWh)					
≤ 0	852	0.01	85.9%	95.5%	99.5%
0–50	510	0.06	76.5%	87.6%	96.3%
50–200	2,091	0.06	69.4%	89.7%	98.1%
200–1,000	437	0.44	56.8%	81.9%	92.9%
$> 1{,}000$	66	0.00	72.7%	72.7%	72.7%

Notes: Replication accuracy of the nempy reclearing engine. For each unique (interval, region) cell in the deviation panel we feed nempy the same MMS-DB and NEMDE-XML inputs that AEMO used at clearing time and run it without any counterfactual bid edit; we then compare the engine's reproduced regional reference price to AEMO's published RRP for the same interval. Δp is the engine price minus the published RRP, in AUD/MWh. Panel D bins the observed RRP to show where replication is tight (sub-cap intervals) and where it degrades (price-cap intervals, where AEMO's full constraint set is harder to reproduce from the public inputs).

($s^{\text{prov}} > 0$); (iii) the focal battery offers positive MW within one band of the regional clearing price (push-down feasibility); and (iv) the focal battery is itself at or near the margin in the interval (its marginal-position score exceeds 0.5), which is the structural condition that makes a push-down deviation actually change dispatch. The *Selected* columns restrict to the focal battery-intervals that appear in the conduct-test panel. The final column is the Kolmogorov–Smirnov p-value comparing the Eligible and Selected distributions. The systematic Full-to-Eligible step in clearing band, marginal-dispatch share, and price reflects the structural restriction the test requires; the Eligible-to-Selected step is small on outcome-relevant variables, consistent with the panel being a stratified draw on the structural pre-conditions rather than on outcomes.

B.8. Conduct Estimator: Numerical Results

Table B16 reports the point estimates, cluster-subsampling confidence sets, and band sample sizes underlying the Q-curves shown in Figure B1. Rows are indexed by focal-provider coalition, market, ERI period, and 10-percentage-point s^{prov} band; bands with fewer than 30 deviations are omitted, as in the figure. The 95% confidence set is constructed by cluster subsampling at the (i, t) level (Section 3.4); Q-reduction is $1 - Q_n(\widehat{\lambda})/Q_n(0)$, equal to the depth of the corresponding curve in Figure B1 expressed as a percentage.

Table B15: Conduct-test sample balance: full evening-peak panel, eligibility set, and selected conduct panel

	Full		Eligible		Selected		
Variable	Mean	Median	Mean	Median	Mean	Median	K–S p
Regional reference price (AUD/MWh)	120	104	155	131	135	120	< 0.001
Regional battery dispatched (MW)	158	70.0	325	273	359	320	< 0.001
Regional battery offered (MW)	1,542	1,615	1,501	1,615	1,583	1,615	< 0.001
Regional spare capacity (MW)	1,384	1,325	1,176	1,099	1,223	1,178	< 0.001
Active batteries in regional stack	10.6	11.0	10.6	11.0	10.9	12.0	< 0.001
Focal offered MW	151	150	168	200	180	200	< 0.001
Focal MW within ± 1 band of clearing	110	100	89.1	65.0	138	150	< 0.001
Clearing band (1–10)	6.09	6.00	3.47	3.00	3.44	3.00	< 0.001
Focal-provider near-margin share s^{prov}	0.403	0.434	0.441	0.482	0.435	0.451	< 0.001
Owner HHI within focal provider	0.594	0.500	0.513	0.483	0.457	0.385	< 0.001
Focal dispatch share at margin	0.162	0.000	0.896	1.00	0.978	1.00	< 0.001
Focal near-offer share	0.094	0.083	0.084	0.057	0.127	0.123	< 0.001
N	433,224		47,401		15,882		

B.9. Robustness: Diversity-Weighted Concentration Moderator

The main-text fit uses the focal provider's near-margin MW share $s^{\text{prov}}_{k_i,r_i,t}$ as the concentration moderator. As a robustness check, we re-fit the conduct estimator using the diversity-weighted moderator

$$C_{it} \;=\; s^{\text{prov}}_{k_i,r_i,t}\left(1 - \text{HHI}^{\text{own}}_{k_i,r_i,t}\right),$$

where $(1 - \text{HHI}^{\text{own}})$ is the Gini-Simpson diversity index of owner shares within the focal provider's near-margin set. This moderator collapses the headline-share moderator and the multi-owner sample restriction into a single $[0, 1]$-bounded index that is zero in single-owner-provider intervals (where the cross-owner spillover channel is mechanically absent) and rises with both larger provider near-margin presence and greater owner dispersion within the provider.

Table B17 reports the per-band fit using C_{it} binned into 10-percentage-point bands. The identifying regime is at $C_{it} \in [0.10, 0.50]$ with the strongest evidence at $C_{it} \approx 0.25$–0.35; under balanced two- and three-owner splits these values correspond to focal-provider near-margin shares of roughly 40–70%, the same regime identified by the main-text s^{prov} binning. The FCAS panels are uniformly null.

B.10. Back-of-Envelope Cost of Identified Conduct

This appendix gives the construction behind the back-of-envelope estimate in Section 3.4. We report two estimates: a consumer-side price-difference estimate that uses the recleared regional clearing price under an owner-only counterfactual deviation and is the headline figure in the main text, and a battery-side diagnostic that considers only the dollar transfer on deviations whose owner-portfolio gain flips sign once same-provider spillovers are internalised. The construction follows the markup logic of Calder-Wang and Kim (2026), adapted to a uniform-price electricity auction in which the consumer side is the regional clearing price times regional demand rather than a demand-system markup.

Figure B1: Conduct objective $Q_n(\lambda)/Q_n(0)$ by coalition, market, and near-margin share band

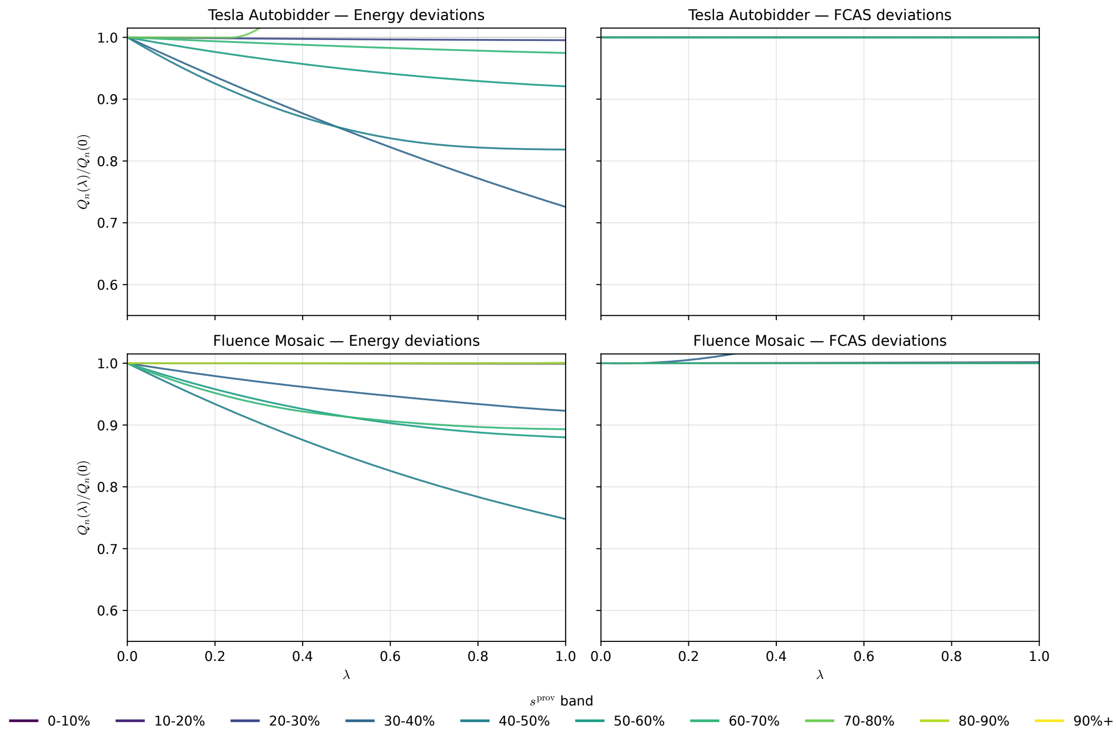

Notes: Each curve plots $Q_n(\lambda)/Q_n(0)$ for one combination of s^{prov} band and the pooled period within the coalition-market panel, on the conduct-test deviation sample of Section 3.4 restricted to multi-owner intervals; colour indexes the s^{prov} band. Bins with fewer than 30 deviations are omitted. The FCAS panels (right column) are uniformly flat: no FCAS curve in either Tesla or Fluence is visually distinguishable from $Q_n(\lambda)/Q_n(0) \equiv 1$. Boundary estimates of $\widehat{\lambda}$ paired with near-zero Q-reduction are uninformative and read as flat curves.

Price-difference estimate (headline). For each focal battery i at interval t inside the identifying range of Section 3.4, define the owner-only counterfactual deviation

$$d^0_{it} \;=\; \arg\max_{d \in \{10\%, 25\%, 50\%\}} \Delta\Pi_{o_i,t}(d) \quad \text{subject to} \quad \Delta\Pi_{o_i,t}(d) > 0,$$

that is, the discrete energy-push deviation that maximises the focal owner's portfolio gain under the owner-only hypothesis. The reclearing engine returns, for that deviation, a counterfactual regional clearing price $p^{\text{cf}}_{rt}(d^0_{it})$ together with the observed baseline price p^{obs}_{rt}. The implied price difference

$$\Delta p_{rt} \;=\; p^{\text{obs}}_{rt} - p^{\text{cf}}_{rt}(d^0_{it})$$

is the increase in the regional clearing price that the focal owner's coordinated restraint preserves. Because the NEM clears each region at a single price in each interval, we collapse to the region-interval level by selecting, among focal batteries with an owner-only counterfactual in (r, t), the focal whose d^0 yields the largest non-negative price difference, and multiply once by regional demand:

$$\text{Cost}_{rt} \;=\; \Delta p_{rt} \times \text{DemandMW}_{rt} \times \tfrac{5}{60},$$

in units of AUD. This avoids double-counting the same regional price difference across focal batteries. The sample-window cost is the sum of $\mathrm{Cost}_{rt} \cdot w_{rt}$ over identified region-intervals, with w_{rt} the inverse-inclusion-probability weight of the representative (i, t) observation, extrapolating from the sample to the universe of evening-peak intervals over the 305-day window. The annualised row scales the weighted total by $365/305 \simeq 1.20$.

The median price difference is small (about $\$1.28$/MWh) but the distribution is fat-tailed (mean $\$2.70$/MWh, 90th percentile around $\$6.24$/MWh, with a maximum of approximately $\$59$/MWh). The annualised total is $\$5.5$m, with Tesla accounting for $\$3.1$m and Fluence for $\$2.4$m. The estimate is bounded below the true cost of coordination for two reasons: only deviations on the discrete $\{10\%, 25\%, 50\%\}$ MW grid in the identifying bands contribute, and the per-(r, t) price difference is the unilateral-counterfactual price difference, which understates the price effect that fully coordinated same-provider bidding could deliver.

Battery-side transfer (diagnostic). A narrower diagnostic isolates the dollar magnitude on the *sign-flipping* subset of the deviation panel. Define the left-on-table set

$$\mathcal{L}^{\star}_{(i,t)} \;=\; \arg\max_{d} \Delta\Pi_{o_i,t}(d) \quad \text{s.t.} \quad \Delta\Pi_{o_i,t}(d) > 0,\ \Delta\Pi_{o_i,t}(d) + \Delta\Pi_{k_i,-o_i,t}(d) < 0,$$

that is, the (i, t) intervals in which same-provider weighting flips the sign of the focal owner's best deviation gain. On $\mathcal{L}^{\star}$ the focal owner foregoes $\Delta\Pi_{o_i,t}$ in portfolio profit, same-provider partners retain $|\Delta\Pi_{k_i,-o_i,t}|$ of inframarginal revenue, and other (different-provider) regional batteries retain $|\Delta\Pi^{\mathrm{nei}}_{t}|$. Table B19 reports these magnitudes by coalition.

The two estimates measure different objects. The price-difference estimate in Table B18 is the consumer-side cost of the higher clearing price across all regional inframarginal MW in the identified region-intervals, while the second estimate in Table B19 is the dollar size of the battery-side transfer on the strict sign-flipping subset $\mathcal{L}^{\star}$. The two differ by roughly two orders of magnitude because the price-difference estimate applies to the broader regional inframarginal generation (not just the same-provider fleet), and because it counts all region-intervals with a positive price difference while the second transfer diagnostic is limited to $\mathcal{L}^{\star}$.

B.11. Robustness of the Conduct Test

This appendix collects five robustness exercises for the conduct test of Section 3.4. The first three address alternative interpretations of the conduct finding – an unobserved owner-level cost, a mechanical explanation based on the marginal distribution of same-provider spillovers, and whether the effect is specific to the provider coalition rather than to any similarly placed set of near-margin batteries. The final two probe the construction of the test itself – whether the finding survives when each bid is dated to its actual submission time, and whether the estimator recovers internalisation in a positive control where theory requires it.

B.11.1. Omitted owner-level cost bounds

The conduct test treats a positive owner-portfolio gain $\Delta\Pi_{o_i,t}(d) > 0$ as a contradiction of owner-level conduct. A natural concern is that the estimated owner payoff omits private components of the owner's objective: contract positions, tolling constraints, degradation or warranty shadow costs, risk limits, or private forecasts. This appendix quantifies how large such an omitted owner-level component would have to be to absorb the conduct evidence.

Write

$$G^O_{itd} \equiv \Delta\Pi_{o_i,t}(d), \qquad G^K_{itd} \equiv \Delta\Pi_{k_i,-o_i,t}(d),$$

for the focal owner's regional portfolio gain and the same-provider, different-owner spillover from deviation d. The conduct estimator asks whether $G^O_{itd} + \lambda G^K_{itd} \leq 0$. Suppose instead that the owner-only objective includes an omitted non-negative deviation cost Ω_{itd}. The owner-only inequality becomes

$$G^O_{itd} - \Omega_{itd} \leq 0.$$

With no structure on Ω_{itd}, the minimum cost needed to rationalise an owner-only violation is simply $\max\{G^O_{itd}, 0\}$, which is tautological. We therefore report two more disciplined benchmarks.

First, consider a band-level linear omitted cost c in AUD/MWh of extra focal discharge. Let

$$x^+_{itd} = \max\{\Delta q^{\text{disp}}_{itd}, 0\} \times \tfrac{5}{60}$$

be the recleared increase in focal discharge, in MWh, under the deviation. For each coalition-concentration band $\mathcal{C}$, define

$$Q^O_{n,\mathcal{C}}(c) = \frac{1}{n_{\mathcal{C}}} \sum_{(i,t,d)\in\mathcal{C}} w_{itd} \max\{G^O_{itd} - c x^+_{itd}, 0\}^2.$$

The first statistic is

$$c^Q_{\mathcal{C}} = \inf\left\{c \geq 0 : Q^O_{n,\mathcal{C}}(c) \leq Q_{n,\mathcal{C}}(\widehat{\lambda})\right\}.$$

This is the smallest common throughput-style owner cost that would reduce the owner-only contradiction objective to the value achieved by the estimated same-provider conduct parameter. It is deliberately favourable to the omitted-cost explanation, because it only has to match the aggregate squared-violation improvement rather than rationalise every individual deviation.

Second, for each focal battery-interval (i, t), define the interval-specific omitted-cost rate

$$\mu^\star_{it} = \sup_{d: G^O_{itd} > 0} \frac{G^O_{itd}}{x^+_{itd}}.$$

This is the smallest AUD/MWh charge on extra focal discharge that would rationalise all sampled owner-profitable deviations for that battery-interval under owner-only conduct. If any owner-profitable sampled deviation has $x^+_{itd} = 0$, then a discharge-denominated omitted cost cannot rationalise that deviation and $\mu^\star_{it} = \infty$.

The table reports two internal benchmarks. The column $c^Q/11$ divides the band-level cost by the 11 AUD/MWh maximum movement in $\widehat{m}_{it}$ across the Bellman grid/control sensitivity checks of Appendix B.3; a value above one means the required omitted owner cost exceeds anything that Bellman discretisation can plausibly produce. The last two columns report the share of owner-violating battery-intervals for which $\mu^\star_{it}$ exceeds \$100/MWh and \$$1{,}000$/MWh, the same materiality cutoffs used in the Bellman incentive-compatibility diagnostics.

For Tesla Autobidder, two of the four identifying bands (40–50% and 60–70%) require an infinite uniform charge. On these bands the positive-own-gain mass is supported by deviations with no corresponding focal-discharge exposure, so no per-MWh charge on extra discharge can reduce the moment objective below $Q_n(\widehat{\lambda})$. The remaining two Tesla bands require \$16/MWh ($c^Q/11 = 1.4$) at 30–40% and \$59/MWh ($c^Q/11 = 5.4$) at 50–60%. For Fluence Mosaic, the three corner bands at $\widehat{\lambda} = 1$ require \$11, \$15, and \$28/MWh ($c^Q/11$ from 1.0 to 2.6); only the 30–40% interior band, the weakest in the identifying set, sits below the Bellman sensitivity benchmark at \$8/MWh ($c^Q/11 = 0.7$).

The battery-interval benchmark $\mu^\star_{it}$ delivers the same verdict. Across the eight identifying bands, the share of owner-violating battery-intervals individually requiring an omitted cost above \$100/MWh ranges from 37% (Tesla 30–40%) to 80% (Tesla 40–50%), and the share above \$$1{,}000$/MWh ranges from 32% to 78%. The bands with infinite c^Q have the highest battery-interval shares: a substantial fraction of the deviations the conduct test flags are not rationalisable by any finite per-MWh discharge cost.

The omitted-cost alternative therefore cannot account for the conduct evidence at any reasonable benchmark. The two Tesla bands with infinite required charge are decisive on their own, and the remaining bands need omitted costs an order of magnitude above the Bellman discretisation margin. The single band where the implied charge sits below the benchmark, Fluence 30–40%, is also the band where $\widehat{\lambda}$ is interior at 0.74 rather than at the corner, and where the conduct signal is weakest.

The bounds in this appendix are denominated in AUD per MWh of extra focal discharge and therefore do not cover owner objectives denominated in price exposure, such as inframarginal generation or contract positions that gain when the regional price stays high. The matched-placebo exercise of Appendix B.11.3 addresses these directly: any objective that scales with the recleared price change would be proxied equally well by a capacity-matched different-provider coalition, yet the same-provider coalition fits strictly better in every draw.

B.11.2. Permutation placebo

This appendix tests whether the per-deviation pairing between the focal owner's deviation gain G^O_{itd} and the same-provider, different-owner spillover G^K_{itd} has identifying content beyond the marginal distribution of G^K. We draw a placebo null by, within each provider coalition (Tesla / Fluence), randomly reassigning G^K_{itd} across focal deviations. This shuffle preserves the marginal distribution of the spillover within coalition but destroys its per-deviation joint distribution with the focal's deviation gain. On each of $B = 300$ draws we refit the binned $\widehat{\lambda}$ by $(\text{coalition}, s^{\text{prov}})$ band and record the resulting point estimate and Q-reduction. We report empirical p-values with the standard plus-one finite-sample correction, $p = (1 + \#\{b : \text{stat}_b \geq \text{stat}_{\text{actual}}\})/(B + 1)$.

For Fluence Mosaic, both $\widehat{\lambda}$ and the Q-reduction lie outside the null distribution in every identifying band (30–70%) at $p \leq 0.007$. For Tesla Autobidder, the $\widehat{\lambda}$ corner is preserved under shuffling because Tesla's spillover marginal is sufficiently mean-negative that random pairings still pin λ at one. The $\widehat{\lambda}$ statistic alone has no power against the marginal-distribution explanation for Tesla; the Q-reduction comparison does. The actual Q-reduction lies at 13.8–27.8% across the four Tesla identifying bands while the null 95th percentile sits at 1.5–5.1% and the empirical p-value is 0.003 uniformly. Outside the identifying range ($s^{\text{prov}} < 30\%$ and $s^{\text{prov}} > 70\%$) the actual Q-reduction is at most 0.5%. The Tesla comparisons lie inside the null distribution; the one nominal rejection, Fluence below 30%, concerns a fit improvement an order of magnitude smaller than in the identifying bands.

Figure B2: Permutation placebo: actual vs null

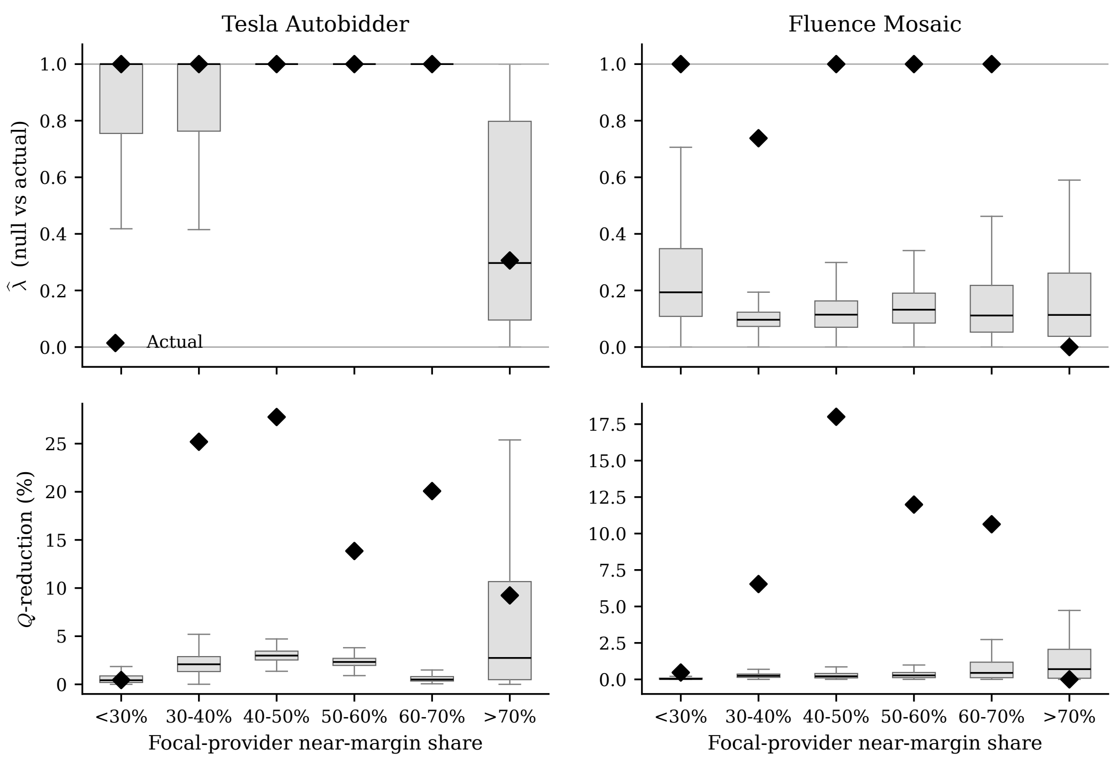

Notes: Box-plots of the $B = 300$ permutation null for $\widehat{\lambda}$ (top row) and Q-reduction (bottom row), with the actual point estimate overlaid as a solid diamond. Within each coalition (Tesla / Fluence) the same-provider spillover G^K_{itd} is randomly reassigned across focal deviations on each draw; whiskers extend to the full range of the null.

B.11.3. Provider-specificity: matched placebo coalitions

The permutation placebo shows that the per-deviation pairing matters, but not that provider identity does – shuffling also destroys the matching on price impact and coalition size. This exercise tests provider identity directly. Using the recleared profit change that each deviation imposes on every regional battery, we form placebo coalitions from the different-provider, different-owner batteries near the margin in the same region-interval, matched to the actual same-provider coalition on battery count, and separately on both count and installed capacity. We then compare the actual coalition's conduct fit improvement to a null of $B = 500$ matched placebo coalitions. Table B22 reports the result. For both providers the actual same-provider fit improvement exceeds that of every count- and capacity-matched placebo draw ($p \leq 0.010$). Capacity matching raises the placebo baseline – as it must, since the matched batteries are then comparably exposed to the price change – yet the same-provider coalition still rationalises the observed restraint significantly better. The signal is therefore specific to the provider coalition, not a generic consequence of any similarly sized and similarly exposed set of near-margin batteries losing revenue when the price falls.

B.11.4. Lead-time split

The reclearing engine values each deviation at the realised market outcome, whereas the no-profitable-deviation restriction concerns the bidder's expected profit given the information available when the operative bid was submitted. An apparent owner-level violation could therefore reflect hindsight rather than restraint. We date each interval's operative quantity bid to its submission timestamp and split the identifying-range estimator by the lead time to dispatch. The bulk of operative rebids are lodged close to dispatch (median 7.6 minutes). Table B23 shows that the same-provider Q-reduction is concentrated in the bids submitted within fifteen minutes of dispatch, where five-minute predispatch forecasts are accurate and the realised outcome closely approximates the bidder's information set, and vanishes for bids lodged more than an hour ahead. For Tesla the share of owner-profitable deviations falls with lead time in the same way. A hindsight artefact would produce the opposite pattern, strongest for the longest-lead bids.

B.11.5. Same-owner positive control

An owner should fully internalise the price effect of a deviation on its own other batteries, so the conduct weight on same-owner, different-battery profits should equal one. As a positive control we estimate that weight – rather than imposing it, as the headline test does – on the battery-intervals in which the focal owner operates at least one other battery in the region. Table B24 reports $\widehat{\lambda}_O = 1.00$ for Tesla Autobidder with a 12 percent improvement in fit, confirming that the estimator detects joint-profit internalisation when it is present by construction. The control is uninformative for Fluence Mosaic, whose owners rarely operate more than one battery in the same region, so same-owner spillovers are almost never present.

B.12. Installed vs Near-Margin Provider Concentration

The conduct test in Section 3.4 uses the focal provider's per-interval near-margin MW share $s^{\text{prov}}_{k,r,t}$. Installed-capacity shares are the more familiar way to express a provider's footprint, and are the basis for the static index reported in Section 3.1. This appendix documents that the two concentration objects are tightly linked in our sample, so the conduct test's identifying near-margin range can be mapped back to a range of installed-capacity shares.

Figure B3 plots, for each region, the per-interval near-margin share against the installed-capacity provider share for every provider with non-zero installed capacity. For each provider-region pair we mark the median per-interval near-margin share and the 10–90% band. Three patterns are visible. First, the median per-interval near-margin share tracks the installed share closely: for the two headline providers, the median near-margin share lies within roughly 5 percentage points of the installed share in every region. Second, per-interval dispersion around the installed-share mean reflects which batteries are dispatchable near the margin in that interval, and varies across provider-region pairs from tight (QLD1 Tesla: inter-decile range ≈ 17 percentage points) to wide (NSW1 Fluence: inter-decile range ≈ 47 percentage points). Third, providers with installed shares above roughly 20% spend the majority of evening-peak intervals in the conduct-test identifying near-margin band $s^{\text{prov}} \in [0.30, 0.70]$: 98% of Tesla's QLD1 intervals, 80% of Fluence's VIC1 intervals, 74% of Tesla's VIC1 intervals, and 61% of Fluence's NSW1 intervals. The conduct test's identifying near-margin range thus maps on average to installed-capacity shares of roughly 20–60%.

Figure B3: Installed-capacity vs per-interval near-margin provider share

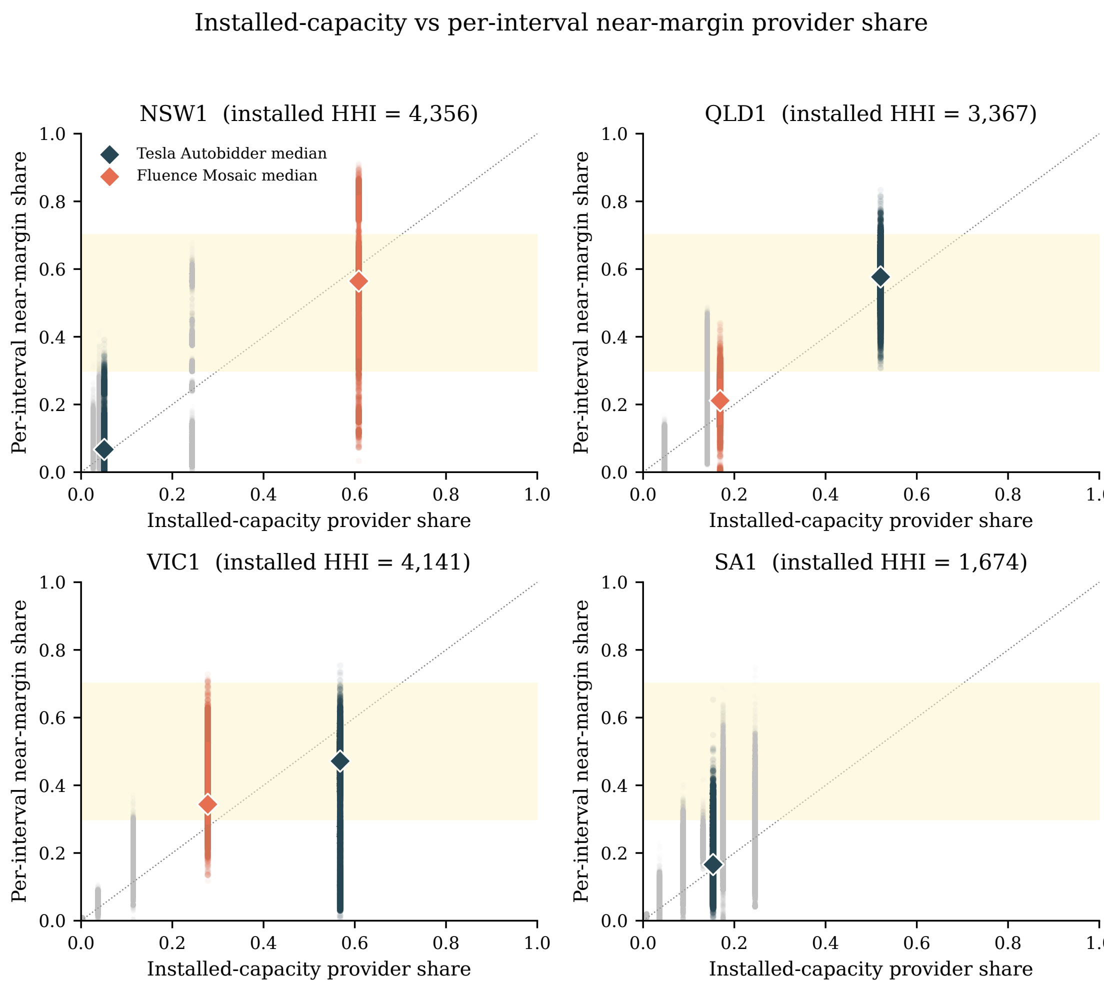

Notes: One panel per NEM region. Horizontal axis: provider's MW-weighted installed-capacity share. Vertical axis: per-interval near-margin MW share averaged over all evening-peak intervals in the sample. Coloured diamonds mark the median per-interval near-margin share for Tesla Autobidder (dark teal) and Fluence Mosaic (orange); the vertical line spans the 10–90% inter-decile range. Grey points are all other providers in that region. The dashed $45°$ line marks equality of installed and near-margin shares. The shaded horizontal band marks the conduct-test identifying range $s^{\text{prov}} \in [0.30, 0.70]$.

Figure B4: Schematic FCAS trapezium constraints

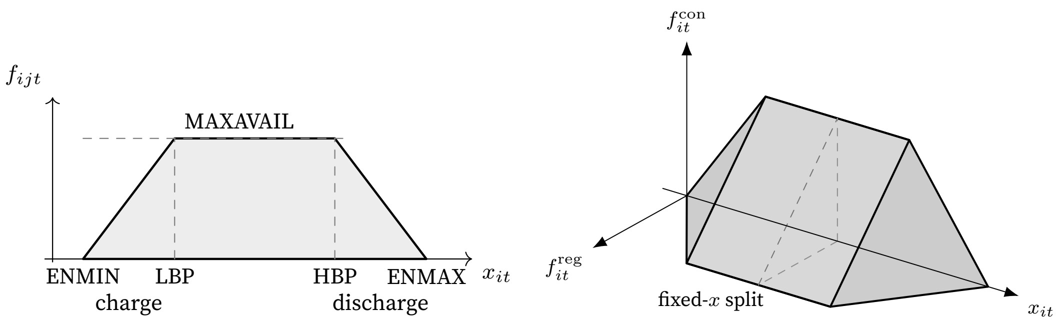

(a) Service-level trapezium (b) Joint FCAS allocation

Notes: Panel a shows the service-specific NEM validation object: enabled FCAS MW must lie below a piecewise-linear availability function of the energy operating point. Panel b illustrates the joint energy-FCAS constraint for a battery. The dashed triangle is a fixed-operating-point cross-section: regulation and contingency services are separate markets, but their enabled quantities draw on the same physical headroom.

B.13. FCAS Trapezium and Technical Constraints

FCAS enablement is feasible only conditional on the battery's energy operating point. This appendix gives the compact version of the AEMO trapezium constraint used to interpret the bid problem and the counterfactual reclearing exercise (Australian Energy Market Operator, 2021; Karimi-Arpanahi et al., 2024). Let

$$x_{it} := q_{it} - r_{it}$$

denote the battery's net energy operating point in interval t, where $x_{it} > 0$ denotes discharge and $x_{it} < 0$ denotes charging. For FCAS service j, let f_{ijt} denote enabled FCAS MW. AEMO validates f_{ijt} against a service-specific trapezium in the energy operating point. Figure B4 shows both the service-level validation object and the joint capacity-allocation logic emphasized by Karimi-Arpanahi et al. (2024): energy, regulation FCAS, and contingency FCAS all draw on the same physical headroom.

Write the AEMO trapezium parameters as

$$\underline{x}_{ij} := \mathrm{ENMIN}_{ij}, \quad \ell_{ij} := \mathrm{LBP}_{ij}, \quad u_{ij} := \mathrm{HBP}_{ij}, \quad \overline{x}_{ij} := \mathrm{ENMAX}_{ij}, \quad \overline{f}_{ij} := \mathrm{MAXAVAIL}_{ij}.$$

The market trapezium imposes

$$0 \le f_{ijt} \le T_{ij}(x_{it}), \tag{44}$$

where

$$T_{ij}(x) = \begin{cases} 0, & x < \underline{x}_{ij}, \\ \overline{f}_{ij} \dfrac{x - \underline{x}_{ij}}{\ell_{ij} - \underline{x}_{ij}}, & \underline{x}_{ij} \le x < \ell_{ij}, \\ \overline{f}_{ij}, & \ell_{ij} \le x \le u_{ij}, \\ \overline{f}_{ij} \dfrac{\overline{x}_{ij} - x}{\overline{x}_{ij} - u_{ij}}, & u_{ij} < x \le \overline{x}_{ij}, \\ 0, & x > \overline{x}_{ij}. \end{cases} \tag{45}$$

The flat part of the trapezium is the operating range in which the unit can provide the full enabled quantity for service j. The two sloped sides capture the fact that FCAS availability falls as the unit approaches the edge of its feasible charge or discharge range.

For batteries, the market trapezium is not the only relevant restriction. Let F_{it}^{R} and F_{it}^{L} denote the raise and lower response MW that must be physically deliverable at the operating point. A compact representation of the headroom constraints is

$$F_{it}^{R} \le \bar{P}_i^{\text{dis}} - x_{it}, \qquad F_{it}^{L} \le x_{it} + \bar{P}_i^{\text{ch}}, \tag{46}$$

where $\bar{P}_i^{\text{dis}}$ and $\bar{P}_i^{\text{ch}}$ are the discharge and charge power limits. Raise FCAS requires upward headroom: the battery must be able to increase net injection or reduce net load. Lower FCAS requires downward headroom: the battery must be able to reduce net injection or increase net load.

FCAS also uses scarce energy or scarce empty room when called. For a service with delivery duration Δ_j, a conservative energy-duration restriction is

$$\frac{F_{it}^{R} \Delta_j}{\eta_i^{\text{dis}}} \le S_{it} - \underline{S}_i, \qquad F_{it}^{L} \eta_i^{\text{ch}} \Delta_j \le \bar{S}_i - S_{it}. \tag{47}$$

These inequalities show why FCAS belongs in the same dynamic problem as energy dispatch. Raise services consume stored energy if activated; lower services consume empty room. A change in the energy stack therefore changes the FCAS quantities that can be feasibly enabled, and a change in FCAS enablement changes the energy headroom left for dispatch.

Table B16: Conduct estimator by coalition, market, ERI period, and focal-provider near-margin share band

Period	s^{prov} band	Deviations	(i,t) cells	Mean s^{prov}	$\widehat{\lambda}$	95% CS	Q-reduction
Panel A: Tesla Autobidder – Energy deviations							
Pooled	0–10%	148	54	0.08	1.00	[0.42, 1.00]	1.0%
	10–20%	441	160	0.15	1.00	[0.90, 1.00]	0.1%
	20–30%	873	273	0.24	1.00	[0.87, 1.00]	0.5%
	30–40%	1,840	594	0.36	1.00	[0.95, 1.00]	25.2%
	40–50%	8,065	2,721	0.46	1.00	[0.99, 1.00]	27.8%
	50–60%	9,111	3,064	0.55	1.00	[0.99, 1.00]	13.8%
	60–70%	3,197	1,070	0.63	1.00	[0.95, 1.00]	20.1%
	70–80%	120	38	0.73	0.31	[0.00, 0.97]	9.2%
Panel B: Tesla Autobidder – FCAS deviations							
Pooled	20–30%	194	70	0.24	0.00	[0.00, 0.55]	$< 0.1\%$
	30–40%	331	113	0.36	1.00	[0.69, 1.00]	$< 0.1\%$
	40–50%	151	48	0.46	0.00	—	$< 0.1\%$
	50–60%	72	24	0.55	0.00	—	$< 0.1\%$
	60–70%	36	11	0.65	0.00	—	$< 0.1\%$
Panel C: Fluence Mosaic – Energy deviations							
Pooled	20–30%	2,861	948	0.28	1.00	[0.93, 1.00]	0.5%
	30–40%	10,059	3,328	0.34	0.74	[0.70, 0.78]	6.5%
	40–50%	3,244	1,025	0.46	1.00	[0.99, 1.00]	18.0%
	50–60%	2,655	869	0.55	1.00	[0.98, 1.00]	12.0%
	60–70%	683	223	0.62	1.00	[0.90, 1.00]	10.6%
	70–80%	148	60	0.77	0.00	[0.00, 0.94]	$< 0.1\%$
	80–90%	133	60	0.81	0.00	—	$< 0.1\%$
Panel D: Fluence Mosaic – FCAS deviations							
Pooled	20–30%	121	41	0.28	0.00	[0.00, 0.83]	$< 0.1\%$
	30–40%	388	127	0.34	0.04	[0.00, 0.52]	$< 0.1\%$
	40–50%	276	86	0.46	0.00	—	$< 0.1\%$
	50–60%	272	87	0.54	0.00	—	$< 0.1\%$
	60–70%	81	25	0.63	0.00	—	$< 0.1\%$

Notes: Conduct estimator $\widehat{\lambda} = \arg\min_{\lambda\in[0,1]} Q_n(\lambda)$ from (17), fit separately by focal-provider coalition, market, period, and 10-percentage-point bands of the focal provider's near-margin MW share $s^{\text{prov}}_{k_i,r_i,t}$. The sample is the conduct-test deviation panel of Section 3.4, restricted to cells with at least two distinct owners inside the focal provider's near-margin set; cells with fewer than 30 rows or with no cross-cluster identifying variation are omitted. "Q-reduction" is $1 - Q_n(\widehat{\lambda})/Q_n(0)$, the share of the unrationalised deviation evidence at $\lambda = 0$ that the conduct hypothesis at $\widehat{\lambda}$ accounts for; a Q-reduction below 1% means the test is essentially flat in λ and $\widehat{\lambda}$ is uninformative. 95% confidence sets are obtained by cluster subsampling over (i,t) cells and are reported as "—" when the cell is too small to subsample reliably. Coalitions with empty same-provider, different-owner partner sets in the region (Major-IOU and Other providers) are omitted because $\Delta\Pi_{k_i,-o_i,t}(d) \equiv 0$ leaves $\widehat{\lambda}$ structurally unidentified.

Table B17: Robustness: conduct estimator by diversity-weighted moderator C_{it}

Period	C_{it} band	Deviations	(i,t) cells	Mean C_{it}	$\widehat{\lambda}$	95% CS	Q-reduction
Panel A: Tesla Autobidder – Energy deviations							
Pooled	0–10%	2,906	934	0.03	0.00	[0.00, 0.01]	$< 0.1\%$
	10–20%	1,091	357	0.17	1.00	[0.93, 1.00]	2.5%
	20–30%	11,223	3,756	0.26	1.00	[1.00, 1.00]	27.9%
	30–40%	8,411	2,838	0.34	1.00	[1.00, 1.00]	14.8%
	40–50%	1,610	541	0.42	0.62	[0.35, 0.89]	0.7%
Panel B: Tesla Autobidder – FCAS deviations							
Pooled	0–10%	490	167	0.04	1.00	[0.79, 1.00]	$< 0.1\%$
	10–20%	92	29	0.17	0.00	—	$< 0.1\%$
	20–30%	321	106	0.24	0.00	—	$< 0.1\%$
	30–40%	84	28	0.35	0.00	—	$< 0.1\%$
	40–50%	30	9	0.44	0.00	—	$< 0.1\%$
Panel C: Fluence Mosaic – Energy deviations							
Pooled	0–10%	1,810	583	0.01	1.00	[0.94, 1.00]	$< 0.1\%$
	10–20%	5,517	1,848	0.18	1.00	[0.99, 1.00]	1.1%
	20–30%	9,495	3,126	0.23	0.75	[0.69, 0.80]	7.4%
	30–40%	4,443	1,428	0.34	1.00	[0.97, 1.00]	16.0%
	40–50%	159	51	0.41	1.00	[0.32, 1.00]	33.0%
Panel D: Fluence Mosaic – FCAS deviations							
Pooled	0–10%	137	42	0.03	0.00	—	$< 0.1\%$
	10–20%	231	77	0.17	0.00	[0.00, 0.62]	$< 0.1\%$
	20–30%	469	152	0.24	0.50	[0.18, 0.81]	0.8%
	30–40%	354	113	0.34	0.00	[0.00, 0.41]	$< 0.1\%$

Notes: Robustness fit of the conduct estimator using the diversity-weighted moderator $C_{it} = s^{\text{prov}}_{k_i,r_i,t}\,(1 - \text{HHI}^{\text{own}}_{k_i,r_i,t})$ instead of the headline focal-provider near-margin share $s^{\text{prov}}_{k_i,r_i,t}$. $(1 - \text{HHI}^{\text{own}})$ is the Gini-Simpson diversity index of owner shares within the provider's near-margin set; cells with a single-owner provider are excluded by construction because $C_{it} = 0$ there. Conduct estimator $\widehat{\lambda} = \arg\min_{\lambda\in[0,1]} Q_n(\lambda)$ from (17), fit separately by focal-provider coalition, market, period, and 10-percentage-point bands of C_{it}. "Q-reduction" is $1 - Q_n(\widehat{\lambda})/Q_n(0)$. 95% confidence sets are obtained by cluster subsampling over (i, t) cells and are reported as "—" when the cell is too small to subsample reliably.

Table B18: Consumer-side cost of identified same-provider conduct (price-difference estimate)

	(r,t)	Δp (AUD/MWh)			Sample	Annual
Coalition	cells	Median	Mean	p_{90}	(AUD)	(AUD/yr)
Fluence Mosaic	457	1.29	2.80	6.44	\$1.98m	\$2.36m
Tesla Autobidder	439	1.28	2.59	6.02	\$2.58m	\$3.09m
Total	896	1.28	2.70	6.24	\$4.56m	\$5.45m

Notes: Sample comprises the 19 focal batteries (12 Tesla Autobidder, 7 Fluence Mosaic) of the conduct panel, restricted to evening-peak intervals (16:00–22:00) in the identifying bands (energy market, focal-provider near-margin share s^{prov} in the identifying regime of Table B16, Q-reduction $\geq 1\%$ and CS excluding zero). (r, t) counts region-intervals with a positive recleared price difference under the owner-only counterfactual d^0_{it}. Price-difference percentiles are taken over the same set. The sample-window cost is the inverse-inclusion-probability-weighted total $\sum_{(r,t)} \Delta p_{rt} \cdot \text{DemandMW}_{rt} \cdot \frac{5}{60} \cdot w_{rt}$; the annualised cost multiplies by $365/305 \simeq 1.20$.

Table B19: Battery-side dollar transfer on sign-flipping deviations (diagnostic)

Coalition	$\mathcal{L}^\star$ cells	Focal foregone	Same-prov. retained	Other-batt. retained	Battery transfer
Sample totals (305-day window)					
Fluence Mosaic	307	\$10.2k	\$18.4k	\$11.1k	\$29.5k
Tesla Autobidder	401	\$18.3k	\$35.7k	\$16.2k	\$51.9k
Total	708	\$28.6k	\$54.2k	\$27.3k	\$81.5k
Annualised ($\times 1.20$)					
Fluence Mosaic		\$12.2k	\$22.1k	\$13.3k	\$35.4k
Tesla Autobidder		\$21.9k	\$42.7k	\$19.4k	\$62.1k
Total		\$34.2k	\$64.8k	\$32.7k	\$97.5k

Notes: As Table B18 but restricted to the sign-flipping subset $\mathcal{L}^\star$ (708 region-intervals in the sample) and tabulating battery-side dollar magnitudes rather than the consumer-side price effect. The diagnostic is intentionally narrower than Table B18: it considers only the discrete deviations that flip sign between the two hypotheses, and excludes both the consumer cost on non-battery inframarginal generation and the magnitude-shrinking contributions from deviations that remain profitable under both hypotheses. The annualised row scales sample totals by $365/305 \simeq 1.20$.

Table B20: Omitted owner-cost bounds for conduct-identifying energy deviations

Coalition	Period	s^{prov} band	(i,t) cells	c^Q	$c^Q/11$	Med. $\mu^\star$	p90 fin. $\mu^\star$	$\mu^\star > 100$ share	$\mu^\star > 1{,}000$ share
Tesla	Pooled	30–40%	594	16	1.4	25	77	36.4%	32.0%
Tesla	Pooled	40–50%	2,721	–	–	24	92	79.7%	78.2%
Tesla	Pooled	50–60%	3,064	59	5.4	27	105	77.1%	74.5%
Tesla	Pooled	60–70%	1,070	–	–	20	79	57.7%	55.0%
Fluence	Pooled	30–40%	3,328	8	0.7	24	89	71.7%	69.4%
Fluence	Pooled	40–50%	1,025	28	2.6	21	70	48.8%	45.9%
Fluence	Pooled	50–60%	869	15	1.4	23	121	62.2%	54.1%
Fluence	Pooled	60–70%	223	11	1.0	14	67	62.5%	59.4%

Notes: The table reports the omitted-owner-cost exercise for conduct-identifying energy-push cells: Q-reduction at $\widehat{\lambda}$ is at least one percent and the cluster-subsampling confidence set excludes zero. c^Q is the smallest cell-level omitted owner cost in AUD/MWh of extra focal discharge that would reduce the owner-only squared-violation objective to $Q_n(\widehat{\lambda})$. The column $c^Q/11$ benchmarks this cost against the 11 AUD/MWh maximum movement in $\widehat{m}_{it}$ across Bellman grid/control sensitivity checks reported in Appendix B.3. $\mu^\star_{it}$ is the battery-interval linear wedge in AUD/MWh of extra focal discharge needed to rationalise all sampled owner-profitable deviations in that battery-interval under owner-only conduct. Quantiles of $\mu^\star_{it}$ are over finite values. Threshold shares are among owner-violating battery-intervals and count $\mu^\star_{it} = \infty$ as above threshold; the 100 and $1{,}000$ AUD/MWh thresholds match the materiality cutoffs used in the Bellman IC diagnostics. Uniform weights match the conduct estimator.

Table B21: Permutation-null vs actual for the conduct estimator, by $(\text{coalition}, s^{\text{prov}})$ band

			$\widehat{\lambda}$			Q-reduction (%)		
Coalition	s^{prov} (%)	n	Actual	Null p95	p	Actual	Null p95	p
Tesla	< 30	1,462	1.00	1.00	0.641	0.4	2.35	0.485
	30–40	1,840	1.00	1.00	0.578	25.2	5.12	0.003
	40–50	8,065	1.00	1.00	0.837	27.8	4.19	0.003
	50–60	9,111	1.00	1.00	0.983	13.8	3.61	0.003
	60–70	3,197	1.00	1.00	0.771	20.1	1.49	0.003
	> 70	123	0.31	1.00	0.495	9.2	44.17	0.282
Fluence	< 30	2,876	1.00	0.66	0.023	0.5	0.37	0.037
	30–40	10,059	0.74	0.17	0.003	6.5	0.63	0.003
	40–50	3,244	1.00	0.26	0.003	18.0	0.78	0.003
	50–60	2,655	1.00	0.28	0.003	12.0	0.92	0.003
	60–70	683	1.00	0.46	0.007	10.6	3.44	0.003
	> 70	281	0.00	0.65	1.000	0.0	5.79	1.000

Notes: $B = 300$ permutation draws shuffling G^{K}_{itd} across focal deviations within coalition. "Null p95" is the 95th percentile of the null statistic across draws; p is the empirical upper-tail p-value with plus-one finite-sample correction.

Table B22: Provider-specificity: matched placebo coalitions

		Same-provider	Count-matched placebo		Capacity-matched placebo	
Coalition	n	Q-reduction	null mean [p95]	p	null mean [p95]	p
Tesla	21,815	19.6%	10.5 [13.2]	0.002	13.2 [14.3]	0.002
Fluence	16,151	9.7%	3.2 [6.7]	0.010	2.1 [4.8]	0.002

Notes: For each focal battery-interval in the identifying range ($s^{\text{prov}} \in [0.30, 0.70]$, multi-owner), the placebo coalition is drawn from the different-provider, different-owner batteries near the margin in the same region-interval, matched to the actual same-provider coalition on battery count ("count-matched") or on both count and installed capacity via a Gaussian kernel ("capacity-matched"). Entries are the conduct fit improvement $R = 1 - Q_n(\widehat{\lambda})/Q_n(0)$; the null summarises 500 placebo draws and p is the fraction with $R \geq$ the actual same-provider value (plus-one correction). The same-provider coalition rationalises the observed restraint significantly better than matched different-provider coalitions with the same mechanical price exposure.

Table B23: Conduct estimator by quantity-rebid lead time

Coalition	Rebid lead time	Deviations	Own-profitable (%)	$\widehat{\lambda}$	Q-reduction
Tesla	< 15 min	20,125	42.8	1.00	19.8%
	15–60 min	803	14.1	1.00	2.6%
	> 60 min	1,285	10.7	0.00	0.0%
Fluence	< 15 min	13,602	35.0	0.96	11.2%
	15–60 min	2,649	28.6	1.00	4.9%
	> 60 min	390	36.4	1.00	0.0%

Notes: Conduct estimator $\widehat{\lambda} = \arg\min_{\lambda \in [0,1]} Q_n(\lambda)$ with a single same-provider, different-owner peer term, fit on the evening-peak energy deviation panel restricted to the identifying near-margin range $s^{\text{prov}} \in [0.30, 0.70]$ with at least two owners inside the focal provider's near-margin set. Rows split the sample by the number of minutes between the operative quantity rebid and dispatch. "Own-profitable" is the share of deviations with a positive recleared owner-portfolio gain; "Q-reduction" is $1 - Q_n(\widehat{\lambda})/Q_n(0)$. Under a hindsight alternative the signal would concentrate in long-lead bids; instead it concentrates in the near-dispatch bids, where predispatch foresight is accurate.

Table B24: Same-owner positive control

Coalition	Battery-intervals	With same-owner peer	$\widehat{\lambda}_O$	Q-reduction
Tesla	25,253	73.2%	1.00	12.4%
Fluence	21,424	11.8%	1.00	0.3%

Notes: Positive control estimating the weight $\widehat{\lambda}_O$ the focal owner places on the recleared profit effect on its *own* other batteries in the region, $\arg\min_{\lambda_O} \sum w[\Delta\Pi^{\text{focal}} + \lambda_O \Delta\Pi^{\text{same owner}}]_+^2$, on the evening-peak energy deviation panel restricted to focal battery-intervals with at least one same-owner peer in the region. Economic theory requires $\lambda_O = 1$. "With same-owner peer" is the share of each coalition's battery-intervals that have such a peer.